TRANSMISSION OF SOUND THROUGH A RANDOMLY ROUGH AIR-SEA INTERFACE

BY

James Dixon Hagy

United States
Naval Postgraduate School

THESIS

TRANSMISSION OF SOUND

THROUGH A RANDOMLY ROUGH AIR-SEA INTERFACE

by

James Dixon Hagy, Jr.

September 1970

This document has been approved for public release and sale; its distribution is unlimited.

T136124

Transmission of Sound

Through a Randomly Rough Air-Sea Interface

by

James Dixon Hagy, Jr.
Lieutenant, United States Navy
B.A. Duke University, 1963

Submitted in partial fulfillment of the
requirements for the degree of

ELECTRICAL ENGINEER

from the

NAVAL POSTGRADUATE SCHOOL
September 1970

RARY
AL POSTGRADUATE SCHOOL
TEREY, CALIF. 93940

ABSTRACT

The Helmholtz integral and the Kirchhoff approximation have been used to develop predictions for the transmission of sound through a rough air-sea interface. A model study was conducted with wind-driven surfaces generated in a large anechoic tank. Root mean square wave heights, σ, ranged from .05 to .41 cm, windward correlation lengths, L_u, from 0.8 to 4.2 cm. The frequencies used (10-43 kHz) were scaled to be equivalent to low audio frequencies with moderate seas. Although the coherent component of the transmitted acoustic intensity showed an exponential decrease with increasing values of the roughness parameter, $R\ [= k_2^2\sigma^2\ (c_2/c_1 \cos\theta_1 - \cos\theta_2)^2\ ]$, the decrease was greater than predicted. (Subscript 2 refers to propagation constant, speed and angle of transmission in water; subscript 1, in air.) This lack of agreement appeared to be caused by violation of the Kirchhoff requirement, $L/\lambda_2 >> 1$. An empirical correction factor $\alpha = 1 + 4.8e^{-L_u/1.75}$ was determined to give a corrected roughness, αR. The corrected theory appears to be valid for both coherent and incoherent components of intensity for all values of L/λ_2 provided that $\alpha R < 4.0$. For higher values of roughness there is a "leveling off" of the transmission loss of the coherent component similar to that recently observed but unexplained in rough surface scattering.

TABLE OF CONTENTS

ACKNOWLEDGEMENT

The author is indebted to his thesis advisor, Dr. H. Medwin of the Naval Postgraduate School, for his useful and instructive advice and for the insights gained during many hours of stimulating discussion.

Thanks are also due to Dr. W. M. Wright, who designed and constructed the wave probes and permitted the author to join him in the study of the model sea surfaces.

The computer programming of Mrs. R. S. Lande was very helpful and is appreciated. The assistance of technicians W. Smith, T. Maris, R. Moeller and M. Andrews is acknowledged with thanks.

The support of ASW Systems Project Office, Code ASW 21 and Naval Ordnance Systems Command is acknowledged.

BLANK

p 6
Blank

I. INTRODUCTION

The problem of transmission of airborne sound into the ocean has received very little attention. Only recently has it become apparent that a more detailed study of the problem than has been made in the past should be undertaken. Most of the theoretical studies that have been done in this area have dealt with a smooth air-sea interface and the rough air-water transmission studies reported to date have been with deterministic surfaces [1]. The work reported in this thesis is part of a project in progress at the Naval Postgraduate School that has included a series of ocean-acoustic experiments as well as the theoretical and model studies.

The author has had the satisfaction of participating in two successful ocean experiments with Professor H. Medwin and LCDR R. A. Helbig. LCDR Helbig will report on this phase of the project when the analysis has been completed. These experiments were conducted from the research platform FLIP operated by the Scripps Oceanographic Institution, and involved the recording of the underwater sound fields of several operational Navy aircraft. Ocean wave data were collected simultaneously with the acoustic data collection as were the other important environmental parameters. It is hoped that the results of these experiments can be better interpreted on the basis of the theoretical and model sea studies reported here.

The objective of this thesis has been to reduce the sound transmission problem to the simplest useful case and to apply the Helmholtz integral in the Kirchhoff approximation to develop a theory that parallels that derived for rough surface scattering. The rough surface scattering

problem has received a great deal of attention and this method of approach has given reasonably good results for the scattering of underwater sound from a realistically rough sea surface. Apparently no one has tried to apply this technique to a rough surface transmission problem although there seems to be no reason why this can not be done.

II. THEORY

The development given here applies the Helmholtz integral and the Kirchhoff approximation to describe the transmission of acoustic waves through a randomly rough air-sea interface. The formulation of this problem parallels that used for acoustic scattering from a rough surface by Medwin [2]. The monograph of Beckmann and Spizzichino [3] presents a detailed discussion of the application of the Helmholtz integral to the scattering of electromagnetic waves that, with minor modifications, is directly applicable to the problem of acoustic transmission through a rough interface.

A. AN INTEGRAL EXPRESSION FOR THE RECEIVED ACOUSTIC PRESSURE

The Helmholtz integral,

$$p_2 = \frac{1}{4\pi} \int_S \left(p \frac{\partial \Psi}{\partial n} - \Psi \frac{\partial p}{\partial n} \right) dS \qquad (1)$$

expresses the complex acoustic field, p_2, at a receiver in the far field of an ensonified area, S, in terms of the field and its normal derivative on S and the scalar "Green's Function", $\Psi = \frac{e^{ikr}}{r}$. A single frequency harmonic wave is assumed and the time dependence suppressed. For convenience the quantity p_2 is described as the "received acoustic pressure" with the understanding that it represents the amplitude and phase of the received acoustic wave. The exact value of the field and its normal derivative on S is in general unknown and the Kirchhoff method consists of approximating these values by those that would exist on a tangent plane at that point. Within this approximation the boundary conditions can be stated in terms of the incident field, p_1 ,

$$p = p_1 + Rp_1 = Tp_1$$

$$\frac{\partial p}{\partial n} = \frac{\partial p_1}{\partial n} - \frac{\partial Rp_1}{\partial n} = i(1 - R)(\vec{k}_1 \cdot \hat{n})p_1 \qquad (2)$$

where R and T are the reflection and transmission coefficients defined for infinite planes.

Before proceeding with the evaluation of (1) it is convenient at this point to specialize and introduce the reflection coefficient appropriate for acoustic transmission from air to water. This results in a simplification of the integral since R may be set equal to one and the normal derivative of the field vanishes at the boundary. It is at this point that the development first diverges from that for underwater scatter, where R = -1 and the field itself must vanish at the boundary. The Helmholtz integral can now be written in a simplified form.

$$p_2 = \frac{1}{4\pi} \int_S 2\, p_1\, (-i\vec{k}_2 \cdot \hat{n}\psi)\, dS \qquad (3)$$

Figure 1 is a sketch of the geometry of the problem that shows the coordinates that will be used and labels the angles that are defined. A list of the notation to be used follows.

p_{1A} = acoustic pressure at unit distance from source

$p_{10} = \frac{p_{1A}}{r_1} e^{i(k_1 r_1 - \omega t)}$, incident acoustic pressure at origin

$p_1 = p_{10}\, e^{i(\vec{k}_1 \cdot \vec{r})}$, incident acoustic pressure at element dS

p_2 = acoustic pressure at the receiver

dS = dxdy/cos γ , the area of a surface element

ζ = $\zeta(x,y)$, the surface height at (x,y)

$\hat{n}$ = $\hat{i}_1(-\sin\gamma\cos\alpha) + i_2(-\sin\gamma\sin\alpha) + \hat{i}_3\cos\gamma$, normal to surface element

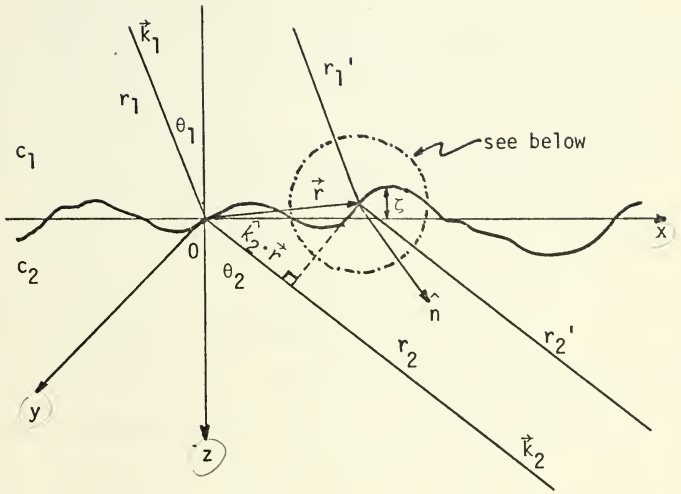

FIGURE 1. THE GEOMETRY OF THE PROBLEM

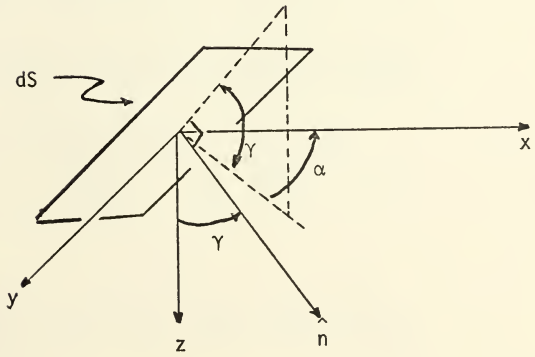

γ = angle the normal makes with the z axis

α = angle the projection of the normal onto the xy-plane makes with the x axis

$\vec{k}_1 = \frac{2\pi f}{c_1}(\hat{i}_1 \sin\theta_1 + \hat{i}_3 \cos\theta_1)$, vector propagation constant of incident field

$\vec{k}_2 = \frac{2\pi f}{c_2}(\hat{i}_1 \sin\theta_2 \cos\theta_3 + \hat{i}_2 \sin\theta_2 \sin\theta_3 + \hat{i}_3 \cos\theta_2)$, vector propagation constant of received field

θ_1 = angle of incidence

θ_2 = angle that $\vec{k}_2$ makes with the z-axis

θ_3 = angle that $\vec{k}_2$ makes with the xz-plane

$\vec{r} = \hat{i}_1 x + \hat{i}_2 y + \hat{i}_3 \zeta$, the radius vector to the surface element

r_1 = distance from source to origin of ensonified area

r_1' = distance from source to surface element

r_2 = distance from origin of ensonified area to receiver

r_2' = distance from surface element to receiver

$\Psi = \frac{e^{ik_2 r_2'}}{r_2'} = \frac{e^{ik_2 r_2}}{r_2} e^{-i\vec{k}_2 \cdot \vec{r}}$, Green's Function

$$\left(\frac{\partial \Psi}{\partial n}\right)_S = -i\vec{k}_2 \cdot \hat{n}\Psi$$

Continuing, equation (3) can be rewritten,

$$p_2 = \frac{-i2p_{10}e^{ik_2 r_2}}{4\pi r_2} \int_S \vec{k}_2 \cdot \hat{n} e^{i\vec{K}\cdot\vec{r}}\, dS \qquad (4)$$

where

$$\vec{K} = \vec{k}_1 - \vec{k}_2 = \hat{i}_1 K_x + \hat{i}_2 K_y + \hat{i}_3 K_z$$

$$K_x = k_1 \sin\theta_1 - k_2 \sin\theta_2 \cos\theta_3$$

$$K_y = -k_2 \sin\theta_2 \sin\theta_3$$

$$K_z = k_1 \cos\theta_1 - k_2 \cos\theta_2$$

and

$$\vec{k}_2 \cdot \hat{n} = k_2 \cos\theta_2 \left[-\tan\theta_2 \sin\gamma \cos\alpha \cos\theta_3 - \tan\theta_2 \sin\gamma \sin\alpha \sin\theta_3 + \cos\gamma\right]$$

Assuming uniform ensonification over a rectangular area 2X by 2Y,

$$p_2 = \frac{-i2p_{10}\, e^{ik_2 r_2}\, k_2 \cos\theta_2}{4\pi r_2} \int_{-Y}^{Y} \int_{-X}^{X} f(\theta_1,\theta_2,\theta_3,\gamma,\alpha) e^{i\vec{K}\cdot\vec{r}}\, dx\, dy \quad (5)$$

where

$$f = -\tan\theta_2 \tan\gamma \cos\alpha \cos\theta_3 - \tan\theta_2 \tan\gamma \sin\alpha \sin\theta_3 + 1 .$$

The smooth surface transmitted pressure has a maximum value p_{20}, where,

$$p_{20} = \left| \frac{-i2p_{10} e^{ik_2 r_2}}{4\pi r_2} A \cos\theta_2 \right| , \qquad A = 4XY \quad (6)$$

The integral of (5) may be written using (6),

$$p_2 = \frac{p_{20}}{A} \int_{-Y}^{Y} \int_{-X}^{X} \left(a \frac{\partial\zeta}{\partial x} + b \frac{\partial\zeta}{\partial y} + 1 \right) e^{i\vec{K}\cdot\vec{r}}\, dxdy \quad (7)$$

where $\frac{\partial\zeta}{\partial x} = \tan\gamma \cos\alpha$

$$\frac{\partial\zeta}{\partial y} = \tan\gamma \sin\alpha$$

and $a = -\tan\theta_2 \cos\theta_3$

$b = -\tan\theta_2 \sin\theta_3$

Now there are three integrals to evaluate two of which must be integrated by parts. Starting with the first term

$$- \iint \frac{a\partial\zeta}{\partial x} e^{i\vec{K}\cdot\vec{r}}\, dx\, dy \qquad (8)$$

let $u = e^{iK_x x}$, $du = iK_x e^{iK_x x}\, dx$

$dv = iK_z e^{iK_z\zeta} \frac{\partial\zeta}{\partial x}\, dx$, $v = e^{iK_z\zeta}$

Then since

$$\int u\,dv = uv - \int v\,du$$

(8) can be evaluated

$$= \frac{a}{iK_z} \int e^{iK_y y} \int e^{iK_x x} \left(iK_z e^{iK_z\zeta} \frac{\partial\zeta}{\partial x}\, dx\right) dy$$

$$= \frac{a}{iK_z} \int e^{iK_y y} \left[e^{iK_x x} e^{iK_z\zeta}\Big|_{-X}^{X} - \int_{-X}^{X} e^{iK_z\zeta} e^{iK_x x} iK_x\, dx \right] dy$$

$$= \frac{a}{iK_z} \left[\int_{-Y}^{Y} e^{iK_x x}\Big|_{-X}^{X} e^{iK_z\zeta}\Big|_{-X}^{X} e^{iK_y y}\, dy - iK_x \int_{-Y}^{Y}\int_{-X}^{X} e^{i\vec{K}\cdot\vec{r}}\, dx dy \right]$$

Similarly for the second term

$$\frac{b}{iK_z} \int e^{i\vec{K}\cdot\vec{r}}\Big|_{-Y}^{Y} dx - \frac{bK_y}{K_z} \int_{-Y}^{Y}\int_{-X}^{X} e^{i\vec{K}\cdot\vec{r}}\, dx dy \qquad (9)$$

combining the three integrals gives,

$$p_2 = p_{20} \frac{F}{A} \int_{-Y}^{Y} \int_{-X}^{X} e^{i\vec{K}\cdot\vec{r}} \, dxdy + B \qquad (10)$$

where

$$F = f(\theta_1,\theta_2,\theta_3) = 1 - \left(\frac{aK_x + bK_y}{K_z} \right)$$

$$F(\theta_1,\theta_2,\theta_3) = 1 + \frac{(c_2/c_1 \sin\theta_1 - \sin\theta_2) \tan\theta_2 \cos\theta_3}{c_2/c_1 \cos\theta_1 - \cos\theta_2}$$

$$- \frac{\sin\theta_2 \tan\theta_2 \sin^2\theta_3}{c_2/c_1 \cos\theta_1 - \cos\theta_2}$$

It can be seen that F reduces to unity when the receiver is in the direction predicted by Snell's law of refraction, that is when $c_2/c_1 \sin\theta_1 - \sin\theta_2 = 0$ and $\theta_3 = 0$. In addition, F diverges significantly from unity only for angles far from the Snell angle for given angle of incidence. The behavior of $F(\theta_1,\theta_2,0)$ is given in Table 1, which may be compared with Table 3.1 in Ref. [3] that gives values for a similar function encountered in the surface scattering problem. A difference that is observed is the appearance of negative values of F for refracted angles far from the Snell angle and nearly horizontal. The acoustic intensity in these directions will be relatively low, since other factors will dominate the behavior of the transmitted field, and it will be difficult to determine experimentally if this effect apparently introduced by F is, in fact, real.

TABLE 1

Values of $F(\theta_1,\theta_2,0)$

$$F(\theta_1,\theta_2,0) = 1 + \frac{(c_2/c_1 \sin\theta_1 - \sin\theta_2)\tan\theta_2}{c_2/c_1 \cos\theta_1 - \cos\theta_2}$$

θ_2 \ θ_1	0°	3°	6°	9°	12°
-80	-0.30	-0.61	-0.93	-0.13	-1.59
-70	0.37	0.21	0.55	-0.11	-0.27
-60	0.62	0.52	0.41	0.31	0.19
-50	0.76	0.68	0.61	0.54	0.46
-40	0.85	0.80	0.75	0.69	0.63
-30	0.92	0.88	0.84	0.80	0.76
-20	0.96	0.94	0.92	0.89	0.86
-10	0.99	0.98	0.97	0.96	0.94
0	1.00	1.00	1.00	1.00	1.00
10	0.99	1.00	1.02	1.03	1.04
20	0.96	0.99	1.01	1.04	1.06
30	0.92	0.96	0.99	1.03	1.07
40	0.85	0.91	0.96	1.01	1.07
50	0.76	0.83	0.91	0.98	1.05
60	0.62	0.72	0.82	0.92	1.03
70	0.37	0.53	0.68	0.84	0.99
80	-0.30	0.28	0.31	0.61	0.92

The second term in (10) represents an "edge effect" and can be shown to be small compared to the remaining integral if the ensonified area is many wave lengths in dimension.

$$B = \frac{p_{20}}{A} \left[\frac{a}{iK_z} \int_{-Y}^{Y} e^{i\vec{K}\cdot\vec{r}} \Big|_{-X}^{X} dy + \frac{b}{iK_z} \int_{-X}^{X} e^{i\vec{K}\cdot\vec{r}} \Big|_{-Y}^{Y} dx \right] \qquad (11)$$

To see this, it is argued that because the conditions at the periphery of a large ensonified area can not be a major factor in the overall result, ζ can be set equal to zero at the edges without significantly altering the predicted field. With this assumption the integration can be performed and gives

$$B = p_{20} \left(\frac{aK_x + bK_y}{K_z} \right) \text{ sinc } K_x X \text{ sinc } k_y Y$$

or

$$B = p_{20} (1 - F) \text{ sinc } K_x X \text{ sinc } k_y Y \qquad (12)$$

It can be observed that because of the sinc terms, B can only have a significant value within a narrow wedge centered on Snell's direction. But in this direction F is approximately equal to unity; so we have $B \ll p_{20}$. On the basis of the above argument the edge contribution is dropped and (10) becomes

$$p_2 = p_{20} \frac{F}{A} \int_{-Y}^{Y} \int_{-X}^{X} e^{i\vec{K}\cdot\vec{r}} \, dxdy \qquad (13)$$

Equation (13) is an integral expression for the received acoustic pressure. The form of this equation is identical to that developed for

the surface scattering problem. The steps from this point on are identical to those in surface scattering but, of course, the results will be somewhat different since the terms in (13) reflect the different geometry and refraction encountered in rough surface transmission. To procede a further specialization will be made by specifying a randomly rough surface and the first and second moments of the transmitted acoustic signal will be derived.

B. ASSUMPTIONS AND APPROXIMATIONS

In order to derive (13) it has been necessary to make a number of assumptions and approximations which may limit the applicability of the theory. To summarize, it has been assumed:

1) The incident wave is plane and ensonifies a limited area.
2) The receiver is sufficiently far from the surface to regard the received waves as plane, i.e., the "far field approximation" is made.
3) Mutual interaction of the surface irregularities may be neglected.
4) The ensonified area is large compared to an acoustic wavelength.
5) The surface is considered perfectly rigid such that the reflection coefficient, R = 1.
6) 5) The Kirchhoff approximation is valid.

Of the above, the last is probably the most serious limitation to the validity of the solution. The Kirchhoff approximation has been noted by Beckmann and others to require that the minimum radius of curvature of the surface be large compared with the wavelength of the incident radiation. For the transmission problem there are two wavelengths at the interface and it seems reasonable that the reradiation wavelength (λ_2), which in this case is the larger wavelength, must be chosen as the critical one. The requirement of the Kirchhoff approximation seems to limit the application of (13) to a certain class of

surfaces. The surface must be a gentle one without a large amount of sharp edges or irregularities with small radii of curvature. For a realistic wind-driven sea this requirement can be expressed in terms of a characteristic length that may be derived from the two-dimensional spatial correlation or equivalently from the sea surface directional spectra.

C. THE MEAN ACOUSTIC PRESSURE

The average received acoustic pressure can be calculated for a statistically rough surface by taking the space average of equation (13).

$$\langle p_2 \rangle = p_{20} \frac{F}{A} \int_{-Y}^{Y} \int_{-X}^{X} e^{i(K_x x + K_y y)} \left\langle e^{iK_z \zeta} \right\rangle \, dx dy \qquad (14)$$

It has been shown that the wave height distribution of ocean waves is very nearly Gaussian. Using a Gaussian probability density function

$$w(\zeta) = \frac{1}{\sigma\sqrt{2\pi}} e^{-\zeta^2/2\sigma^2}$$

Equation (6) can now be evaluated.

$$\langle p_2 \rangle = p_{20} F e^{-R/2} \operatorname{sinc} K_x X \operatorname{sinc} K_y Y \qquad (15)$$

where $R = K_z^2 \sigma^2$.

The significant parameter in equation (7) is a "roughness parameter" similar to one encountered in rough surface scattering and denoted by Beckmann as $g = K_z^2 \sigma^2$. Comparison of R and g shows some interesting differences:

$$R = k_2^2\sigma^2 (c_2/c_1 \cos\theta_1 - \cos\theta_2)^2$$

$$g = k_2^2\sigma^2 (\cos\theta_1 + \cos\theta_2)^2$$

A significant difference is that the strong dependence on geometry seen in g is almost completely absent in R. While g can vanish as the angles approach grazing, the geometry dependence in R is dominated by the term, $c_2/c_1 \cos\theta_1$ and this quantity must remain nearly constant because of the limited range of incident angles, θ_1 , that will result in significant sound transmission for sound traveling from air into water. If R is evaluated for those refracted rays predicted by Snell's Law, it can be seen to be a minimum at normal incidence and to increase gradually as the angle of incidence increases. It is also apparent that, for the same frequency and mean square wave height, the surface appears "rougher" for sound transmission from air into the sea than it does forthe scattering of underwater sound. R will be a minimum of three times greater than g at normal incidence and, of course, much larger if the practically important case of near grazing incidence for surface scatter is compared to nearly horizontal transmission.

D. THE VARIANCE OF THE ACOUSTIC PRESSURE

In order to evaluate the mean received intensity, the variance of the acoustic pressure must be determined in addition to the mean acoustic pressure. The variance of p_2 can be evaluated through the formula

$$V\{p_2\} = \langle p_2 p_2^* \rangle - \langle p_2 \rangle \langle p_2^* \rangle$$

which can be expressed

$$V\{p_2\} = p_{20}^2 \left(\frac{F}{A}\right)^2 \iiiint e^{i(K_x(x-x') + K_y(y-y'))} \quad .....$$

$$..... \left[\left\langle e^{iK_z(\zeta-\zeta')} \right\rangle - \left\langle e^{iK_z\zeta} \right\rangle \right] dxdydx'dy' \qquad (16)$$

For a Gaussian distribution of heights,

$$- \left\langle e^{iK_z(\zeta-\zeta')} \right\rangle = e^{-R + RC}$$

where C is the correlation coefficient.

It is now assumed that the surface is isotropically rough and a Gaussian correlation function is specified. Although this assumption is quite obviously incorrect for a realistic sea, it has yielded some useful results in the surface scattering problem and it simplifies the mathematics considerably.

The sea surface spatial correlation is assumed to be

$$C(\ell) = e^{-\ell^2/L^2} \qquad (17)$$

Transforming (16) to polar coordinates, using the assumption $L^2 << A$.

$$V\{p_2\} = p_{20}^2 \frac{F^2}{A} \int_0^{\infty} \int_0^{2} e^{i\,(K_x\cos\phi + K_y\sin\phi)} \left[e^{-R(1-C)} - e^{-R}\right] d\phi\,\ell\,d\ell \qquad (18)$$

Using the series expansion for the exponential the bracketed term becomes

$$\left[e^{-R} \sum_{n=1}^{\infty} \frac{R^n}{n!} e^{-n\ell^2/L^2}\right]$$

Integrating over ϕ gives

$$V\{p_2\} = 2\pi\, p_{20}^2\, \frac{F^2}{A} \int_0^\infty J_0(\ell K_{xy}) \left[e^{-R} \sum_{n=1}^{\infty} \frac{R^n}{n!} e^{-n\ell^2/L^2}\right] \ell\, d\ell \qquad (19)$$

where $K_{xy} = K_x^2 + K_y^2$

Uniform convergence permits the change of order of summation and integration. The resulting form

$$V\{p_2\} = 2\pi\, p_{20}^2\, \frac{F^2}{A}\, e^{-R} \sum_{n=1}^{\infty} \frac{R^n}{n!} \int_0^\infty J_0(K_{xy}\ell)\, e^{-n\ell^2/L^2}\, \ell\, d\ell \qquad (20)$$

is a standard integration which gives

$$V\{p_2\} = p_{20}^2\, F^2\, \frac{\pi L^2}{A}\, e^{-R} \sum_{n=1}^{\infty} \frac{R^n}{n\,n!}\, e^{-K_{xy}^2 L^2/4n} \qquad (21)$$

It is possible to get less complicated expressions than (21) for three cases: a) $R \ll 1$ b) $R \gg 1$ c) $K_{xy} = 0$, where $K_{xy} = 0$ corresponds to transmission in Snell's direction.

a) For $R \ll 1$ we may take only the first term of the series and obtain

$$V\{p_2\} \simeq p_{20}^2\, F^2\, \frac{\pi L^2}{A}\, R\, e^{-R}\, e^{-K_{xy}^2 L^2/4} \qquad (22)$$

b) For $R \gg 1$ the mean acoustic pressure approaches zero and $V\{p_2\} \quad \langle p_2 p_2^* \rangle$. Equation (18) becomes

$$\langle p_2 p_2^* \rangle = 2\pi\, \frac{p_{20}^2}{A}\, F^2 \int_0^\infty J_0(K_{xy}\ell)\, e^{-R(1-C)}\, \ell\, d\ell$$

or using the Gaussian correlation coefficient

$$\langle p_2 p_2^* \rangle = 2\pi \frac{p_{20}^2}{A} F^2 \int_0^\infty J_0(K_{xy}\ell)\, e^{-R\,[1 - \exp(-\ell^2/L^2)]}\, \ell d\ell \quad (23)$$

It can be shown that for $R >> 1$ this integral receives significant contributions only from the neighborhood of $\ell = 0$. Therefore, using the first two terms of the expansion of the correlation function, $C(\ell) \quad 1 - (\ell^2/L^2)$, (23) becomes

$$\langle p_2 p_2^* \rangle = 2\pi \frac{p_{20}^2}{A} F^2 \int_0^\infty J_0(K_{xy}\ell) \exp(-R\ell^2/L^2)\, \ell d\ell \quad (24)$$

and we can evaluate this integral

$$\langle p_2 p_2^* \rangle = p_{20}^2 F^2 \frac{\pi L^2}{AR} \exp(-K_{xy}^2 L^2/4R) \quad (25)$$

Using the expression for the mean square slope of the rough surface, $\Sigma^2 = \frac{2\sigma^2}{L^2}$, (25) can be written, again for $R >> 1$

$$V\{p_2\} \simeq \langle p_2 p_2^* \rangle_{R>>1} \simeq p_{20}^2 \frac{2\pi F^2}{K_z^2 A \Sigma^2} \exp\left(-\frac{K_{xy}^2}{2K_z^2\Sigma^2}\right) \quad (26)$$

c) A special case of interest is an evaluation of the variance of the acoustic pressure in Snell's direction, where $K_{xy} = 0$. Using equation (21)

$$V\{p_2\} = p_{20}^2 \frac{\pi L^2}{A} \left(e^{-R} \sum_{n=1}^{\infty} \frac{R^n}{nn!} \right) \quad (27)$$

Medwin [2] has evaluated the function, S(R), where

$$S(R) = e^{-R} \sum_{n=1}^{\infty} \frac{R^n}{nn!} \tag{28}$$

A plot of S(R) is given in Ref. [2]. It can be noted that for $R << 1$, $S(R) \rightarrow R$ and for $R >> 1$, $S(R) \rightarrow 1/R$. Using these asymptotic values and $K_{xy} = 0$, equation (27) agrees with the low roughness case stated in (22) and with the high roughness case given in (25).

E. THE MEAN SQUARE ACOUSTIC PRESSURE

It is now possible to write the general expression for the mean squared acoustic pressure.

$$\langle p_2 p_2^* \rangle = p_{20}^2 F^2 e^{-R} \left[(\text{sinc } K_x X \text{ sinc } K_y Y)^2 + \frac{\pi L^2}{A} \sum_{n=1}^{\infty} \frac{R^n}{nn!} \exp(-K_{xy}^2 L^2/4n) \right] \tag{29}$$

for low roughness, $R << 1$, we have

$$\langle p_2 p_2^* \rangle = p_{20}^2 F^2 e^{-R} \left[(\text{sinc } K_x X \text{ sinc } K_y Y)^2 + \frac{\pi L^2}{A} R \exp(-K_{xy} L^2/4) \right] \tag{30}$$

for high roughness, $R >> 1$, we have

$$\langle p_2 p_2^* \rangle = p_{20}^2 F^2 \frac{2\pi}{K_z^2 A \Sigma^2} \exp\left(\frac{-K_{xy}^2}{2K_z^2 \Sigma^2} \right) \tag{31}$$

The first term in (29) represents the coherent component of the transmitted signal, while the second term is the incoherent component. Since $L^2 \ll A$, the coherent component dominates for $R < 1$. But as R increases the coherent term fades rapidly until we have, for $R \gg 1$, a completely incoherent signal.

F. STATISTICAL DISTRIBUTION OF THE RECEIVED ACOUSTIC PRESSURE

A complete solution to the problem of acoustic transmission through a rough surface requires that the probability distribution of the received signal be known as well as the average field and power. In Chapter Seven of his monograph, Beckmann derives the probability distribution of the sum of arbitrary coplanar random vectors. He then links up this distribution with the mean field and power scattered by a rough surface. This approach provides a general solution, not restricted to mean values, but giving the entire distribution about these mean values. The results of Beckmann's analysis can be applied to the signal transmitted through a rough surface and the same conclusions can be made about both cases.

A qualitative summary of the characteristics of this distribution can be given easily. For the case of low roughness, $R < 1$, the signal observed in Snell's direction will have a near Gaussian distribution of amplitudes. This result reflects the addition of a large coherent component to a small incoherent component. As the roughness increases the amplitude distribution in Snell's direction, $K_{xy} = 0$, approaches Rayleigh, indicating the absence of the coherent component. In the case where the signal is observed from a direction away from Snell's direction

and, therefore, away from the predominant smooth surface field, the incoherent component dominates and the distribution will be near Rayleigh for any roughness.

III. THE MODEL EXPERIMENT

The theory developed in the previous section has been tested in a model experiment that has been scaled to be representative of the conditions at sea for the lower audio frequencies. The significant ratios σ/λ_2 and L/λ_2 (root-mean-square wave height/acoustic wavelength and wave correlation distance/acoustic wavelength) take on values in the model that are comparable to those at sea for the range of acoustic frequencies of particular interest. A result of this scaling has been the choice of L/λ_2 ratios that do not satisfy the requirements of the Kirchhoff approximation. This, of course, should be the objective of a model experiment; to study cases that may be beyond the capability of theorists, but of great practical importance.

A. DESIGN OF THE MODEL — SCALING CONSIDERATIONS

In order to design the particular configuration to be used in the model experiment some compromises were made between what was considered ideal and what was physically realizable with the equipment and facilities available. The fundamental requirement was to achieve the desired σ/λ_2 and L/λ_2 ratios. After that it was attempted to satisfy as nearly as possible the assumptions made in deriving the theoretical results. The basic configuration of the experiment consisted of a source of airborne acoustic waves located above an anechoic tank and transmitting through an aperture so as to create a limited ensonified area on the water surface. A model sea surface was generated by directing a wind stream over the surface of the anechoic tank. The transmitted acoustic signal was received by a hydrophone located far enough from the ensonified area to be considered in the far field.

The Underwater Acoustics Laboratory at the Naval Postgraduate School is equipped with an anechoic tank configured for generating a model sea surface. The development of this facility has taken place over a number of years and the model sea surfaces produced have proven to be quite similar to a well-developed sea of gravity waves. It was decided to scale the acoustic frequency to obtain the desired ratios of σ/λ_2 and L/λ_2 rather than attempt to modify the proven Sea Exciter, (SEX MOD. 2). The model sea surfaces available range from an rms wave height of about 0.1 cm to 0.5 cm. The correlation lengths obtained are scaled to those of ocean waves in approximately the same ratio as the rms wave heights, provided seas with swell (low-frequency gravity waves propagated from long distances) are not considered. In order to choose the range of acoustic frequencies to be used the σ/λ_2 ratio was chosen as the criterion and the Pierson-Moskowitz [4] Ocean Wave Spectrum was integrated to get representative rms wave heights for various wind speeds. At 12 knots, the rms wave height at sea should be about 19 cm.; using this figure for σ and a low frequency limit on the order of 100 Hz (λ_2 = 1500. cm) a σ/λ_2 ratio of at least as small as 19/1500 should be achieved in the model. Frequencies at least as high as 100kHz are of interest at sea and for the same sea the ratio σ/λ_2 = 19/150 . Since a model sea with rms wave height of .19 cm can be achieved, it can be seen that the scale factor should be about 100 and the acoustic frequencies used in the model should range from about 10 kHz to 100 kHz.

B. THE ACOUSTIC ARRANGEMENT

1. The Anechoic Tank

The model experiment was carried out in an anechoic tank 24 feet long, 6 feet wide and 8 feet deep. The tank was designed to be anechoic

at frequencies above 20 kHz by use of a lining of sound absorbent aluminum-loaded rubber. Since it was desired to use frequencies as low as 10 kHz, it became apparent that the anechoic qualities of the tank would have to be studied and improved. An experiment to evaluate the qualities of the anechoic treatment was performed to determine how good (or bad) it was at frequencies below 20 kHz. This experiment involved transmitting tone burst with an electrostatic transducer at normal incidence to the tank bottom. An Atlantic Research LC-32 hydrophone located between the transmitter and the bottom was used to determine the ratio of the bottom reflected pulse to the outgoing pulse. Then, maintaining the same relative geometry but inverting the transducers, the transmitted signal was directed upward past the hydrophone and the ratio of the reflected pulse from the smooth, free surface to the outgoing pulse was determined. From these data an estimate of the normal incidence reflection loss for the tank bottom was computed and the results are given in Table 2.

A second experiment was conducted to study the reverberant field in the tank. A continuous wave, 10 kHz tone was transmitted by a loudspeaker above the tank with the surface acoustically masked except for a 25 cm square area. The incident, nearly plane, acoustic wave on the smooth water surface was at normal incidence and the field in the water was probed vertically beneath the ensonified area with an LC-32 hydrophone. This yielded a plot that showed a spherically spreading field with a small but not insignificant standing wave that became larger close to the tank bottom. Figure 2 shows this plot.

A study by Lastinger [5] indicates that water-saturated wood can be an effective absorber of low frequency (3-8 kHz) sound. In particular,

TABLE 2

Tabulation of normal incidence reflection coefficient for the aluminum-loaded rubber anechoic lining installed on the tank bottom.

Note: p_r reflected pressure amplitude

p_i incident pressure amplitude

FREQ (kHz) =	10	12	14	16	18	20
$20 \log \frac{p_r}{p_i}$ =	-5	-10	-13	-16	-19	-20

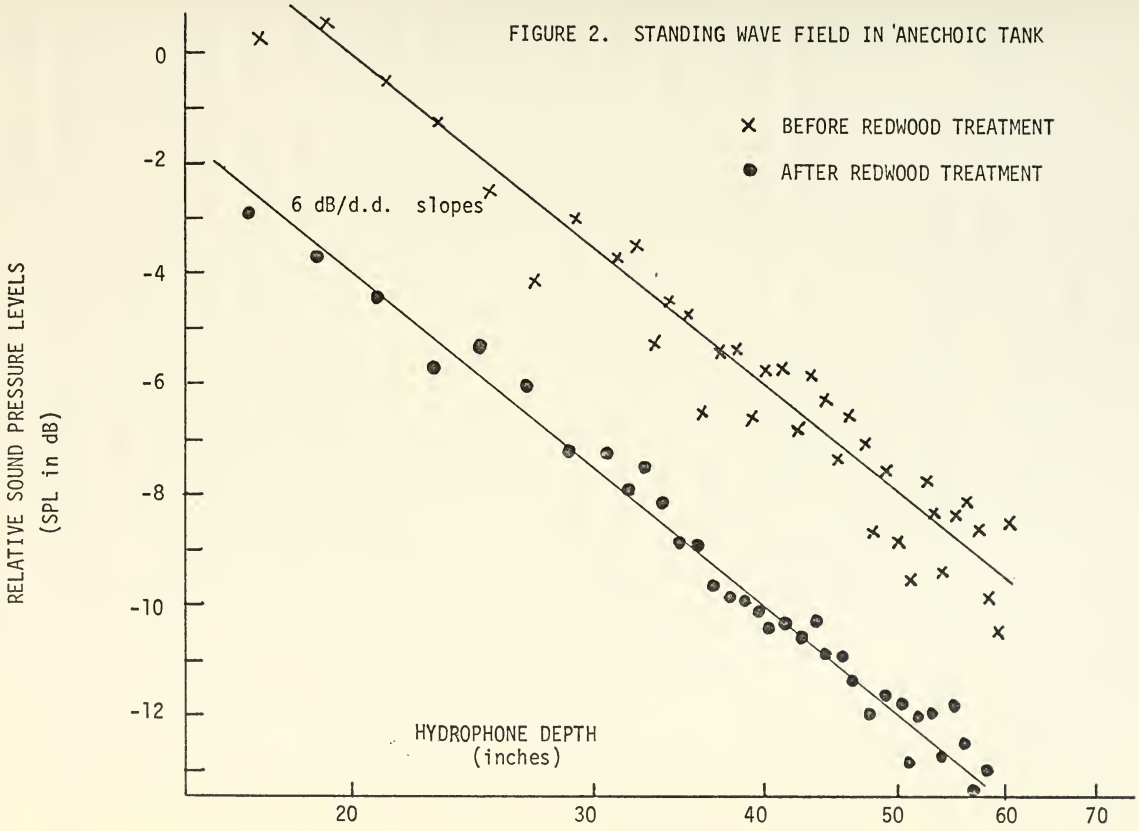
FIGURE 2. STANDING WAVE FIELD IN ANECHOIC TANK
BEFORE REDWOOD TREATMENT
AFTER REDWOOD TREATMENT
6 dB/d.d. slopes
RELATIVE SOUND PRESSURE LEVELS
(SPL in dB)
0
-2
-4
-6
-8
-10
-12
HYDROPHONE DEPTH
(inches)
20
30
40
50
60
70

he reports that redwood can provide an attenuation approaching 35 dB/meter at 8 kHz for sound propagated at 45° to the grain. For sound propagated at 0° to the grain the acoustic characteristics are said to be similar to those obtained for 45° orientation. Perpendicular propagation provided the least absorption.

Since the model experiment would result in sound directed primarily at the tank bottom, it was felt that additional treatment of the bottom was necessary and that a layer of redwood between the concrete bottom and the absorbent rubber lining would be useful. Redwood boards 8 by 4 by 1 inch were cut and wet by first being placed under water in a large, sealed, metal container that was then evacuated to a nominal vacuum of 29 inches of Hg for approximately 72 hours. These boards were then wired together in blocks 8 by 8 by 4 inches and placed under water in the four foot deep runways between the two anechoic tanks in the Acoustics Lab. When enough saturated redwood blocks had been fabricated to cover approximately 12 feet of the tank bottom, the tanks were drained and the redwood installed with the grain oriented vertically. This provided a 4 inch deep layer of redwood on 12 feet by 6 feet of the bottom beneath the area that would be ensonified during the model experiment. Based on Lastinger's study this should have provided additional attenuation of 7 dB. The absorbent rubber lining was placed on top of the redwood blocks, which reduced the depth of the tank to approximately 190 cm. After the redwood was in place a reverberation experiment identical to that described above was conducted and a noticeable improvement was evident. Figure 2 is a plot comparing the field in the anechoic tank before and after the installation of redwood.

The acoustic data in the model experiment was taken approximately two months after the redwood was in place and at that time an additional

test was made to evaluate the significance of the backscattered signal from the tank bottom. An electrostatic transducer with an active area approximately equal to that of the ensonified area used in the model experiment was located just below the surface in the same position as the ensonified area. The receiving hydrophone was positioned as it had been during the experiment. The arrangement approximated the conditions that were present during the experiment but permitted the utilization of a source in a pulsed mode in order to observe the magnitude of the backscattered signal relative to outgoing signal. Measurements were taken for 0°, 30° and 60° incidence with the bottom and the outgoing pulse amplitude received at the on-axis hydrophone was compared to the backscattered pulse amplitudes. Table 3 is a summary of the results of this test. The results for 10 kHz and the normal incidence can be compared with the first evaluation of the loss at the bottom outlined above and an estimate of the attenuation of the redwood can be made.

The 20 dB difference between outgoing and backscattered pulses can be attributed to spreading losses, losses introduced by the metal-loaded rubber and losses introduced by the redwood. Since the hydrophone was located about 90 cm below the source and 100 cm above the concrete tank bottom, the difference due to spreading can be estimated to be about 10 dB. The loss introduced by the rubber anechoic lining, when rigidly backed, has been evaluated as 5 dB. If these figures are used, then it appears that the redwood treatment has resulted in a 5 dB improvement at 10 kHz. A similar analysis for 20 kHz indicates that the addition of redwood has apparently reduced the effectiveness of the anechoic treatment by 7 dB. A possible explanation may be that the rubber absorbant material is less effective when not rigidly backed. Although it is difficult to

TABLE 3

Tabulation of backscattered amplitudes relative to outgoing amplitudes received by hydrophone at one meter and θ_2 degrees from center of ensonified area. Redwood layer has been installed on tank bottom with anechoic lining on the redwood. The first backscattered return was from the bottom — the second was predominantly from the water surface.

FREQUENCY (kHz)	θ_2	FIRST RETURN	SECOND RETURN
10.0	0	0.10	0.07
13.5	0	0.10	0.06
17.5	0	0.09	0.02
20.0	0	0.07	0.02
24.0	0	0.06	0.02
30.0	0	0.05	0.03
40.0	0	0.04	0.02
10.0	30	0.10	0.10
13.5	30	0.06	0.04
17.5	30	0.06	0.03
20.0	30	0.04	0.01
24.0	30	0.03	0.01
30.0	30	0.01	0.01
40.0	30	0.01	0.01
10.0	60	0.09	0.09
13.5	60	0.04	0.03
17.5	60	0.02	0.01
20.0	60	0.01	0.01
24.0	60	0.01	0.01
30.0	60	0.01	0.01
40.0	60	0.01	0.01

estimate the nature of the reverberant field that existed during the rough surface transmission experiments, a conservative evaluation of this problem would seem to indicate that the data, particularly the mean square acoustic pressure data, should be subject to close examination. A more detailed discussion of this problem will be given in a later section.

2. The Ensonified Area

The theory is expressed in terms of a limited area that has a uniform acoustic field over dimensions 2X by 2Y and zero acoustic field outside these boundaries. In addition the incident wave is required to be plane and the area ensonified must be larger than the acoustic wavelength in water. The assumption that the receiver is in the far field necessarily limits the size of the ensonified area, while the description of the rough surface requires a Gaussian distribution of heights and an isotropic surface that has a Gaussian spatial correlation function. Other than the desire to test the theory for a realistic sea surface that is anisotropic and does not have the prescribed spatial correlation, it was felt that the experimental ensonified area should be a reasonable approximation to the idealized description of the theory and yet flexible enough in design to permit the investigation of some of the theoretical limitations.

A number of ideas for implementing this critical component of the experiment were tried out and rejected. A parabolic reflector 20 inches in diameter with an acoustic feedhorn at the focus failed to produce a satisfactory field primarily because the horn required to give sufficient directivity was so large as to severely disturb the reflected wave. This approach was later successful when a reflector from a portable microwave relay station was obtained and used in conjunction with the basic arrangement. The result of this combination will be discussed later.

Another source for generating a limited ensonified area was an 8 foot long fiberglass-lined plywood frame enclosure with the Altec 740A driver and catenoidal horn mounted at one end and directed through the tube of fiberglass absorbing material designed to shape the desired field. An arrangement in the anechoic chamber that tracked a microphone across the mouth of the enclosure permitted the measurement of the amplitude and relative phase of the resultant field. The performance of this enclosure was improved by flaring the lower end so as to form a sort of fiberglass horn 20 by 20 inches at one end and 48 by 48 inches at the other. The bottom end had a wire grid supporting more fiberglass absorbing material to form an aperture that could be adjusted to any desired size. The enclosure was installed above the center of the anechoic tank supported by 9/16 inch diameter steel rods pivoting from two steel angle A-frames along either side of the tank. Although this system seemed reasonably workable, it was decided to go to a similar arrangement that provided more positive masking of the surface outside the desired region of ensonification.

a. The Basic Arrangement

The basic arrangement finally settled on consisted of a 56 by 56 inch masking pad placed over the anechoic tank with an aperture in the center that was 50 cm square but fitted with an insert that could reduce it to 25 cm square. The pad was constructed of three inches of fiberglass absorbing material on either side of a 1/4 inch plywood center. The underneath side of the pad was covered with a protective sheet of 1 mil mylar. The fiberglass sound absorbing material was tested in the anechoic chamber and found to introduce a transmission loss of about 7 dB per inch for the 10-20 kHz frequency range and no detectable

reflective properties. The total transmission loss of the pad including the plywood septum was approximately 65 dB.

The masking pad was installed 6 inches above the water level in the tank so as to permit the sea generating wind stream to pass under it. Ten feet above the pad was the Altec driver and horn mounted on a three foot long fiberglass-lined enclosure that was pivoted from the A-frame supports described previously. The height of the mouth of the catenoidal horn was approximately 305 cm above the water level. A light plywood frame strung with a three inch square grid of fine wire that supported fiberglass absorbing material was positioned over the tank just beneath the source enclosure and formed the roof of a fiberglass enclosure that was fitted over the masking pad.

The A-frames and therefore the acoustic source could be positioned along the length of the tank to allow various angles of incidence from the source to the ensonified area. The aperture insert could be oriented perpendicular to the indident field for angles within about 20 degrees of the vertical.

An LC-32 hydrophone, mounted on a traverse, was swept across the ensonified area to measure a cross-section of the amplitude and relative phase of the incident field. The traverse could be positioned to sweep the hydrophone just below the water surface ($\sim$1 cm) and either along the longitudinal axis or across the anechoic tank. A potentiometer linked to the drive of the traverse was used to supply position information to the x-axis of a Varian F-100 X-Y Plotter. The y-axis was supplied with a signal from either a Hewlett Packard (Mod. 7035) Logarithmic Converter or an Acton Laboratories Phase Meter (Mod. AB) in order to plot

either the amplitude or relative phase distribution across the ensonified area. Figure 3 is a sketch of the basic acoustic arrangement.

The properties of the field produced on the surface were investigated with the arrangement described above. In general, it was found that the ensonified area for all the frequencies used was characterized by a central area of nearly uniform sound level that abruptly decreased with a slope of about 2 1/2 dB per centimeter as the probe was moved beyond the limits of the aperture. The dimensions of the ensonified area, taken at the 3 dB points was approximately 24 cm by 24 cm. The Acton Laboratories Phase Meter compared the phase of the driving voltage to the source with that of the hydrophone and provided a d.c. voltage proportional to the relative phase that was plotted on the x-y recorder as the hydrophone was traversed across the ensonified area. The results showed wavefront curvatures that were consistent with a spherically diverging wave from a source at a distance on the order of three meters.

A calculation of the expected wavefront curvatures can be made using the formula for the sagitta of an arc:

$$(2R - x)\, x = d^2$$

where R is the radius of curvature, $2d$ is chord of the arc and x is the sagitta of the arc. Using $R = 300$ and $d = 12$, the sagitta turns out to be .24 cm. If the curvature of the incident wavefront is expressed in terms of the fraction of a wavelength phase difference between the center of the ensonified area and the edge, assuming normal incidence, then the ratio of the sagitta of the arc and the acoustic wavelength should give this fraction. For an incident 10 kHz wave,

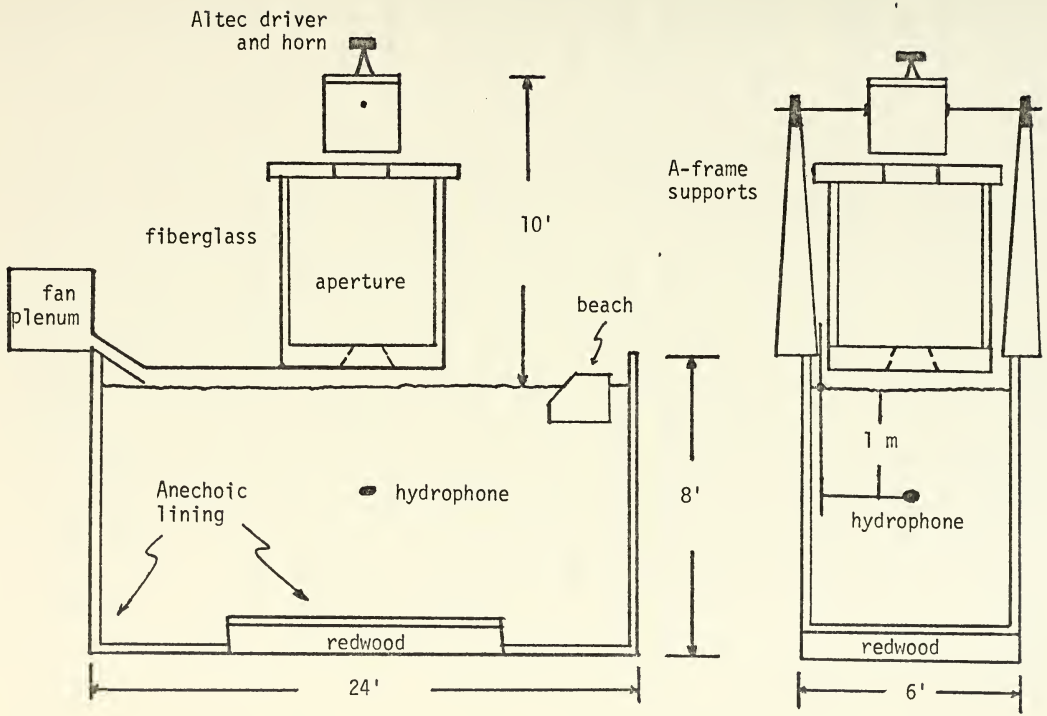

FIGURE 3. THE BASIC ARRANGEMENT (not to scale)

therefore, the expected value of wavefront curvature is about $.07\ \lambda_1$. This value compares to the $0.1\ \lambda_1$ value obtained in the experiment and plotted in Figure 4. The highest frequency used with this source and configuration was 24.3 kHz. The wavefront curvature obtained at this frequency was approximately $.17\ \lambda_1$. A criterion for permitting the plane wave approximation that has been given by Medwin and Clay [6] is a-maximum curvature of $\lambda/8$. In this experiment this has been exceeded somewhat and an opportunity has been provided to test the criterion.

An indicator of how closely the experimental ensonified area approximated the theoretical description is given by a comparison of the smooth surface radiated field measured in the experiment with that predicted by the theory. Since for a smooth surface the theoretical predictions reduce to a relatively straight-forward expression for the radiation pattern of a piston with a particular linear phase shading, there should be reasonably good agreement at least for the main features. The plots in Figures 5-8 are representative of those obtained with the basic acoustic arrangement. Each plot compares the theoretical and experimental directivity patterns of the ensonified area for a given frequency (10.0 kHz or 24.3 kHz) and angle of incidence, θ_1, (0°, 6°, 12° or 16°). The angles are those used in the rough surface study and were selected to be below and above the critical angle, θ_c, for infinite plane waves incident on a plane surface (about 13°). The incident angles were measured by the geometry of the arrangement and are estimated to be accurate to within one degree. Since angular position of the main lobe is very sensitive to small changes of incident angle, some of the theoretical patterns have been rotated as much as 5° to obtain the best fit.

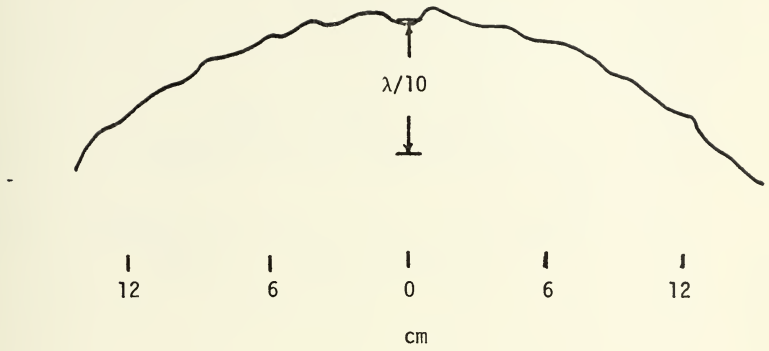

FIGURE 4. PHASE AND AMPLITUDE CROSS-SECTION AT ENSONIFIED AREA

SOURCE: Altec driver and horn at 10.0 kHz

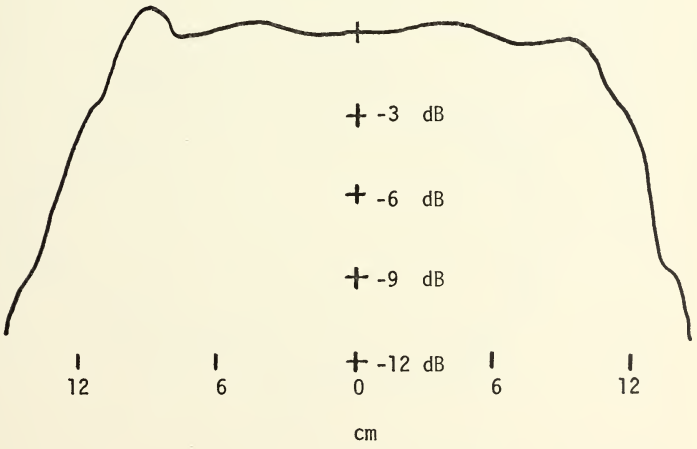

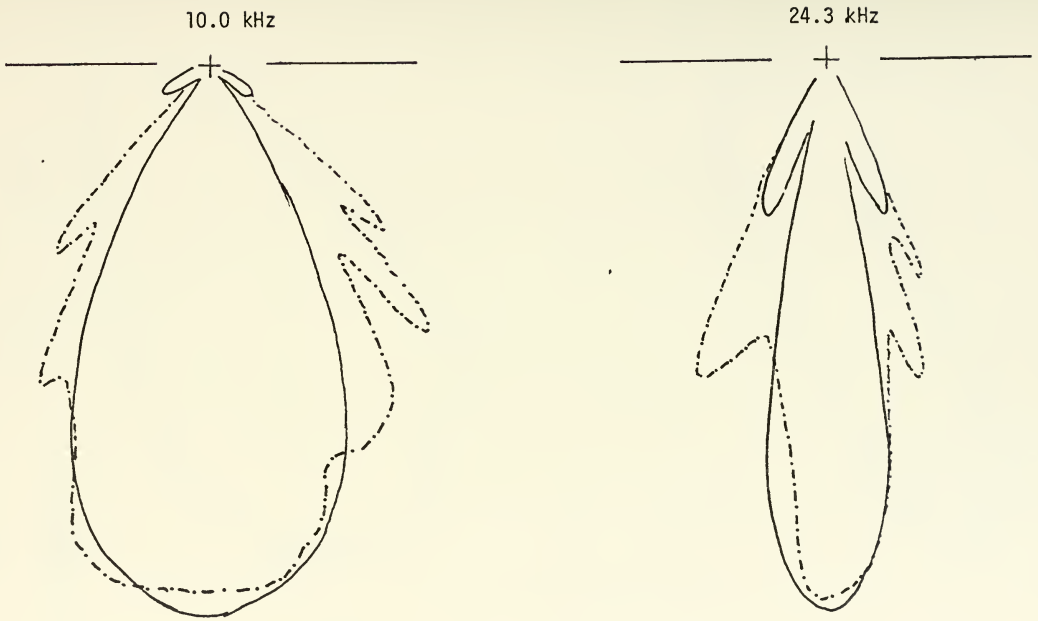

FIGURE 5. DIRECTIVITY PATTERNS MEASURED AT 1 METER FROM ENSONIFIED AREA (24 x 24 cm)

$\theta_1 = 0°$

——— THEORY -·-·-· EXPERIMENT

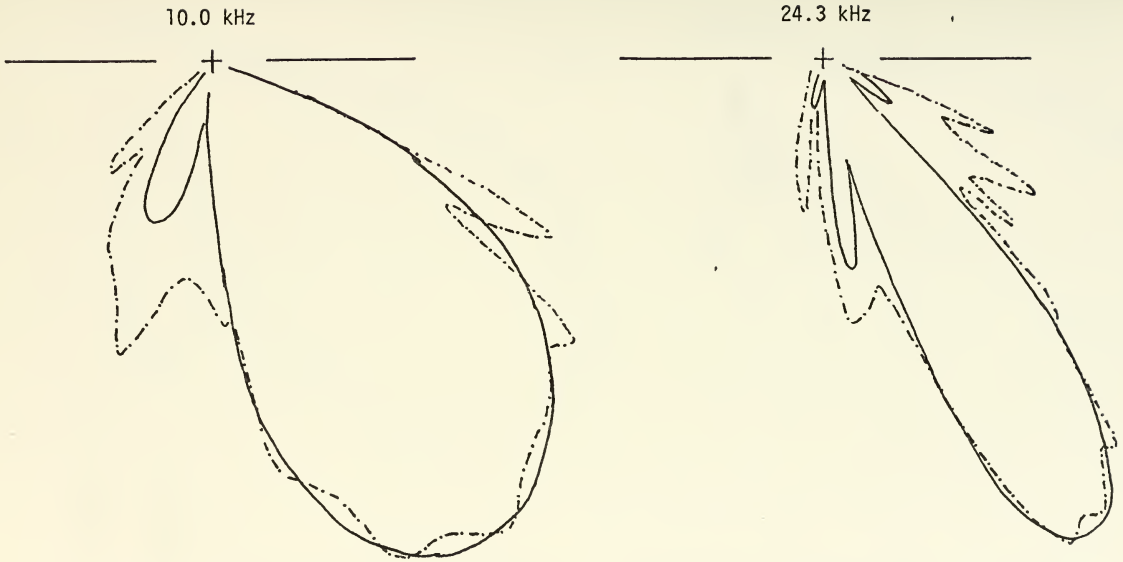

FIGURE 6. DIRECTIVITY PATTERNS MEASURED AT 1 METER FROM ENSONIFIED AREA (24 x 24 cm)

$\theta_1 = 6°$

——— THEORY —·—·— EXPERIMENT

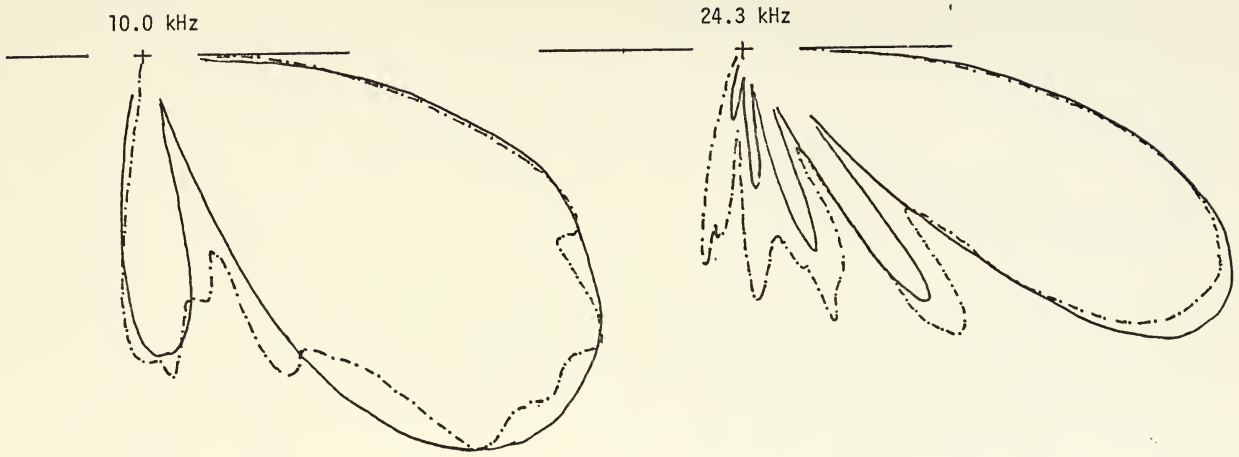

FIGURE 7. DIRECTIVITY PATTERNS MEASURED AT 1 METER FROM ENSONIFIED AREA (24 x 24 cm)

$\theta_1 = 12°$

——— THEORY —·—·— EXPERIMENT

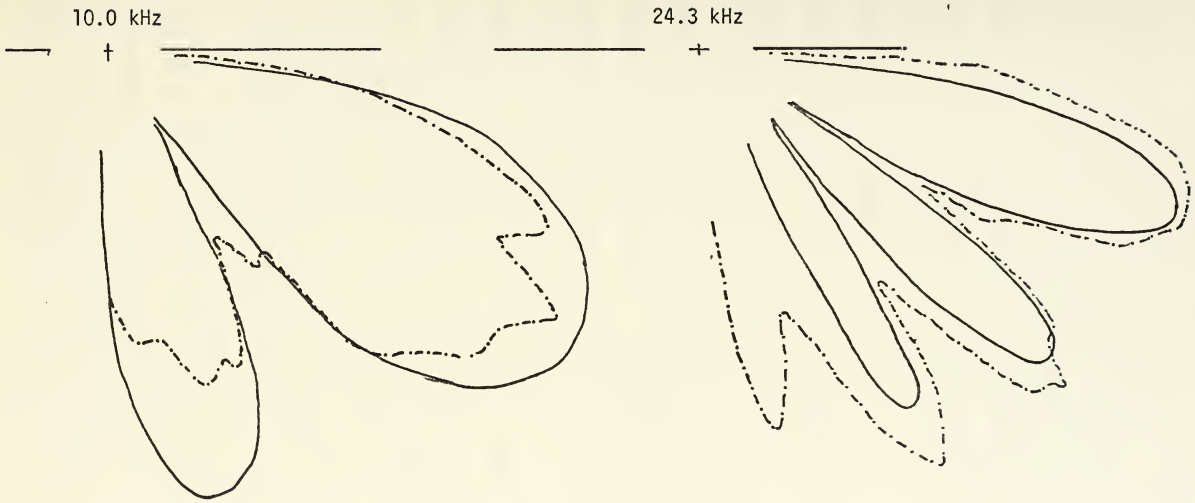

FIGURE 8. DIRECTIVITY PATTERNS MEASURED AT 1 METER FROM ENSONIFIED AREA (24 x 24 cm)
$\theta_1 = 16°$

——— THEORY -·-·-·- EXPERIMENT

b. The Parabolic Reflector

In an effort to extend the frequency range of the experiment it became necessary to use a new acoustic source. Two requirements were placed on the new source; it had to be able to transmit sufficient sound pressure levels at the higher frequencies and it should have produced a nearly plane wave incident on the ensonified area. A parabolic section reflector from a AN/TRC-27 Portable Microwave Relay Set was obtained which, in conjunction with a Western Electric 640AA condenser microphone used as a transmitter, produced a most satisfactory incident wave and permitted the extension of the experiment to 43 kHz. The microwave horn was removed from its mount at the focal point of the reflector and the 640AA transmitter was installed. The reflector was positioned approximately 1.8 meters above the water surface and directly over the aperture in the masking pad. Provisions for making fine adjustments of the reflector unit were built into the reflector. Adjustment of the reflector until a maximum signal was obtained on the receiving hydrophone located at $\theta_2 = 0°$ was easily accomplished. The surface hydrophone was traversed across the ensonified area and an amplitude and phase cross-section was obtained. The amplitude distributions were essentially the same as had been obtained with the original source but the phase distributions showed no discernable curvature even at 37 kHz. See Figure 9 for the plots obtained at 37 kHz.

The source level of the W.E. 640AA transmitter was on the order of 0 dB re 1 μbar at 30 cm when polarized at 180 volts and driven with 30 vrms. The signal levels obtained at the hydrophone were considerably lower than those experienced with the Altec 740A source. Since the signal levels were about 20-25 dB below those obtained previously,

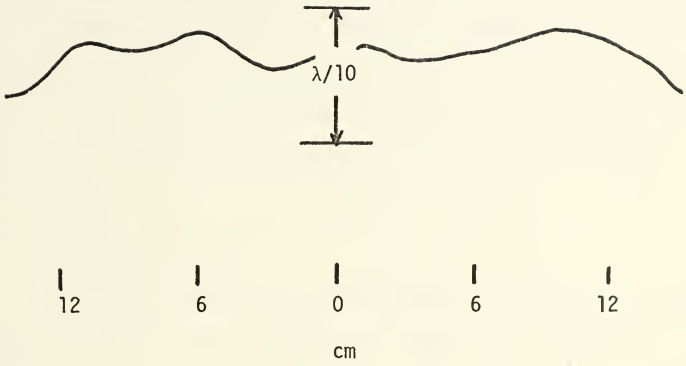

FIGURE 9. PHASE AND AMPLITUDE CROSS-SECTION OF "PLANE WAVE" AT ENSONIFIED AREA

SOURCE: Parabolic Reflector and W.E. 640AA at 37.0 kHz

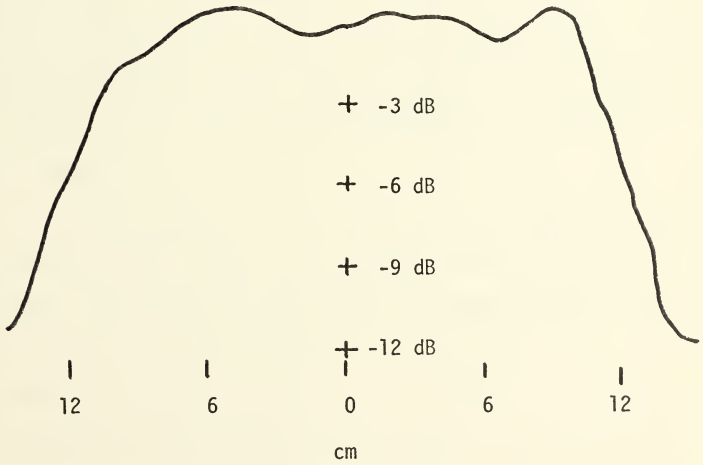

the noise in the receiving electronics precluded computation of the relative mean square pressure until the narrower filter of a wave analyzer was inserted to improve the signal-to-noise ratio. This uncorrelated additive noise was not a problem in computing the relative mean acoustic pressure but the low signal levels did cause difficulties because of a small, pervasive, correlated electrical feedthrough from the transmitting electronics that became a factor when the acoustic level decreased.

c. The Point Source

In a supplementary experiment the transmission of a nearly omnidirectional point source through the rough air-sea interface without an unlimited ensonified area was studied. The source used was the Western Electric 640AA condenser transmitter, which has an active element diameter of 1.7 cm. Reference [7] discusses the characteristics of this microphone used as a transmitter. The field of the transmitter is piston-like and for the frequencies used would be a reasonable approximation to an omnidirectional point source out to angles greater than the critical angle defined by Snell's Law. Figures 10 and 11 show the free field patterns of the transmitter used obtained at 10 and 20 kHz in the anechoic chamber.

In this experiment the masking pad was removed and the microphone was positioned 1 meter above the water surface and over the center of the tank. An enclosure of fiberglass absorbing material was constructed over the tank with the sides extending down to within about 3 cm of the water surface and the top supported by a fram with a fine wire grid just above the height of the transmitting microphone. This left about 16

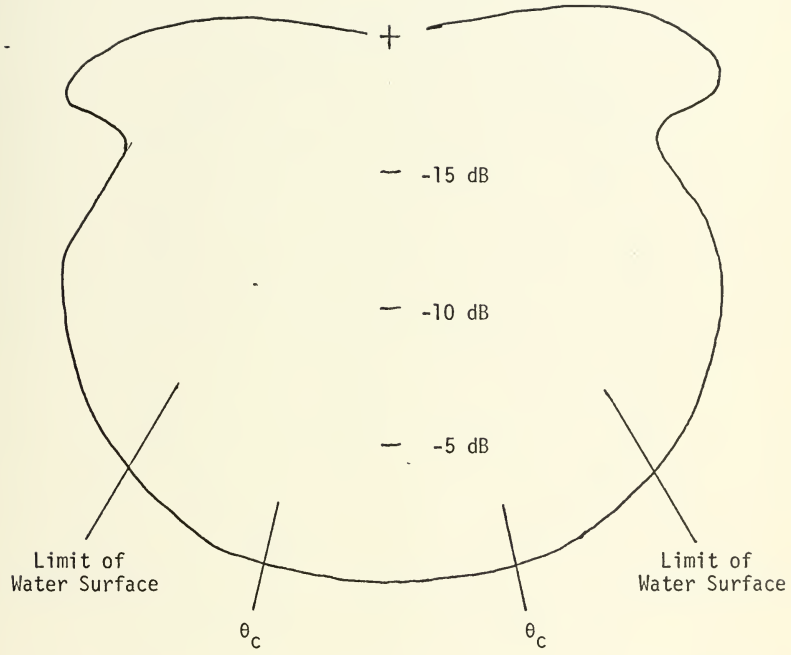

FIGURE 10. FREE FIELD DIRECTIVITY PATTERN AT 1 METER FROM W.E. 640AA TRANSMITTER AT 10.0 kHz

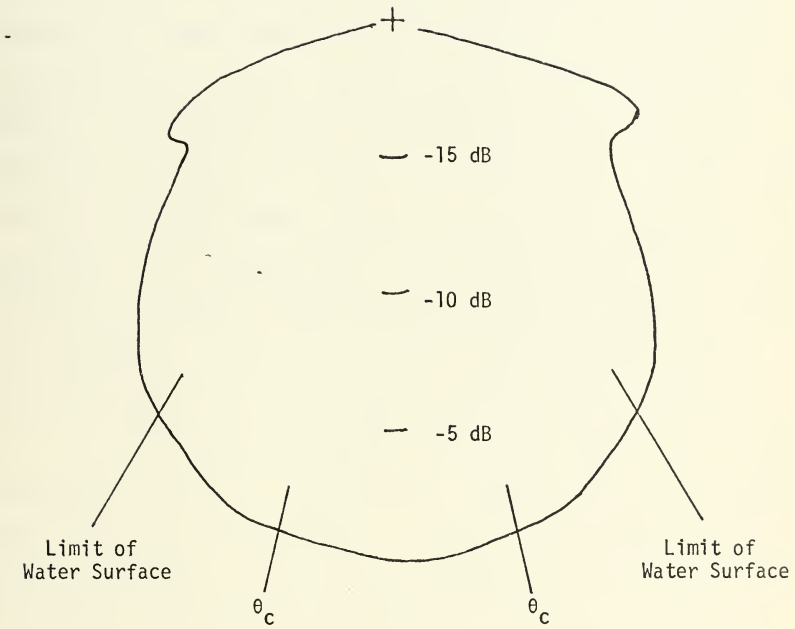

FIGURE 11. FREE FIELD DIRECTIVITY PATTERN AT 1 METER
FROM W.E. 640AA TRANSMITTER AT 20.0 kHz

square feet of water surface exposed to the nearly omnidirectional source and reduced the contributions of secondary scattering to the field over the ensonified area.

3. The Receiver and Associated Electronics

An Atlantic Research LC-32 hydrophone with active element dimensions of 3/4 by 1/4 inches was used as the reciever. The hydrophone was mounted on a L-shaped support that pivoted at the water surface and positioned the hydrophone in the plane passing through the source, the center of the ensonified area, and the central axis of the tank. A potentiometer pickoff at the pivot point supplied a d.c. voltage proportional to the angle between the center of the ensonified area and the hydrophone. This arrangement was used to swing the hydrophone through a 180° arc to obtain the smooth surface polar plots and also to position the hydrophone at a given angle for measuring the relative average transmitted acoustic field and intensity for the rough surface.

An NUS low noise preamplifier (Model #2110) amplified the hydrophone signal by 30 dB. Since the sound pressure levels in the experiment were low (on the order of 20 dB re 1 μbar) and the hydrophone sensitivity was about -110 dB re 1 volt/μbar, an additional 60 dB of amplification by a Hewlett-Packard 465A Precision Amplifier was required to bring the signal level to the one volt range. An SKL variable electronic filter was used to bandpass filter the signal with an effective bandwidth of about 1 kHz. A variation on the above filtering technique was the use of a Hewlett-Packard 3590A wave analyzer with a bandwidth of 100 Hz. This was used to obtain the mean square accoustic pressures when the Western Electric 640AA transmitter was used. The filtered output was supplied

to one input of the PAR Model 101 Correlation Function Computer which was used to process all of the acoustic data.

The requirement that the receiver be in the far field was estimated by applying the far field criterion for a piston source; i.e., the far field was taken to be at a range greater than $2a^2/\lambda_2$ from the source with half width "a". For the highest frequency used, 43 kHz, $2a^2/\lambda_2$ is approximately 84 cm. Accordingly the hydrophone range was chosen to be at 1 meter; a position in the far field and also not too close to the more reverberant field near the bottom of the anechoic tank.

C. THE MODEL SEA SURFACE

The north anechoic tank in the Underwater Acoustics Laboratory is equipped to generate a wind-driven model sea surface. The wind generator is located at the east end of the tank and consists of five separately controllable centrifugal fans feeding a common plenum that discharges a uniform wind stream across the width of the tank. The output of the wind generator is confined to the water surface by plexiglass covers suspended six inches above the water level. The sea surface is effectively terminated at the west end of the tank by a sloping beach made of redwood chips packed loosely in a plastic insect screen

The author assisted Dr. W. M. Wright in a study of two different sea surfaces that were later to be used in this model experiment. The wave probe system used was of a design similar to that used by Mayo [8] and had been fabricated and tested by Dr. Wright. The two surfaces, one a "high sea" and the other a "low sea", were studied in some detail and spatial correlation functions, directional surface wave spectra, and wave height probabilities, as well as the mean square wave heights, were

obtained for a location centered at the ensonified area. Later in the experiment, when it became desirable to generate other sea surfaces with particular characteristics, the author used the same wave probe system to make a limited study of these supplementary seas.

1. The Wave Probe System

Reference [9] gives a detailed discussion of the design, construction, and testing of the wave probes and associated electronics. The probes were based on the expectation that the conductance between two, long conducting cylinders is proportional to the depth of immersion of the cylinders. The circuit incorporating the wave probe was designed to detect the water level by measurement of the conductance between the probe electrodes. Figure 11 shows the complete circuit for wave probe "A". The probe is driven by an oscillator with low source resistance and the current is measured by means of the 10 ohm resistor. A passive filter removes any contribution at the carrier frequency of wave probe "B" from the amplitude-modulated signal. This signal is amplified, detected and filtered to produce the wave record which is again amplified before processing by the PAR Correlator. The "AC Input" of the correlator was used, which provided a lower cutoff frequency of about 0.2 Hz. Data recorded on the PI-6200 FM tape recorder was passed through a 50 μF blocking capacitor into the 50 kΩ input impedance of the tape recorder.

When it was desired to make calibrated measurements with the wave probe, a procedure was followed that provided a calibration of the entire wave probe system including the correlator. This was necessary since it was apparent that the sensitivity of the probe was not stable over a long term; possibly due to a changing conductivity in the water in the anechoic tank.

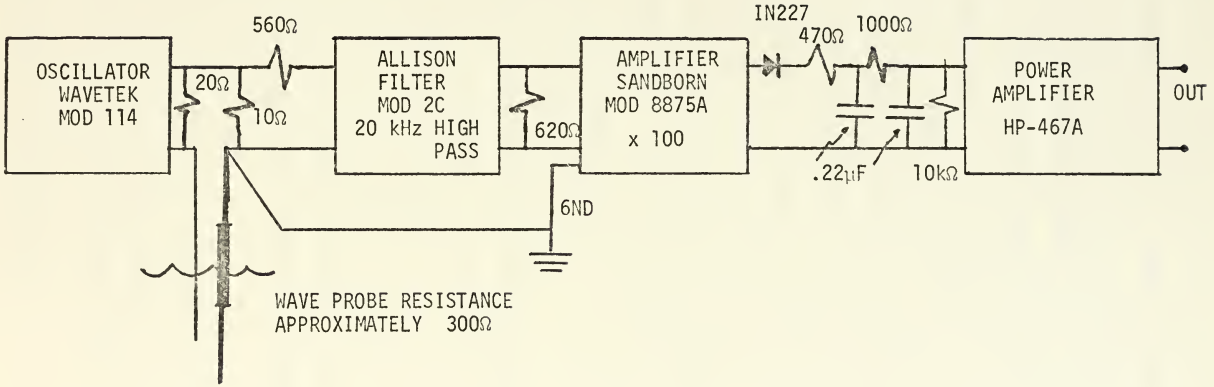

FIGURE 11. CIRCUIT FOR WAVE PROBE A

The calibration procedure consisted of oscillating the probe vertically in the anechoic tank with a motor driven apparatus. A sinusoidal variation of immersion with time was obtained, with a frequency of 2.72 Hz and a peak-to-peak amplitude of 2 cm. The signal generated by this method was applied to the correlator and the autocorrelation at $\tau = 0$, the mean square voltage, was computed. The resulting system calibration was given by $.707 \text{ cm}/[C(0)]^{1/2}$ volt and averaged about .55 cm/volt. The d.c. level of the wave record was noted and the correct immersion depth was obtained after calibration by adjusting the depth to produce the same d.c. voltage. Calibration for the data to be processed by the digital computer was accomplished by recording a ten minute record of the calibration signal at the beginning of the tape containing the wave records. Again, the same d.c. level observed during the calibration run was maintained during the recording of the wave record by adjusting the wave probe depth.

2. Statistical Considerations in Processing the Wave Record

Since the rms wave height is a fundamental quantity in describing the "roughness" of the air-sea interface in terms of the theory, the measurement of this quantity was considered fundamental to the study of the sea surface. Studies in the past had indicated that the mean square wave height of the model seas exhibited temporal fluctuations that appeared to be statistical in nature [8].

Bendat and Piersol [10] give a discussion of the statistical errors to be encountered in parameter estimates. For the variance of the estimate for the mean square of a zero mean process they find:

$$\text{Var}\,[\hat{\sigma}_x^2] \simeq \frac{2}{T} \int_{-\infty}^{\infty} C_x^2(\tau)\, d\tau$$

for large T, where $|\tau| \ll T$. It can be seen that $\hat{\sigma}_x^2$ is a consistent estimate of σ_x^2 since $\mathrm{Var}[\hat{\sigma}_x^2]$ will approach zero as T approaches infinity assuming $C_x^2(\tau)$ is absolutely integrable over $(-\infty,\infty)$.

If the wave record is for simplicity taken to be band limited white noise with a bandwidth, B, and length, T. Then it can be shown that the above becomes

$$\mathrm{Var}[\hat{\sigma}_x^2] \simeq \frac{R_x^2(0)}{BT} \simeq \frac{\sigma_x^4}{BT}$$

or

$$\varepsilon^2 = \frac{\mathrm{Var}[\hat{\sigma}_x^2]}{\sigma_x^4} \simeq \frac{1}{BT}$$

The square root of this last expression gives the normalized standard error, ε.

For the case of an RC integrator as used in the PAR Correlator, the averaging time T used above can be given by the formula:

$$T = \frac{2RC\left[1 - e^{-T_r/RC}\right]^2}{\left[1 - e^{-2T_r/RC}\right]}$$

where T_r is the length of the record available. Since there was no reason the record could not be as long as desired, the effective averaging time in the correlator could be considered to be 2RC or 40 seconds. If the effective bandwidth of the wave record is taken to be about 3 Hz, then the normalized standard error can be computed to be, $\varepsilon = .09$, which would account for the ±20% fluctuations in the mean square wave height reported by Mayo and, in fact, observed in this experiment as well.

In order to reduce the error in the estimate of the mean square wave height it was necessary to increase the averaging time. This was accomplished by plotting a 500 second record of the mean square wave height as computed by the PAR Correlator and visually averaging this record. It was found that this technique consistently produced repeatable results. A quantitative check on the stationarity of the random sea surface generated was performed by processing a wave record in a digital computer. In this analysis a 20 minute wave record for each sea studied was recorded on the PI-6200 FM tape recorder in analog form. This sample was converted to digital information by the A to D conversion capability of the CI5000-XDS9300 hybrid computer facility and processed digitally to obtain mean square values for two ten-minute blocks and the entire 20-minute block. The values obtained for the ten-minute blocks were within 1% of that obtained for the twenty-minute block and the computed mean square wave heights agreed with those obtained through the use of the correlator in the manner outlined above.

3. Description of the Sea Surfaces Generated

For the basic experiment the two sea surfaces studied were characterized as a "low" sea and a "high" sea. The root-mean-square wave heights at the center of the tank, where the ensonified area was to be located, were determined to be 0.17 cm and 0.41 cm for the two seas. Using the scale factor of 100 and assuming a Gaussian wave height distribution, ocean waves with a peak-to-peak height ($\pm 3\sigma$) of about 3.5 feet and 8 feet such as would be expected in a fully developed sea generated by 12 and 18 knot winds, were simulated by the two model seas. These seas were designated A and B respectively and were used as the rough surfaces for most of the acoustic measurements. Three supplementary

seas were generated during the course of the acoustic data collection in an attempt to study an apparent effect introduced by varying the correlation length of the sea surface. These seas were designated C, D, and E. A summary of the basic parameters of the five seas used is found in Table 4.

a. Mean Square Wave Height

The mean square wave height was obtained for all seas used. As noted above, a particular technique was required to obtain satisfactory values for the mean square wave height using the PAR Correlator with its limited 20 second time constant. The study of seas A and B was accomplished approximately two months prior to the time the bulk of the acoustic data were taken; however, mean square wave heights for these seas were measured again with the acoustic arrangement in place over the anechoic tank and found to be unchanged.

An investigation of the fetch-limited variation of the wind-driven seas was made by measuring the mean square wave heights at positions along the center line of the tank but 30 cm upwind and 30 cm downwind of tank center. For both seas the mean square wave height was smaller by about 5% in the upwind direction and larger by the same amount in the downwind direction. For the 25 cm dimensions of the ensonified area using the mean square value obtained at the center of the area as an average value for the entire area seems to be a valid approximation.

Assignment of an interval of high confidence for the measured mean square wave heights is possible if it assumed there was no consistent error introduced by the calibration technique. The normalized standard error, ε , for a single 500 second average of the correlator-computed mean square value is about .025. Using a conservative criterion that

TABLE 4

SEA SURFACE CHARACTERISTICS

SEA	σ(cm)	L_u (cm)	L_c (cm)	How Generated
A	0.173	2.1	5.2	Three back fans
B	0.410	3.5	11.0	All five fans
C	0.170	3.2	-	Four fans - with deflector
D	0.320	4.2	-	Five fans - with deflector
E	0.050	0.8	-	One fan

Definitions:

σ is the root-mean-square wave height

L_u is the smallest separation for a correlation of e^{-1} (upwind-downwind)

L_c is the largest separation for a correlation of e^{-1} (crosswind)

assumes the correct value must lie within $\pm 3\varepsilon$ of the estimate, a figure of ±7.5% is arrived at for the accuracy of the mean square wave heights. During the study of the two basic sea surfaces many calibrations and subsequent mean square computations were performed using both the correlator and the digital computer. Essentially all those runs were well within 7.5% of the mean. It is felt that the point of the above exercise is simply to demonstrate the outer limits of the error that might be introduced by these wave height measurements.

b. Wave Height Probability Distributions

The theory assumes that the probability distribution of wave heights of a randomly rough sea will be Gaussian. This assumption is a reasonable one since the wave height distributions that have been observed at sea are nearly Gaussian. Because ocean waves are characterized by sharp peaks and long smooth troughs, the distributions observed are usually skewed with larger positive values possible but low negative values more likely. This departure from the ideal Gaussian distribution is usually characterized by higher order moments defining the "Skewness" and "Kurtosis". Wave height distributions were obtained for seas A and B and a detailed discussion of this phase of the sea surface study is given in Appendix A along with plots of the resultant distributions. The distributions are nearly Gaussian and show the characteristic skewed shape.

c. Spatial Correlation and the Directional Spectrum

A more complete description of a sea surface than simply stating the mean square wave height is given by specifying also the two-dimensional spatial correlation function or its Fourier Transform, the

normalized directional wave spectrum. The details concerning the determination of this description are given in Appendix A. In the theory it is assumed that the sea is isotropic and has a Gaussian correlation function. Figures A3-A10 in Appendix A show that the model seas were close to the real ocean, that is, decidedly anisotropic.

The parameter that is defined in the theory as the correlation length, L, is not obviously defined for this type of surface. Since an important theoretical criterion concerning the shape of the surface deals with the requirement of the Kirchhoff approximation for the minimum radius of curvature to be much greater than the acoustic wavelength, a characteristic length is taken to be that distance at which the two-dimensional spatial correlation first falls to e^{-1}. This length has been designated the experimental correlation length, L_u, and it turns out that it is always located along the wind line.

A correlation length is presented in Table 4 for all seas. However, for seas C, D, E a complete spatial correlation was not taken and only enough of the upwind-downwind spatial correlation was measured to determine the separation required for the normalized cross-correlation to reach 0.368. Although the primary reason for introducing these three supplementary seas was to observe the effect that modifying the surface "shape" had on sound transmission, a time limitation precluded a more complete study of the characteristics of these surfaces.

Seas C and D were both produced by deflecting the wind up off the water surface at a distance of approximately 60 inches upwind of the ensonified area. This eliminated much of the high frequency energy of the surface wave. The resulting seas were somewhat similar to ocean swell that is generated in one area and propagates into another. Sea surface C

was adjusted to have the same mean square wave height as A, but greater correlation length, by adjusting the location of the deflector, by varying the height of the deflector so that some wind could continue along the surface, and also by selecting an appropriate combination of fans to be operated. This technique produced a 50% longer correlation length than was found with sea A and although the two surfaces had the same mean square wave height, sea C appeared considerably smoother. Sea surface D was the result of an attempt to generate the largest possible correlation length and at the same time a moderate mean square wave height somewhere between those of seas A and B. This was accomplished by relocating the ensonified area 60 inches downwind of the tank center to allow increased fetch for sea build-up and by adjustment of the wind deflector.

Sea E was generated to produce a small correlation length. Only the center fan was operated and the resultant sea observed at tank center was small but not so small as to be in the capillary wave regime (defined to be where the wave length is less than 1.73 cm).

D. PROCESSING THE RECEIVED ACOUSTIC PRESSURE

All processing of acoustic data was done with a PAR Model 101 Correlation Function Computer. This instrument is a special purpose hybrid computer that computes 100 points of the correlation function of two input voltages. The correlator converts one input channel to a sampled digital signal and introduces 100 discrete delays. The undelayed input channel is multiplied with the output of each of the 100 delay steps and each product is averaged in an RC integrator with a 20 second time constant. The result is an estimate of the cross-correlation of the

two input signals computed for 100 values of τ , the delay time. The output of the correlator was displayed on an oscilloscope when all 100 points were to be observed. If the autocorrelation at $\tau = 0$ was desired, the output for this single point was displayed on an X-Y recorder with a time base input to the x-axis.

The acoustic data are presented in terms of relative quantities referenced to the smooth surface value. This procedure is convenient and it yields a result that can be directly compared to theory. A simple modification of Equations (15) and (29) is all that is necessary to express those results in terms of relative quantities.

1. The Relative Mean Acoustic Pressure Squared (Relative Coherent Intensity)

Since $[p_{20} F \operatorname{sinc} K_x x \operatorname{sinc} K_y y]$ is the received acoustic pressure for the smooth surface for a given geometry, the ratio of the mean received acoustic pressure for the roughened surface to the smooth surface pressure can be written:

$$\langle \rho \rangle = \frac{\langle p_2 \rangle}{p_{20} F D} = e^{-R/2} \tag{32}$$

where D is the directivity of the ensonified area, $\operatorname{sinc} K_x x \operatorname{sinc} K_y y$, and $\langle \rho \rangle$ is defined as the relative mean acoustic pressure at the receiver. The quantity that is of more direct interest is the coherent component of the acoustic intensity which is simply the square of (32) and may be written:

$$\langle \rho \rangle \langle \rho \rangle^* = \frac{|\langle p_2 \rangle|^2}{p_{20}^2 F^2 D^2} = e^{-R} \tag{33}$$

2. The Relative Mean Square Acoustic Pressure (Relative Total Intensity)

A similar definition can be made for the total relative acoustic intensity.

$$\langle \rho\rho^* \rangle = e^{-R} + \frac{\pi L^2}{AD^2} e^{-R} \sum_{n=1}^{\infty} \frac{R^n}{nn!} e^{-K_{xy}^2 L^2/4n} \qquad (34)$$

These definitions put the theoretical predictions in a form easily compared to experiment and also limit considerations to the effects of the rough surface only.

3. Data Collection Procedure

The correlator was used in a different mode for each of the two quantities measured. The procedures used were simple but required a good deal of time to perform. The time requirement was a result of taking sample averages of the correlator output to obtain each data point. The variations of correlated acoustic signal were generally less than those encountered in the measurement of the mean square wave height because the received sound scatters from many points of the surface. Nevertheless it was apparent that the 20 second integration time of the correlator was too short to obtain a good average for the acoustic signal without additional averaging as described below.

a. Obtaining the Relative Mean Acoustic Pressure Squared

A cross-correlation technique was used to isolate the coherent component of the acoustic signal from the incoherent component. Since the driving voltage for the source could be used to supply a reference signal proportional to the transmitted acoustic pressure and the amplified and band-pass filtered signal from the hydrophone was proportional to the

received acoustic pressure, a reference value for the smooth surface could be obtained by cross-correlating those two signals. The result of this cross-correlation was proportional to the smooth surface received acoustic pressure. The computation performed by the correlator yielded 100 sample points of the following integral.

$$\hat{C}_o(\tau) = \frac{1}{20} \int_0^{20\,\text{sec}} p_{20}\, F\, D \cos \omega(t-\tau) \cos \omega(t-t') \; dt$$

where $\hat{C}_o(\tau)$ is an unbiased estimate of the cross-correlation function and the integral including the uncorrelated additive noise has been set equal to zero. Smooth surface cross-correlation yielded:

$$C_o(\tau) = \frac{p_{20}\, F\, D}{2} \cos [\omega\tau - \phi]$$

This function was displayed on the oscilloscope and the peak-to-peak value was adjusted to be full scale (10 cm) on the scope. Then without changing the driving voltage to the source the surface was roughened and the resultant correlation function was observed. It was noted that the phase of the correlation function did not change but that the amplitude was reduced when the surface was roughened. In most cases the gain settings of the correlator made for the smooth surface were optimum for the rough surface case as well and no further adjustments of the correlator or oscilloscope were necessary while the rough surface value was being computed. In a few cases the correlator gain was changed and the ratio of the two gains was multiplied times the computed rough surface correlation before the relative value was determined. For the rough surface case the amplitude of the correlation function computed was

proportional to the mean acoustic pressure received at the hydrophone.

$$C(\tau) = \frac{|\langle p_2 \rangle|}{2} \cos(\omega\tau - \phi) \tag{35}$$

After 60 seconds of initial integration, the peak-to-peak value of this function was read 10 times with the readings taken approximately 20 seconds apart. The average value of these readings was recorded as a "run". The reading was recorded as a fraction of the full scale reading and represents the relative mean acoustic pressure. To see this it is noted that the smooth surface correlation function was set to equal full scale and therefore the peak-to-peak value of the rough surface correlation function is equivalent to the ratio:

$$\frac{|\langle p_2 \rangle|}{p_{20\ F\ D}} = |\langle \rho \rangle| \tag{36}$$

At least two and usually three runs were made and averaged to obtain each data point. The final value was squared to yield the relative mean acoustic pressure squared.

A procedure was followed to ensure that undesirable electrical feed-through of the driving voltage into the receiving electronics was not introducing error. The correlator gains and oscilloscope settings were adjusted to get optimum correlator performance and full scale reading for the smooth surface condition. Then without making further adjustments the aperture was blocked so that no sound could reach the hydrophone. The cross-correlation function was observed. In most cases the correlation function dropped to zero; however, in the parts of the experiment where the low source level Western Electric 640AA condenser

transmitter was used, there was a small amount of coherent electrical noise detected that was not eliminated from the system. In no case did this exceed .03 times the smooth surface correlation amplitude.

b. Obtaining the Relative Mean Square Acoustic Pressure

A similar procedure was used to compute the relative mean square acoustic pressure. In this case, however, an auto-correlation was performed with the input from the receiving hydrophone going to both correlator channels. Since the mean square value of a signal is defined to be the auto-covariance evaluated at $\tau = 0$, the output of the correlator for this point was displayed on a Varian F-100 X-Y Recorder. This computation does not eliminate the uncorrelated additive noise introduced by the hydrophone and the receiving electronics. The input can be expressed as $e(t) = p_2(t) + n(t)$ and auto-covariance evaluated at $\tau = 0$ yields,

$$R(0) = R_2(0) + R_n(0) \tag{37}$$

where $R_2(0)$ is the mean square acoustic pressure received and $R_n(0)$ is the noise power. For the smooth surface condition,

$$R_{20}(0) = p_{20}^2 F^2 D^2 \tag{38}$$

In the experiment, the value for the smooth surface mean square acoustic pressure was computed first and plotted against time on the X-Y plotter. The surface was roughened and the correlator output was recorded for approximately 200 seconds after it had undergone the initial decay from the smooth surface to rough surface value (approximately 60 seconds). The average value during the "run" was determined visually and divided by the smooth surface result.

$$\frac{R(0)}{R_0(0)} = \frac{R_2(0) + R_n(0)}{R_{20}(0) + R_n(0)} \tag{39}$$

In most cases in the acoustic experiment the ratio $\frac{R_n(0)}{R_{20}(0)}$ was less than .01 and the noise terms did not contribute significantly to the relative mean square values obtained. However, in some cases, which will be pointed out later, tank reverberation became a source of possible error which could not be ignored. If the noise terms are neglected then the expression for relative mean square acoustic pressure by the procedure outlined above may be written as

$$\langle \rho\rho^* \rangle = \frac{\langle p_2 p_2^* \rangle}{p_{20}^2 F^2 D^2} \quad . \tag{40}$$

IV. PRESENTATION AND ANALYSIS OF THE EXPERIMENTAL DATA

A. THE BASIC ACOUSTIC EXPERIMENT

The greatest part of the acoustic data was obtained using the basic acoustic arrangement and the two well-studied seas, A and B. The source was operated in four positions, either directly above or at angles upwind of the aperture, in order to study transmission for angles of incidence varying from normal to somewhat greater than the "critical angle" for plane waves. The receiver was at an angle either in the Snell direction or near grazing; these two cases were believed to be of particular interest. Five frequencies were used, ranging from 10.0 kHz to 24.3 kHz. In terms of the theoretical roughness parameter, a range of roughness from $R = .06$ to $R = 2.8$ was observed. Study of higher roughness was precluded by the limited frequency range of the source used. For each source-receiver position, (θ_1, θ_2), both relative mean coherent intensity and total intensity (coherent plus incoherent) were computed with the correlator for each sea and all available frequencies. The resultant data have been plotted against the roughness parameter, R, and are presented in Figures 12-17. Figures 18-22 use the same data plotted against R but each graph shows the relative mean acoustic pressure squared (coherent intensity) results for a particular frequency.

1. The Relative Mean Coherent Intensity

Theory predicts that the coherent component of the received acoustic intensity will decrease exponentially with increasing R . $[R = k_2^2\sigma^2(c_2/c_1 \cos\theta_1 - \cos\theta_2)^2]$. The results of the basic experiment have been graphed against R in a semilog plot; the theoretical e^{-R} dependence is shown on each graph. The first observation that can be

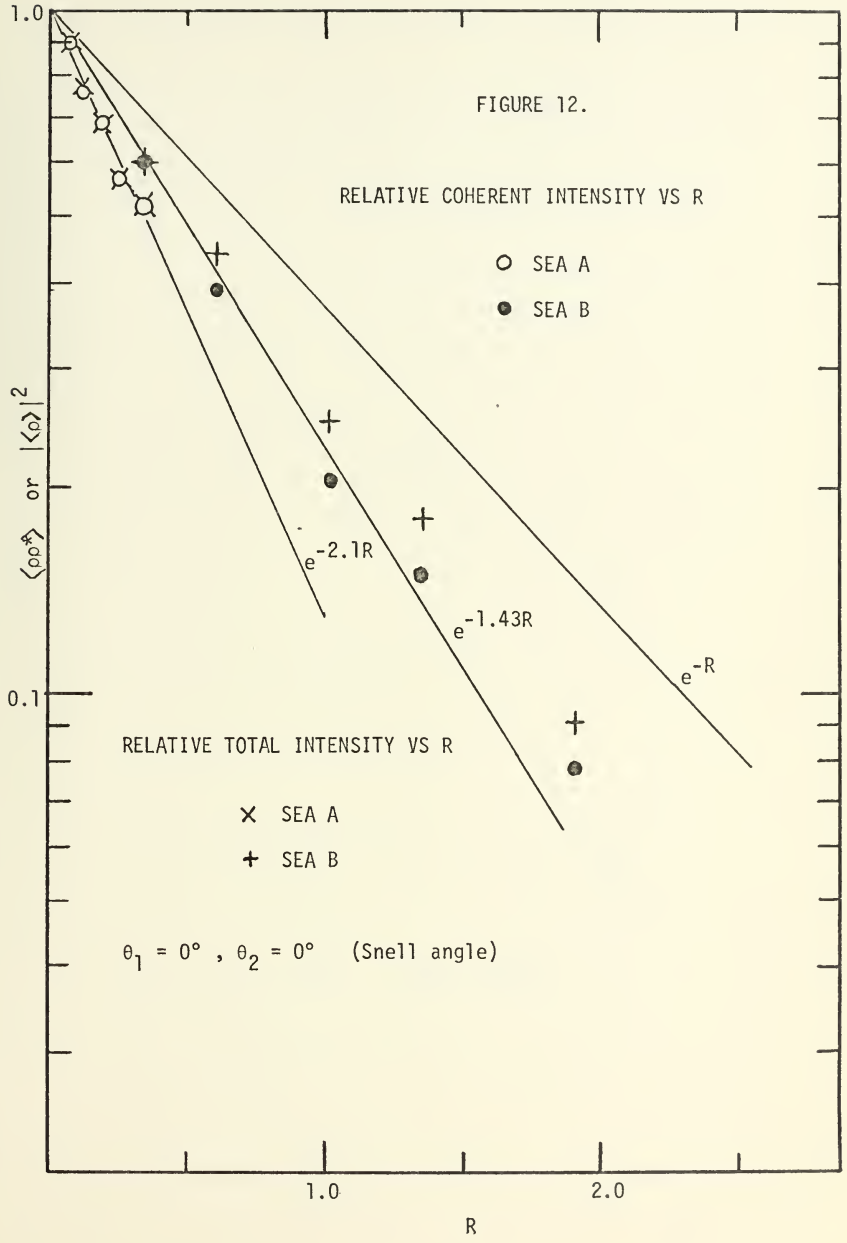
1.0
0.1
$\langle \rho\rho^* \rangle$ or $|\langle \rho \rangle|^2$
FIGURE 12.
RELATIVE COHERENT INTENSITY VS R
SEA A
SEA B
$e^{-2.1R}$
$e^{-1.43R}$
e^{-R}
RELATIVE TOTAL INTENSITY VS R
SEA A
SEA B
$\theta_1 = 0°$, $\theta_2 = 0°$ (Snell angle)
1.0
2.0
R

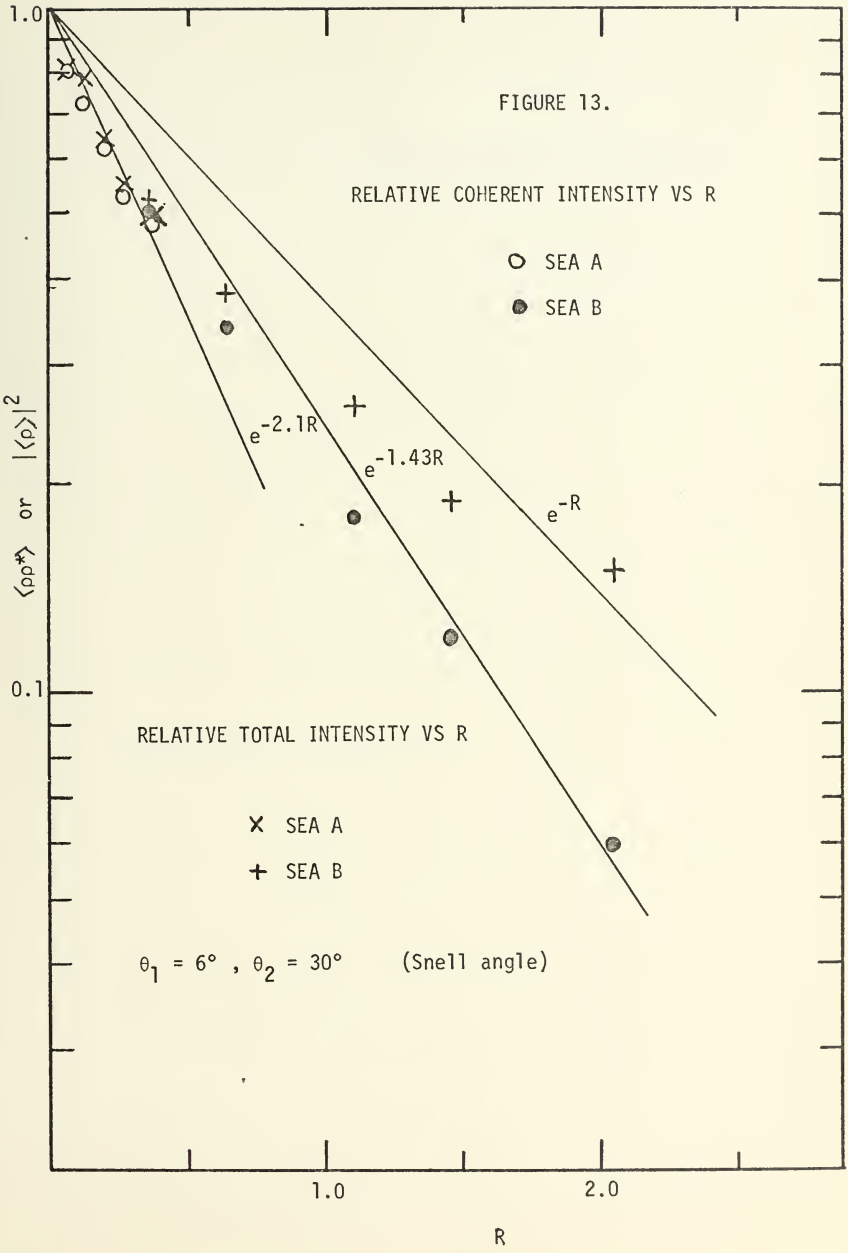
1.0
0.1
1.0
2.0
R
$\langle \rho\rho^* \rangle$ or $|\langle \rho \rangle|^2$
FIGURE 13.
RELATIVE COHERENT INTENSITY VS R
SEA A
SEA B
$e^{-2.1R}$
$e^{-1.43R}$
e^{-R}
RELATIVE TOTAL INTENSITY VS R
SEA A
SEA B
$\theta_1 = 6°$, $\theta_2 = 30°$ (Snell angle)

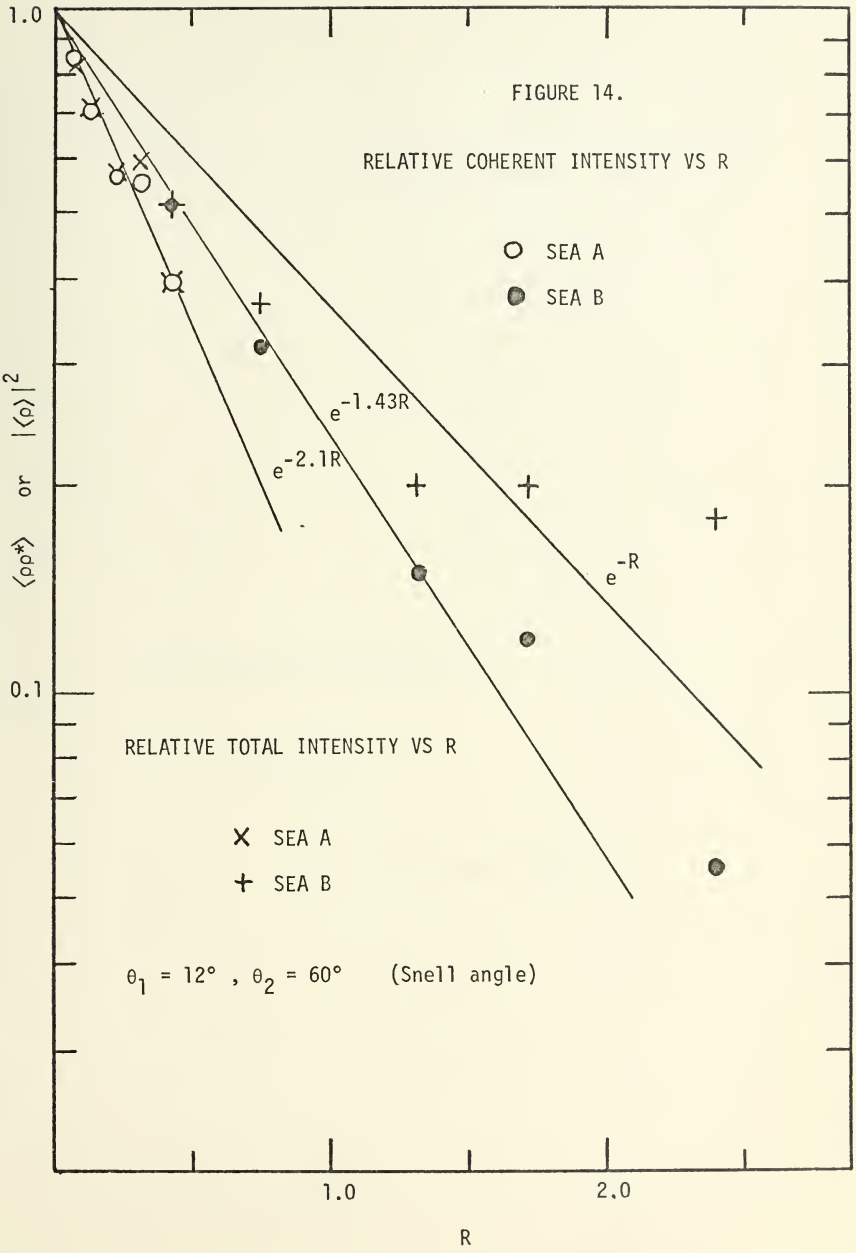
1.0
0.1
$\langle \rho\rho^* \rangle$ or $|\langle \rho \rangle|^2$
FIGURE 14.
RELATIVE COHERENT INTENSITY VS R
SEA A
SEA B
$e^{-1.43R}$
$e^{-2.1R}$
e^{-R}
RELATIVE TOTAL INTENSITY VS R
SEA A
SEA B
$\theta_1 = 12°$, $\theta_2 = 60°$ (Snell angle)
1.0
2.0
R

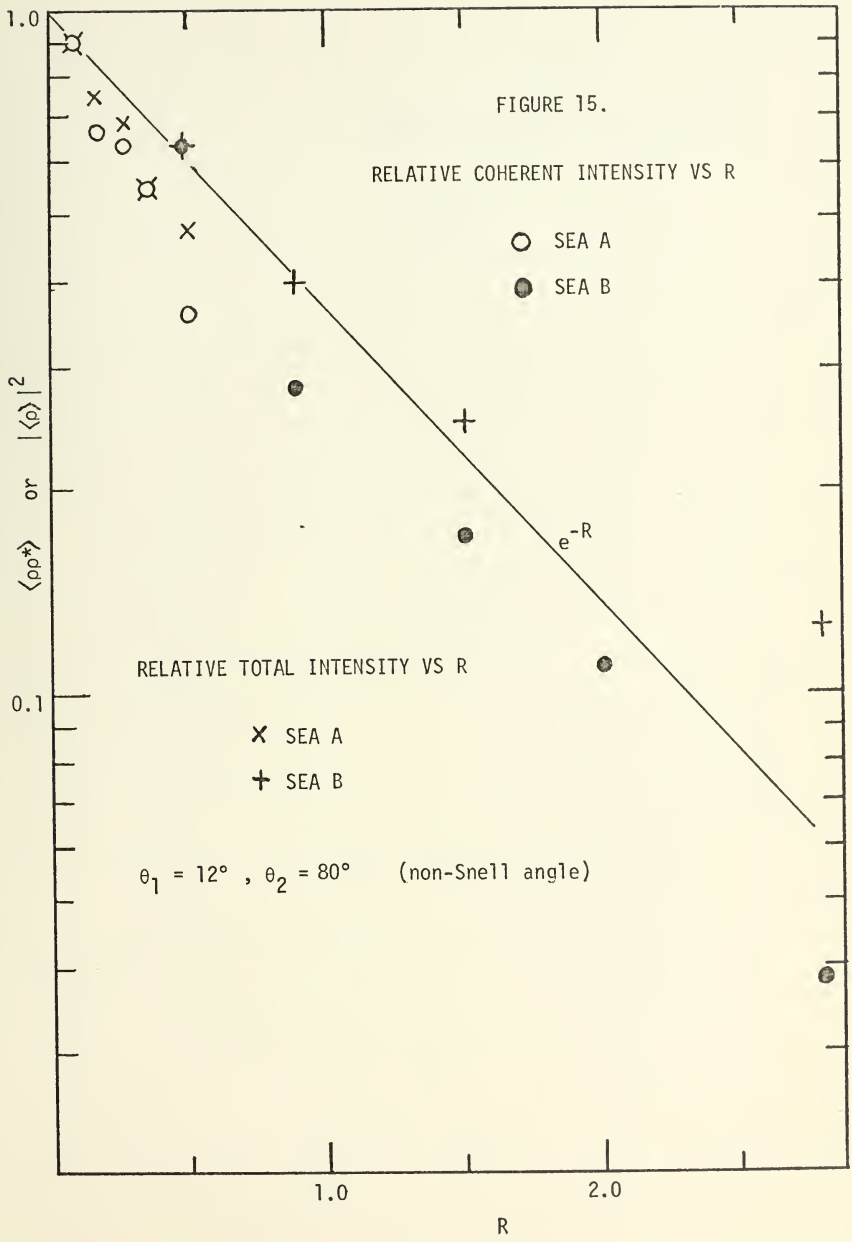
1.0
0.1
$\langle \rho\rho^* \rangle$ or $|\langle \rho \rangle|^2$
FIGURE 15.
RELATIVE COHERENT INTENSITY VS R
SEA A
SEA B
e^{-R}
RELATIVE TOTAL INTENSITY VS R
SEA A
SEA B
$\theta_1 = 12°$, $\theta_2 = 80°$ (non-Snell angle)
1.0
2.0
R

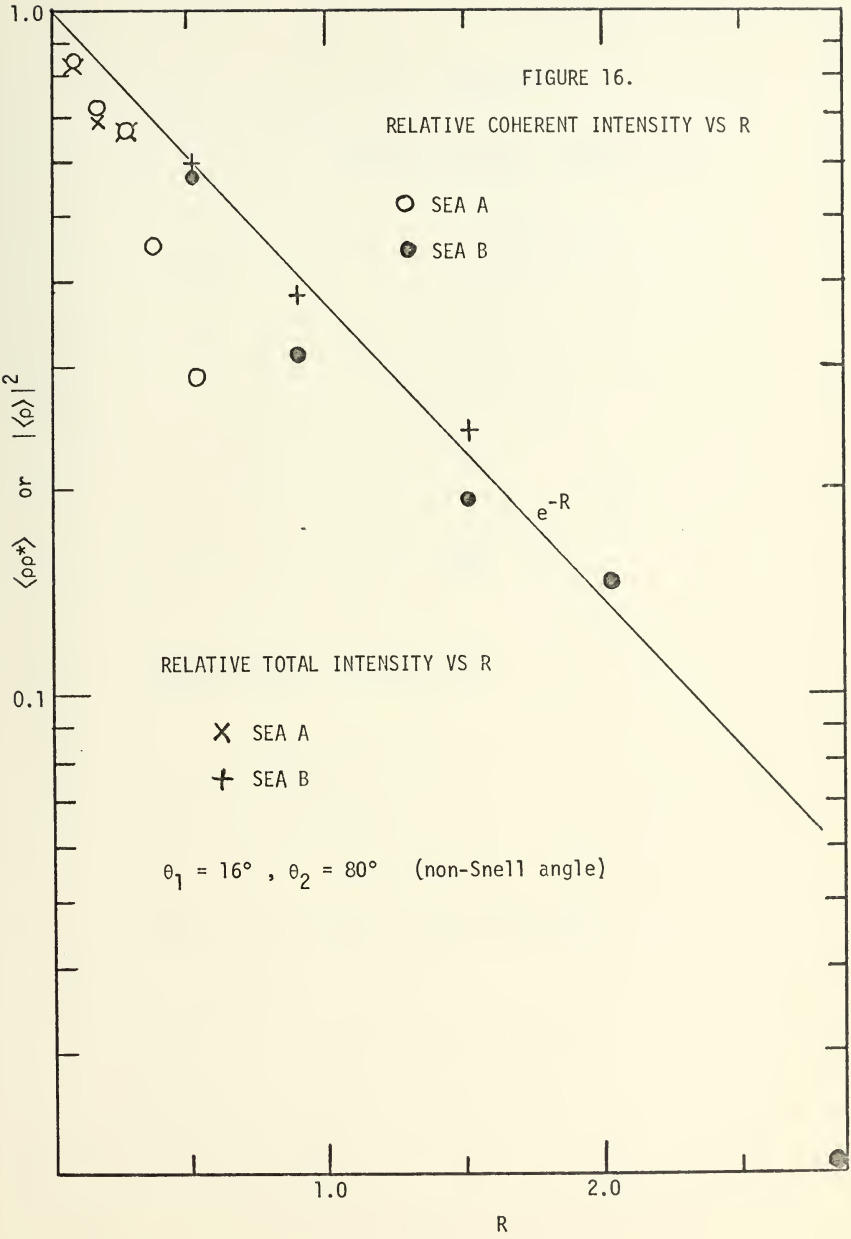
FIGURE 16.
RELATIVE COHERENT INTENSITY VS R
SEA A
SEA B
e-R
RELATIVE TOTAL INTENSITY VS R
SEA A
SEA B
θ1 = 16° , θ2 = 80° (non-Snell angle)
1.0
0.1
1.0
2.0
R
⟨ρρ*⟩ or |⟨ρ⟩|2

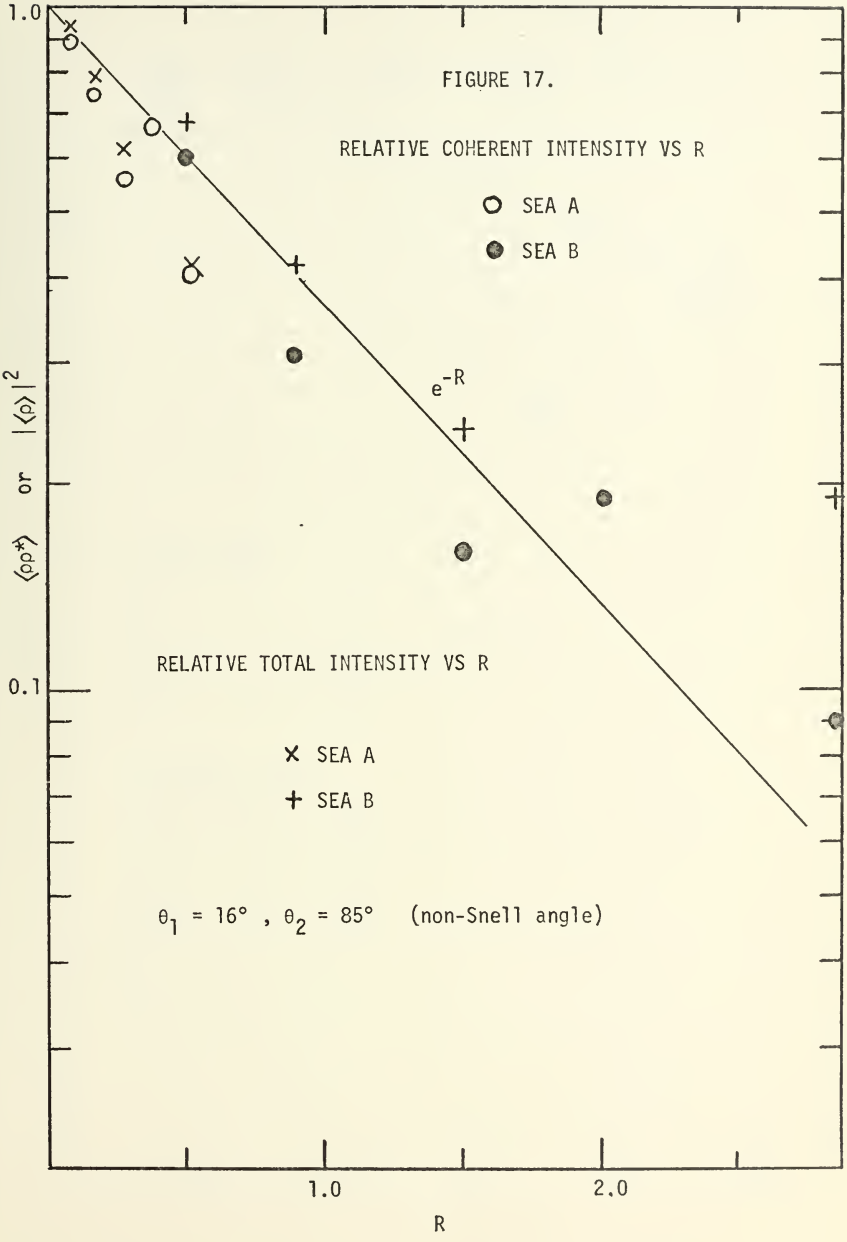
1.0
0.1
FIGURE 17.
RELATIVE COHERENT INTENSITY VS R
SEA A
SEA B
e^{-R}
$\langle \rho \rho^* \rangle$ or $|\langle \rho \rangle|^2$
RELATIVE TOTAL INTENSITY VS R
SEA A
SEA B
$\theta_1 = 16°$, $\theta_2 = 85°$ (non-Snell angle)
1.0
2.0
R

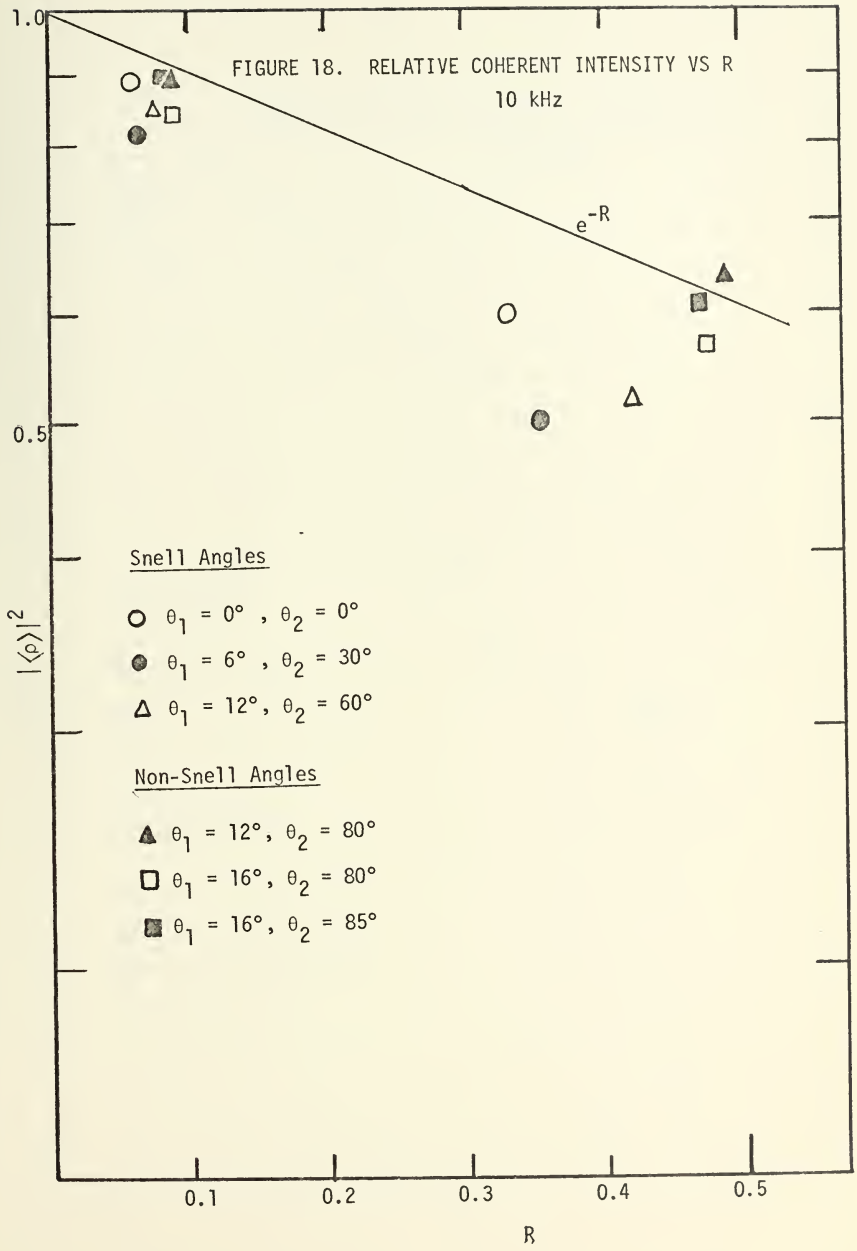

FIGURE 18. RELATIVE COHERENT INTENSITY VS R
10 kHz

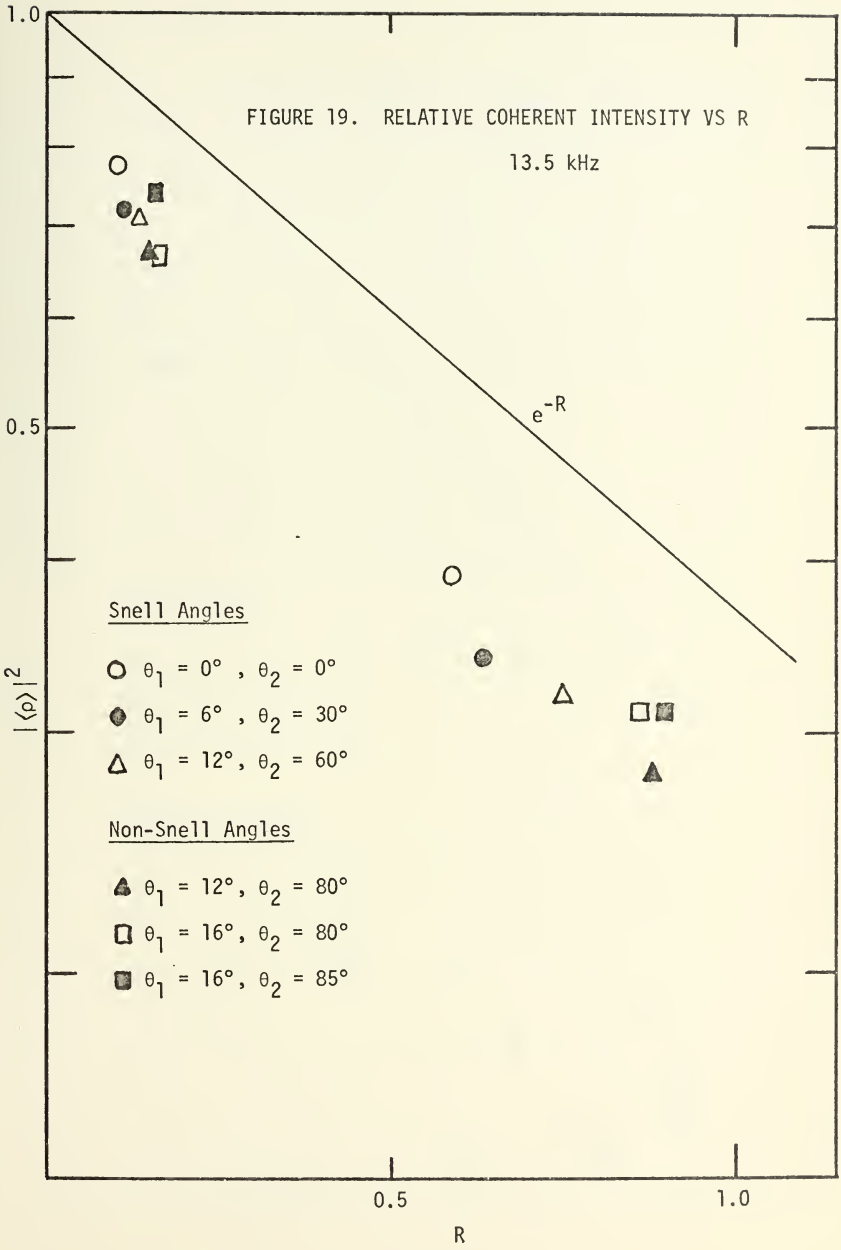

FIGURE 19. RELATIVE COHERENT INTENSITY VS R

13.5 kHz

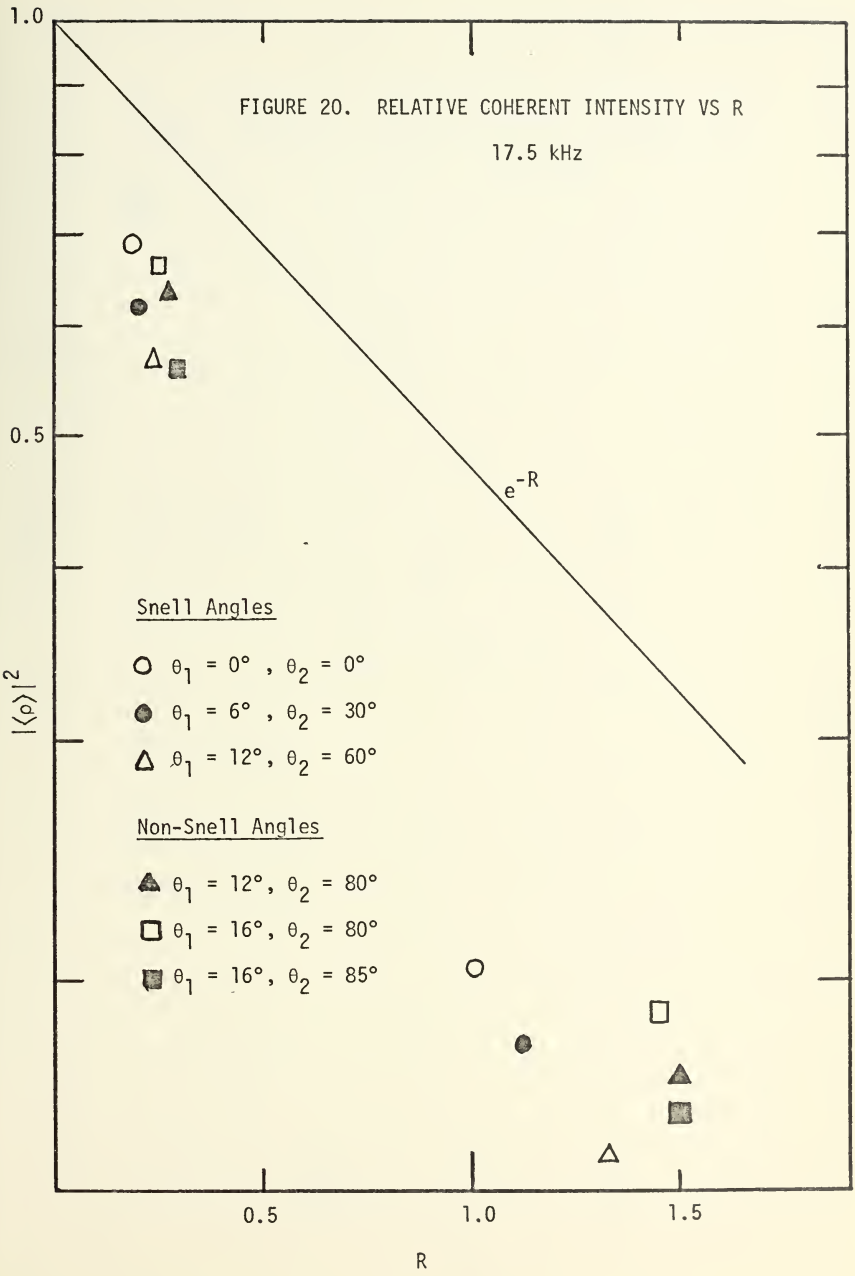

FIGURE 20. RELATIVE COHERENT INTENSITY VS R

17.5 kHz

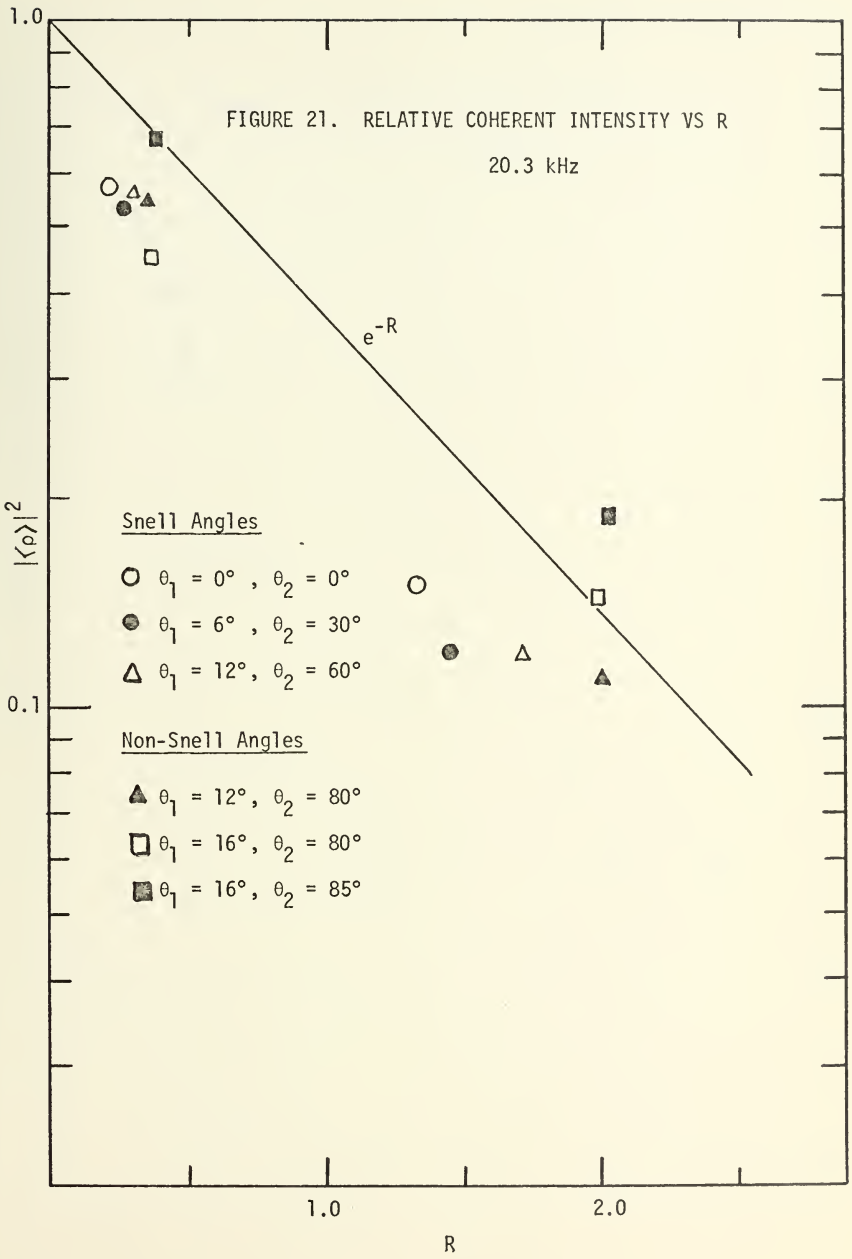

FIGURE 21. RELATIVE COHERENT INTENSITY VS R

20.3 kHz

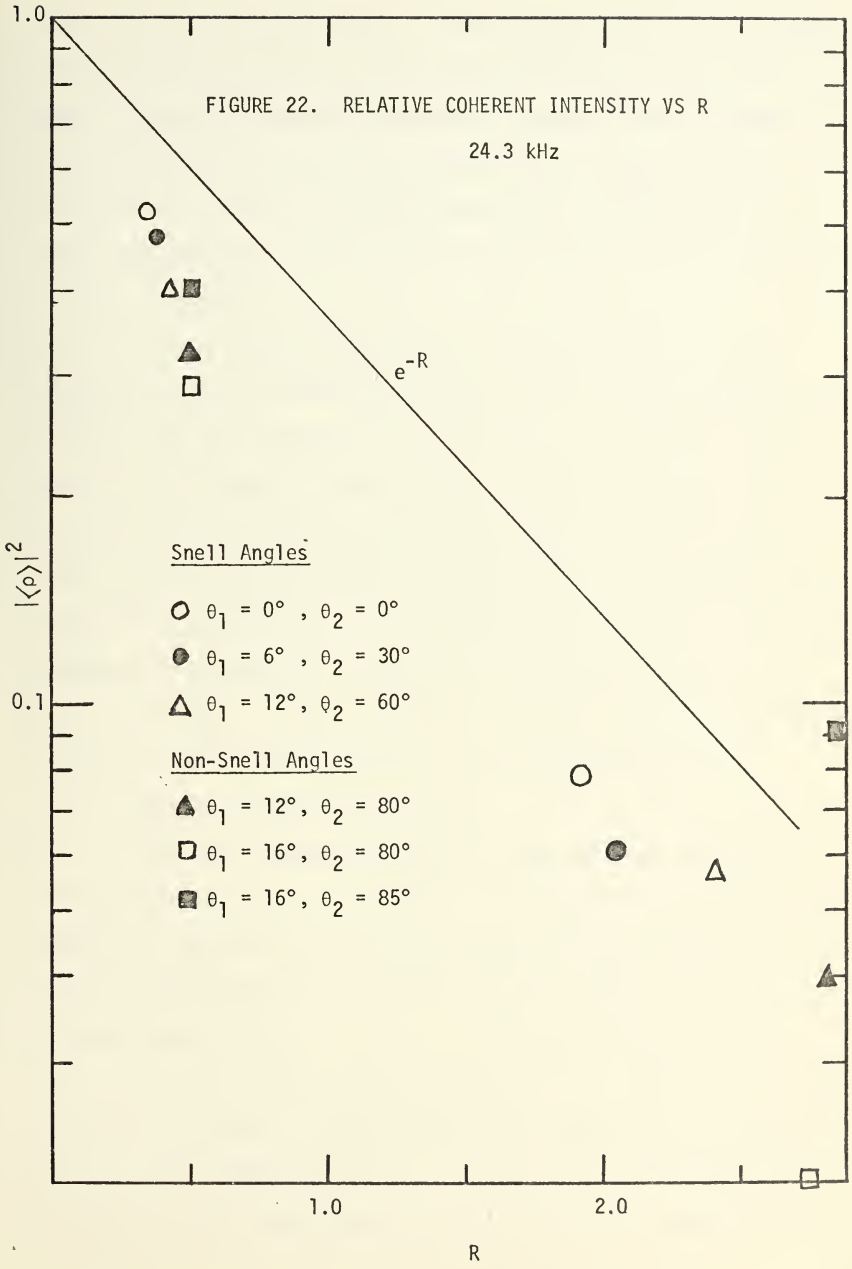

FIGURE 22. RELATIVE COHERENT INTENSITY VS R

24.3 kHz

made is that the surface appears "rougher" than theory admits. Otherwise stated, although there is an exponential decrease with increasing roughness, the empirical roughness parameter is greater than the theoretical value. When this trend was first noted during the experiment the reaction was to reinstall the wave probe and to re-measure the mean square wave heights of the two seas to ensure that the surface had not changed. It had not.

A closer examination of the data revealed that there was a distinct difference between the results for the two sea surfaces. The data for each sea appeared to fit an exponential of the form $e^{-\alpha R}$, where α is a constant greater than unity for a given sea. The smaller sea, A, produced a greater deviation from theory. The conclusion was that, unless the observed results were products of experimental errors, the "acoustical roughness" of these surfaces was dependent on some other parameter, or parameters of the sea surface in addition to the mean square wave height. However, before pursuing this interesting hypothesis it would be well to explore the sources of experimental error.

2. Analysis of Experimental Error

There were a number of factors in the experiment that may have introduced uncertainty in the results. The very fact that the process studied is a stochastic one will introduce a variance dependent on how well the quantities being measured have been averaged. How much this variance might be is, of course, a function of the process itself and must be estimated from the experimental data. As noted in the preceding section on procedures, an effort was made to ensure that the technique used was giving repeatable results. Since each run consisted of a series of samples of the values computed by the correlator, a sample variance

could be calculated and a confidence interval established. But the technique used in this processing produced an unbiased estimator and, therefore, this source of uncertainty seems an unlikely candidate to explain a consistent trend away from theory.

The uncertainty in the determination of the mean square wave height might appear to be a likely candidate. An error here would show up as a trend such as that observed. The fact that the two surfaces, and therefore, the two determinations of mean square wave height gave different results reinforces the suspicion. But the surface was measured and re-measured quite carefully, and the calibration technique seemed adequate. Recalling that a 7.5% error in the mean square wave height was held to be the maximum expected, the apparent error in the mean square wave height can be calculated and compared. For sea A the experimental data can be fit approximately to e^{-2R}. This would indicate a mean square wave height double that measured or a 100% error. Similarly the apparent error for sea B is about 50%. Clearly the observed result can not be explained by errors in wave height measurement.

As noted in the discussion of the anechoic tank, the reverberant field in the tank was not insignificant. An analysis of the possible effect of this factor is in order. In the case of the mean acoustic pressure, only the coherent component need be considered, and a simplified description of the field produced at the receiver can be used to predict the effect of the reverberant field.

We consider that the hypothetical field at the receiver is determined by the vector sum of components from three sources: 1) the ensonified area, 2) a coherent reflection from the bottom and 3) a second coherent reflection from the surface. In determining the relative mean

field the smooth surface value is computed first; then the surface is roughened. The contribution direct from the ensonified area is reduced in amplitude, similarly the contribution from the bottom bounce is reduced in amplitude, although perhaps not in quite the same proportion as the direct contribution because of the geometry factor in the surface roughness parameter. But a more significant effect may be caused by the third component, which is reduced a second time by surface scattering. This should be most noticeable at the higher frequencies, where the loss due to surface scattering is more pronounced. The disproportionate reduction in the amplitude of this third component may cause a larger or smaller result for the relative mean field, depending on the relative phases of the vectors concerned.

Although the preceding argument is for a simple case, the result should hold for the complicated reverberant field that actually existed. This effect would be as likely to produce errors in one direction as in the other, and can not explain a consistent trend away from theory. The net effect of reverberation must be to introduce some uncertainty into the experimental results. That this has caused some problems is evident, particularly for the higher frequencies and near horizontal transmission. For example, Figure 22 gives the results for 24.3 kHz and the inconsistencies of these data are quite apparent. For the (θ_1,θ_2) combinations, (12°,80°), (16°,80°), and (16°,85°) the roughness parameter, R, is about the same. But there was large variation observed in the relative coherent intensity. This effect can be noted for both the "high" and the "low" sea but is more pronounced for the "high" sea. It is not surprising that reverberation becomes a more significant factor for this particular geometry. Consider the field plot for 24.3 kHz and θ_1 = 16°

field the smooth surface value is computed first; then the surface is roughened. The contribution direct from the ensonified area is reduced in amplitude, similarly the contribution from the bottom bounce is reduced in amplitude, although perhaps not in quite the same proportion as the direct contribution because of the geometry factor in the surface roughness parameter. But a more significant effect may be caused by the third component, which is reduced a second time by surface scattering. This should be most noticeable at the higher frequencies, where the loss due to surface scattering is more pronounced. The disproportionate reduction in the amplitude of this third component may cause a larger or smaller result for the relative mean field, depending on the relative phases of the vectors concerned.

Although the preceding argument is for a simple case, the result should hold for the complicated reverberant field that actually existed. This effect would be as likely to produce errors in one direction as in the other, and can not explain a consistent trend away from theory. The net effect of reverberation must be to introduce some uncertainty into the experimental results. That this has caused some problems is evident, particularly for the higher frequencies and near horizontal transmission. For example, Figure 22 gives the results for 24.3 kHz and the inconsistencies of these data are quite apparent. For the (θ_1,θ_2) combinations, (12°,80°), (16°,80°), and (16°,85°) the roughness parameter, R, is about the same. But there was large variation observed in the relative coherent intensity. This effect can be noted for both the "high" and the "low" sea but is more pronounced for the "high" sea. It is not surprising that reverberation becomes a more significant factor for this particular geometry. Consider the field plot for 24.3 kHz and θ_1 = 16°

of Figure 8 ; the SPL at 85° is 6 dB less than that at 30° which, when scattered from the bottom, no doubt produced a proportionately large reverberant field at the receiver. It seems reasonable to conclude that if the data appear well behaved and consistent then the effects of the reverberant field must be small; but when the data become inconsistent, with large swings in the experimental value for small changes in roughness, the reverberation must be introducing significant errors. Despite these apparent errors in some parts of the experiment, the fact remains that, in general, there was an unexplained trend that clearly indicated that the experimental acoustical roughness is greater than theory predicts.

3. The Relative Mean Total Intensity

Theory predicts that for low roughness the incoherent component of the acoustic intensity is dominated by the coherent component and, therefore, the relative mean square acoustic pressure should follow an e^{-R} dependence. As R increases the mean square value should depart from e^{-R} and, for transmission in the Snell direction at very high roughness, the relative mean acoustic intensity should be proportional to R^{-1}. In this experiment R has been limited to values less than 3.0 and reverberation effects further restricted the range of roughness where reliable results have been obtained. In general, it would seem prudent to dismiss as unreliable the mean square data for those cases which showed significant reverberation effects in the relative coherent intensity. When the more reliable data is considered it can be seen that the qualitative predictions of theory are correct, at least over the limited range of R that has been observed.

B. THE SUPPLEMENTARY ACOUSTIC EXPERIMENTS

The validity of the theory within the limitations imposed by the model (and therefore for realistic "real world" conditions) must be seriously questioned based on the results of the basic experiment. It is true that the qualitative behavior of rough surface transmission appeared to fit the description of the theory but it is also true that the surfaces were considerably "rougher" acoustically than predicted. There were a number of assumptions and approximations that were required to derive the theoretical results and the model experiment was designed with the knowledge that some of these assumptions were incorrect and some of the approximations were questionable.

The following are the significant violations of theoretical constraints:

1) An anisotropic sea with a non-Gaussian spatial correlation function and a near Gaussian but skewed wave height probability distribution was used.

2) The incident wave was not plane.

3) The requirements of the Kirchhoff approximation, $L >> \lambda_2$, were not satisfied.

4) For the incoherent component, $\sqrt{A}$ was not much greater than L.

Of these, the third violation was considered to be the most serious. The first seemed less critical because the only specification of the rough sea in the derivation of the mean acoustic field requires that the distribution of heights be Gaussian and this was nearly so. The non-plane wave front was not considered to be the primary cause for the observed deviation but it was desired to eliminate this possible cause in order to isolate other effects. The fact that different seas gave

different results in the basic experiment motivated the attempt to perform some supplementary experiments that would investigate the effect of changing the sea surface "shape".

1. Dependence on Sea Surface Characteristics

The first supplementary experiments to be tried were with the newly generated and measured seas C and E. All other components of the basic experiment were unchanged but as described in Section III, Sea C had a greater correlation length than A but had approximately the same mean square wave height. Sea E was a very small sea (short correlation length) that violated the Kirchhoff assumption more strongly than did sea A.

In all the supplementary experiments only the normal incidence case with the hydrophone in the Snell direction ($\theta_2 = 0°$) was studied. In the basic experiment normal incidence appeared to be the least affected by reverberation.

Figure 23 compares the results obtained for seas A and C. Sea C appears "smoother" acoustically. If the upwind downwind correlation distance, L, is taken to be representative of the minimum radius of curvature of the surface, then the Kirchhoff approximation assumes that $L/\lambda_2 >> 1$. For sea A the ratio L_u/λ_2 is less than or equal to .35 and for sea C, $L_u/\lambda_2 \leq .52$. The obvious conclusion is that sea C has produced results closer to theory because the "shape" of the surface was more nearly like the class of surfaces for which the theory was derived, that is L_u/λ_2 is larger at each frequency (or roughness).

The results obtained with sea E, shown in Figure 24, were obtained by a slightly different technique than that outlined in the data collection procedures section. Since very small transmission losses were

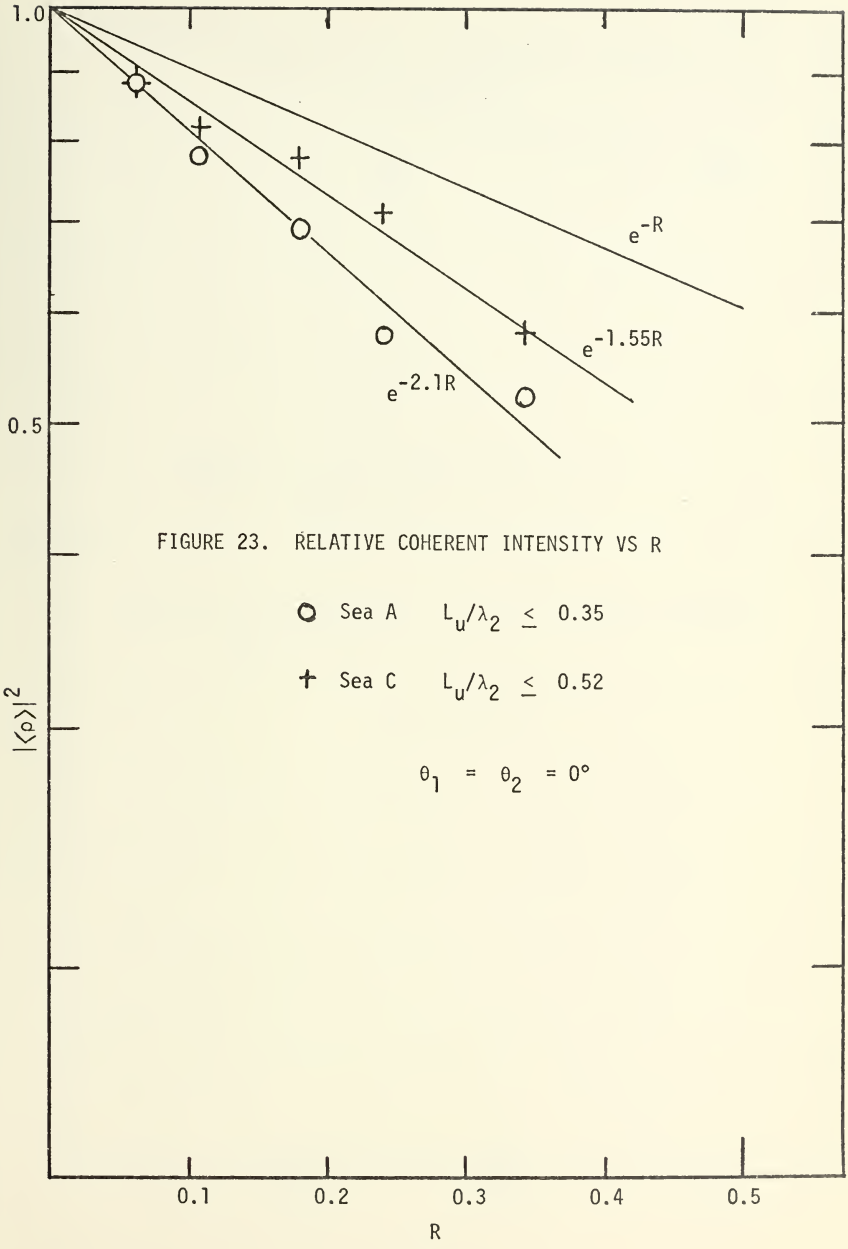

FIGURE 23. RELATIVE COHERENT INTENSITY VS R

○ Sea A $L_u/\lambda_2 \leq 0.35$

+ Sea C $L_u/\lambda_2 \leq 0.52$

$\theta_1 = \theta_2 = 0°$

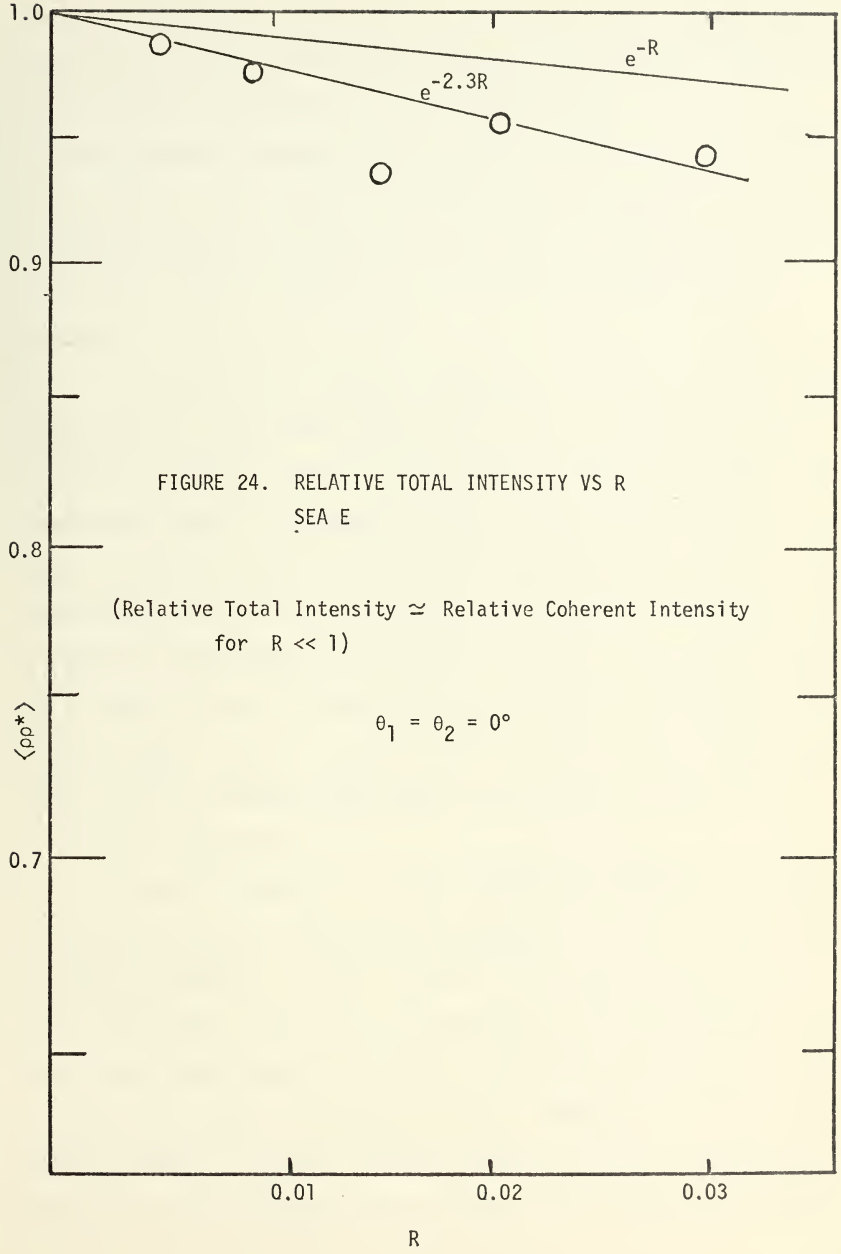

FIGURE 24. RELATIVE TOTAL INTENSITY VS R
SEA E

(Relative Total Intensity $\simeq$ Relative Coherent Intensity
for $R \ll 1$)

$\theta_1 = \theta_2 = 0°$

involved, the relative mean square acoustic pressure was assumed to be equal to the relative mean acoustic pressure squared and the latter value was estimated by computation of the autocovariance at $\tau = 0$. This technique permitted greater resolution since the quantity calculated was the square of a value slightly less than one, and, therefore, is easier to differentiate from one than the value itself. In addition the computed value could be plotted on an X-Y recorder and read with more accuracy.

In spite of this approach, experimental uncertainties must have been relatively large when compared to the small transmission losses. With these reservations noted it can be observed that the deviation from theory does appear to be somewhat greater than that seen for sea A. For sea E the maximum L_u/λ_2 ratio is .13 . Another way of expressing the results obtained with sea E is that for the very small seas, where the Kirchhoff approximation is most strongly violated, the transmission loss is so small that the absolute error introduced by the violation of theory doesn't amount to much. However, for sea E which had the greatest deviation from the Kirchhoff approximation, the empirical slope, $e^{-2.4R}$, is furthest from theory.

Since the constraint of the Kirchhoff approximation is expressed in terms of the ratio, L/λ_2 , it was desirable to extend the experiments to higher frequencies with the same seas. This would supplement the data of the basic experiment by increasing the range of roughness observed and, it was hoped, would provide some more information on the observed deviation from theory. In order to do this without the influence of the non-plane wave, a parabolic reflector source was used. This permitted extension of the experiment up to 43.0 kHz, while maintaining a nearly

plane incident wave. The source was also used with a new sea that was generated with the longest possible correlation length and a moderate mean square wave height.

2. Dependence on Wavefront Curvature

The plane wave results (obtained with the parabolic reflector source) are given in Figures 25, 26 and 27 where they are compared with data from Figure 12. An additional source of experimental error was encountered in the plane wave experiments. A small but not insignificant electrical feedthrough of correlated noise could not be eliminated. The relative amplitude of this interference was estimated as described in Section III-B, and the error flags in the plots correspond to the cases where this component either added in phase or 180° out of phase. The data points without error flags were obtained with no detectable electrical feedthrough.

Comparing the results obtained with seas A and B and the plane-wave with those for the diverging wave (Figures 25, 26), it appears that there is no appreciable difference due to wave front curvature. This would seem to indicate that wavefront curvatures at least as large as $.17\lambda_1$ across the ensonified area do not significantly effect the coherent pressure received and that a Fresnel correction is not required.

3. Dependence on Sea Surface Correlation Length

The great advantage of a model experiment is that it can move into areas relatively unexplored by theorists and, by studying the effects of various parameters in the model gain insights about a process that may be quite difficult to describe analytically. The parameter that seemed to have a significant effect not predicted by theory was the correlation length, L. The correlation length was measured for all sea surfaces used,

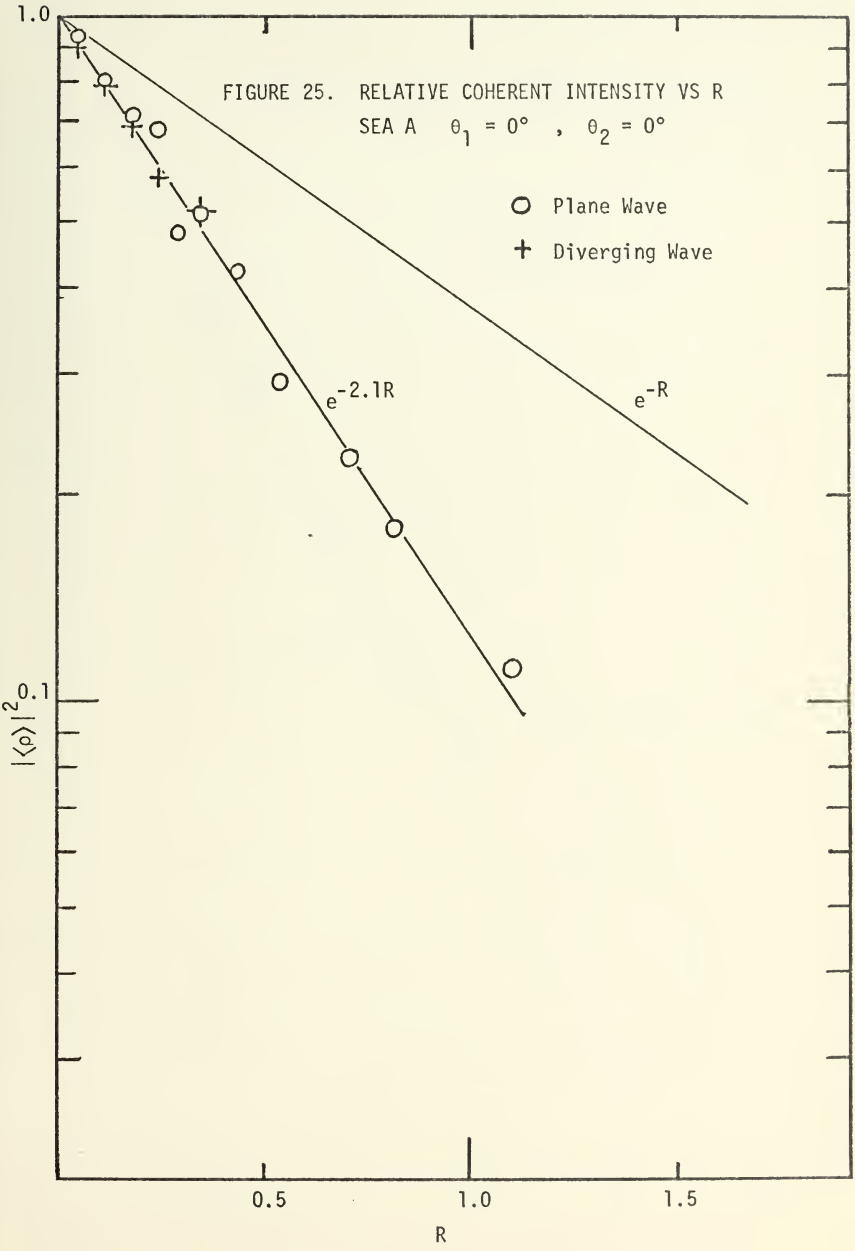

FIGURE 25. RELATIVE COHERENT INTENSITY VS R
SEA A $\theta_1 = 0°$, $\theta_2 = 0°$

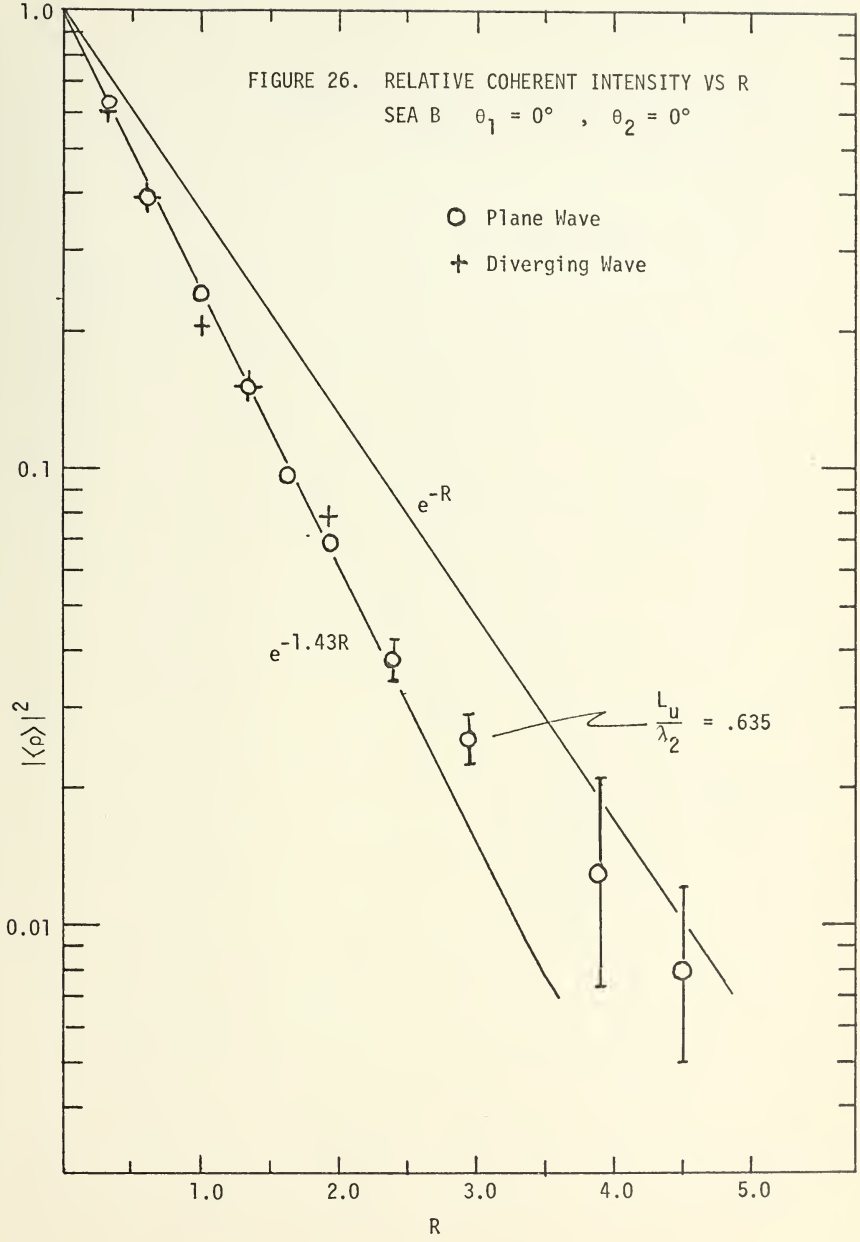
FIGURE 26. RELATIVE COHERENT INTENSITY VS R
SEA B $\theta_1 = 0°$, $\theta_2 = 0°$
Plane Wave
Diverging Wave
e^{-R}
$e^{-1.43R}$
$\frac{L_u}{\lambda_2} = .635$
$|\langle\rho\rangle|^2$
1.0
0.1
0.01
1.0
2.0
3.0
4.0
5.0
R

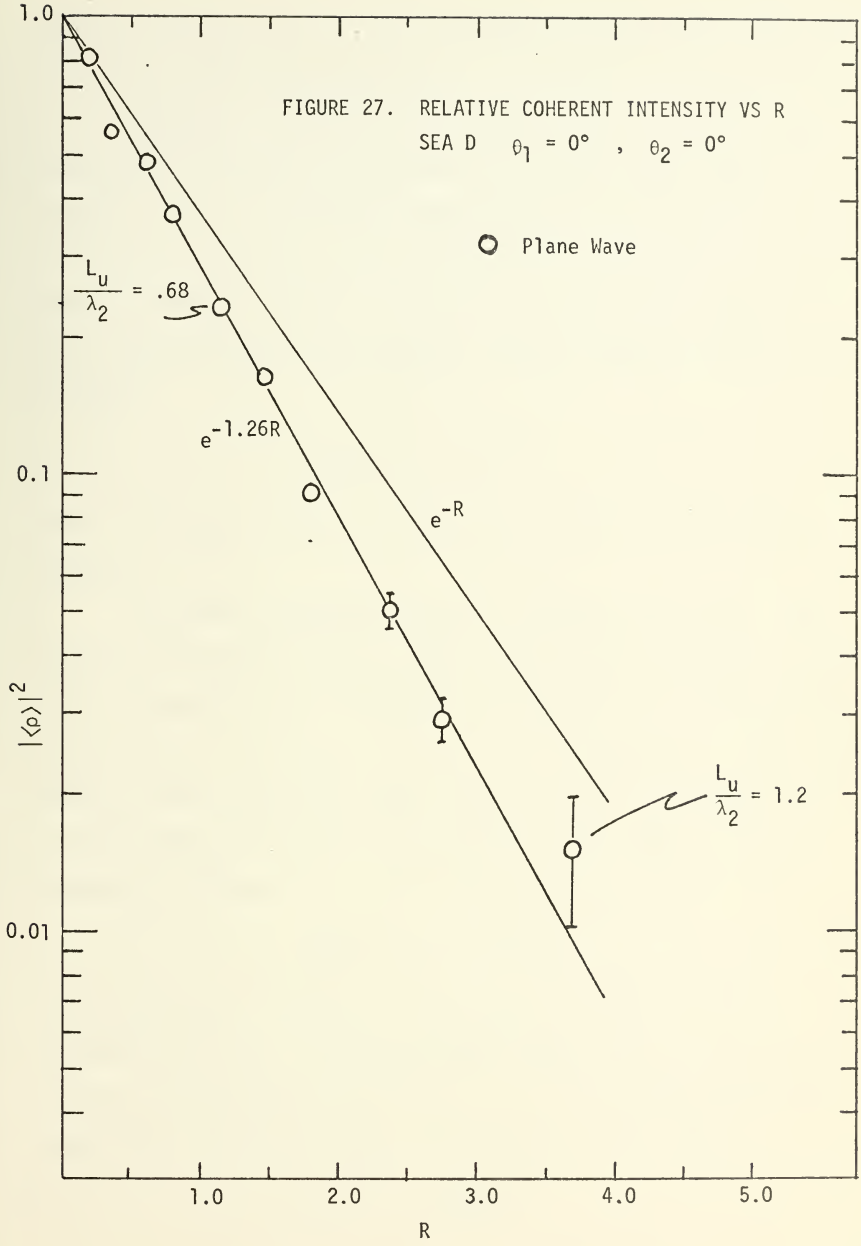

FIGURE 27. RELATIVE COHERENT INTENSITY VS R
SEA D $\theta_1 = 0°$, $\theta_2 = 0°$

and there seems to be a relationship between the correlation length and the amount of deviation from theory.

Although the data that can be used to make an empirical determination of this apparent relationship are limited, there seems to be enough to derive an approximate correction factor to be applied to the theoretical predictions. The correction factor developed here uses the approximation that each sea with correlation length L_u and $L_u/\lambda_2 < 1$, will produce a relative mean acoustic pressure squared that can be predicted by

$$\langle \rho \rangle \langle \rho \rangle^* = e^{-\alpha R}$$

where $\alpha = \alpha(L_u)$. The model study did not extend beyond the regime $L_u/\lambda_2 \leq 1$.

In order to determine an empirical function for $\alpha(L_u)$, the normal incidence data from the model study was used to estimate a value for α for each sea used. A best fit straight line on a semilog plot was drawn for each sea as shown in Figures 23-27. Assuming the theory would hold for large correlation lengths required that $\alpha(L_u)$ approach one as L_u became large. This led to the speculation that $\alpha(L_u)$ could be expressed as follows:

$$\alpha(L_u) = 1 + be^{-L_u/L_o}$$

where b and L_o are constants. To determine the values for these constants and to see if the experimental data actually did fit such a function, the experimental values of $\alpha - 1$ were plotted against the experimental correlation length and compared to the function:

$$\alpha - 1 = be^{-L_u/L_o}$$

Since seas A, B and D were the most thoroughly studied, particular attention was made to fit the empirical relationship to them. A good fit was obtained as shown in Figure 28. The empirical correction to theory thus obtained is given by

$$\alpha(L_u) = 1 + 4.8\, e^{-L_u/1.75} \qquad [L_u \text{ in cm}]$$

In order to demonstrate the effect of this added correction factor all the normal incidence relative coherent intensity data have been plotted against αR, the modified roughness, in a form normalized with the value predicted by the corrected theory. It can be seen from Figure 29 that the bulk of the data plots are within 10% of the predicted value. This scatter is easily attributed to the experimental uncertainties.

It can be noted that for large values of αR Figure 29 shows a rapid departure from the corrected theory. This phenomenon is reminiscent of an effect reported by Mayo [8] and starts at about the same value of roughness. Figures 26 and 27 also show this trend as a leveling off of the transmission loss of the coherent intensity at the higher frequencies. This might have been interpreted as a trend toward theory as the L_u/λ_2 ratio becomes larger. It is noted, however, that sea B (Figure 26) departs from the empirical roughness prediction between $R = 2.5$ and $R = 3.0$, where $L_u/\lambda_2 = .635$, while sea D (Figure 27) departs between $R = 3.0$ and $R = 3.5$, where $L_u/\lambda_2 = 1.2$. It would appear that there is little connection between the observed "leveling off" of the coherent intensity and the L_u/λ_2 ratio. The significant similarity between both of these cases is that they appear to depart from theory at approximately the same value of αR, ~ 4.0.

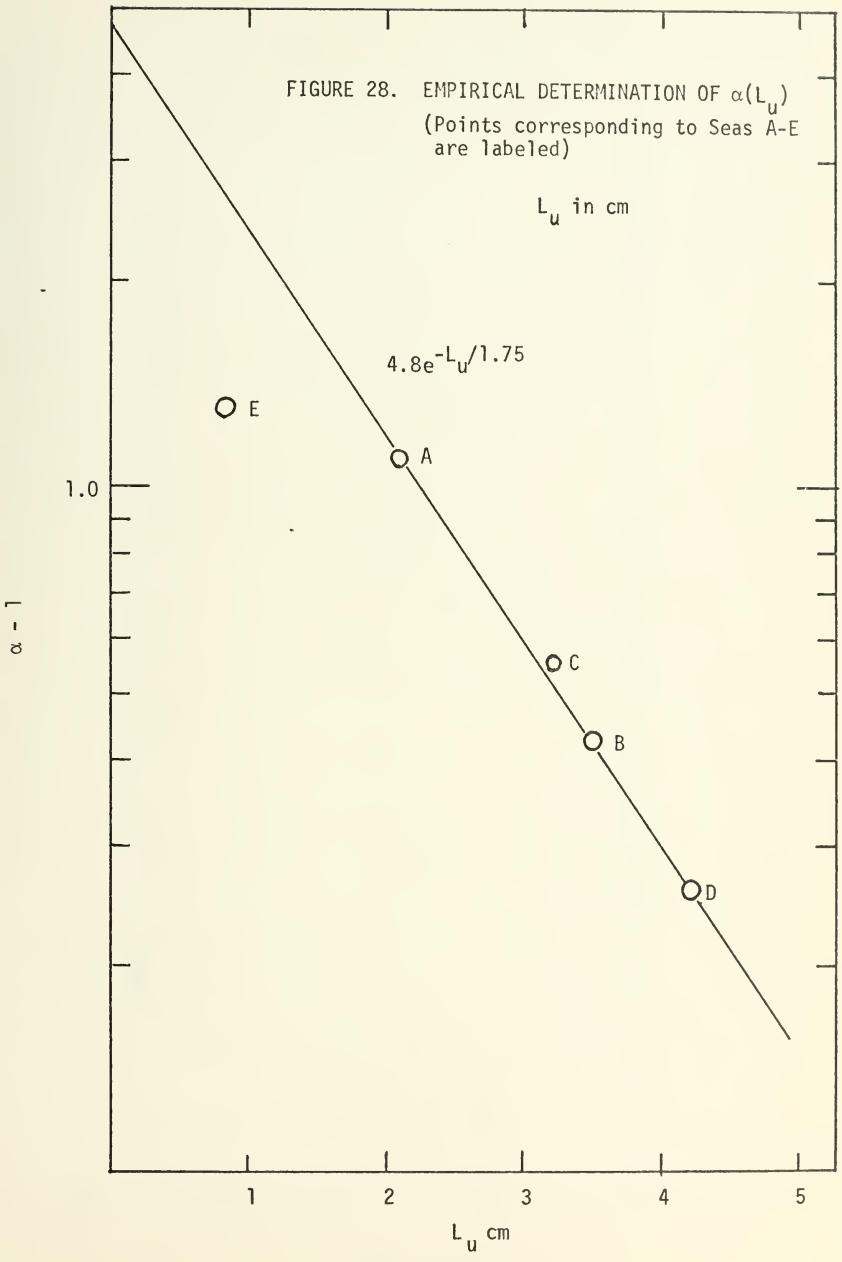

FIGURE 28. EMPIRICAL DETERMINATION OF $\alpha(L_u)$
(Points corresponding to Seas A-E are labeled)

L_u in cm

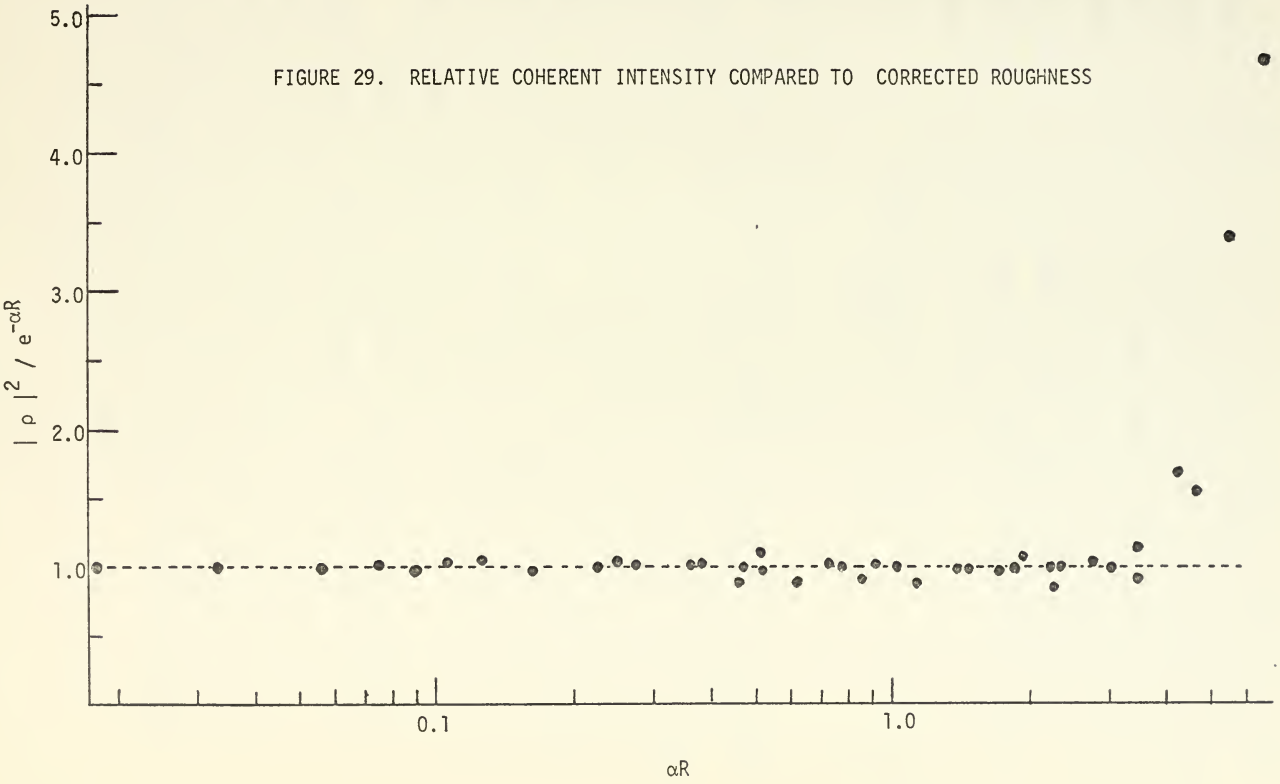

FIGURE 29. RELATIVE COHERENT INTENSITY COMPARED TO CORRECTED ROUGHNESS

The corrected theory can be used to predict the behavior of the incoherent intensity as well as the coherent intensity. The relative incoherent intensity can be obtained by subtracting the relative coherent intensity (33) from the relative total intensity (34). In the present experiment, unfortunately, the difference of two nearly-equal and somewhat uncertain quantities must be taken. Specializing the theory for transmission in the Snell direction, introducing the correction factor, and writing in a convenient form yields:

$$\frac{\langle \rho\rho^* \rangle_{\text{Incoherent}}}{\pi L^2/A} = S(\alpha R) \qquad (41)$$

where $S(\alpha R)$ is the function given in (28).

Recall that the correlation length, L, referred to in the theory is that for an isotropic surface with a Gaussian correlation function. The factor $\pi L^2/A$ is, in effect, a ratio of "correlated area" to ensonified area. To compare the results obtained with the anisotropic sea surfaces one uses $L = L_u L_c$ where L_u and L_c are the upwind and cross-wind correlation lengths, respectively. Using the Snell angle data for seas A and B and (θ_1, θ_2) angles (0°,0°), (6°,30°), (12°,60°), the ratio (41) is plotted against αR in Figure 30.

Comparison with the predicted $S(\alpha R)$ behavior shows reasonable agreement over the range of αR observed. Since the value of $S(\alpha R)$ is changing slowly with αR over the region (αR = 0.5 to 5) where the incoherent component was determined, equally good agreement would have been obtained if the data were plotted against R and compared to S(R). The higher roughnesses will have to be studied to obtain the complete picture of behavior of the incoherent component.

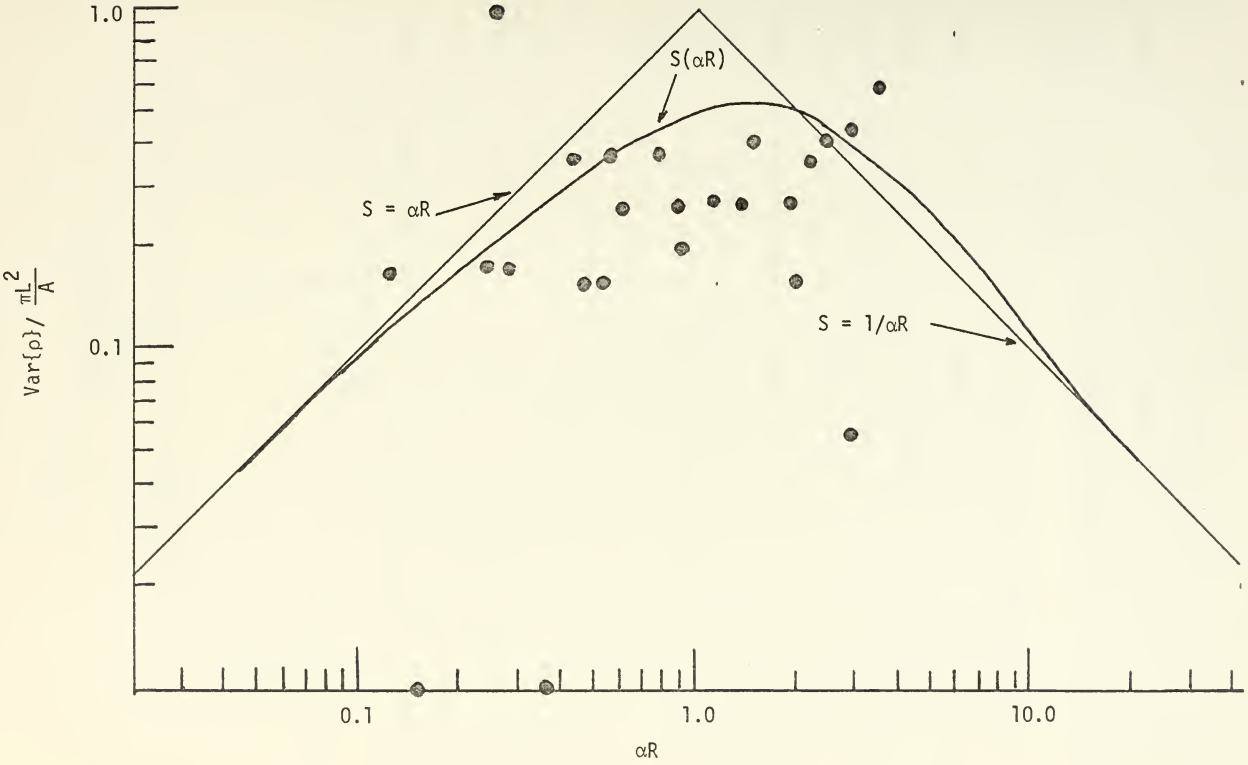

FIGURE 30. RELATIVE INCOHERENT INTENSITY VS αR

4. A Point Source Experiment

A simplified model of the ocean-acoustic experiments conducted with the FLIP was set up in the laboratory. The objective of this model experiment was to gain some insights that might aid in the analysis of the at-sea experiment.

The source used was the Western Electric 640AA transmitter located one meter above the unmasked water surface. A detailed discussion of the source and acoustic arrangement is given in Section III-B. The hydrophone arrangement was the same as that in the basic experiment. It was located one meter from the point on the surface directly below the source and could be positioned accurately at any angle from this point. The filter of the Hewlett-Packard Model 3590A Wave Analyzer was used to provide a 10 Hz bandwidth for the smooth surface data and a 100 Hz bandwidth for the mean square acoustic pressure measurements.

Medwin [11] has developed an expression for the underwater sound field of a point source in air above a smooth surface. The result was derived using a ray theory approach and gives the received acoustic pressure amplitude, p_{2t} , in terms of the pressure amplitude, p_{10} , on the surface directly beneath the point source. The geometry of the problem can be seen in the following figure.

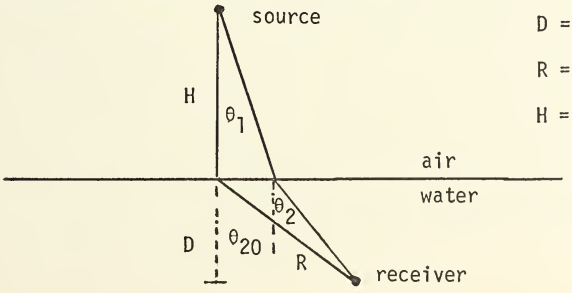

$D = R \cos \theta_{20}$

R = 100 cm

H = 100 cm

The hydrophone position was measured in terms of θ_{20} , while the prediction is expressed in terms of θ_2 as well as θ_1, H, and D.

$$\frac{p_{2t}}{p_{10}} = \frac{(\cos\theta_1 \cos\theta_2)^{1/2}}{1 + \frac{D}{H}\frac{c_2}{c_1}\frac{\cos\theta_1}{\cos\theta_2}}$$

The point source model was used to experimentally determine smooth surface underwater acoustic field. The field was plotted by sweeping θ_{20} (and the hydrophone) from 0° to 180° while the hydrophone output was filtered and detected by the wave analyzer and then plotted in dB vs. θ_{20} . A simple iterative calculation with the IBM 360/67 Computer was used to determine θ_2 from θ_{20} so that the experimental data could be easily compared with the prediction. Reasonable agreement was obtained for the relative sound pressure levels for 10.0 and 20.0 kHz as a function of θ_{20} as shown in Figures 31 and 32. The absolute SPL's are not compared in these figures because of the possible interference of the reverberant field.

A second probe of the underwater sound field as a function of depth for a frequency of 20 kHz produced a plot of SPL relative to that at the surface that can be compared to the prediction of Medwin's formula with more confidence. This plot is given in Figure 33, where the solid line indicates the predicted field. The increased variation of the experimental SPL with depth is attributed to the reverberant field. The experimental and predicted fields are in substantial agreement and appear to be approaching a spherical spreading dependence with depth as would be expected in the "far field".

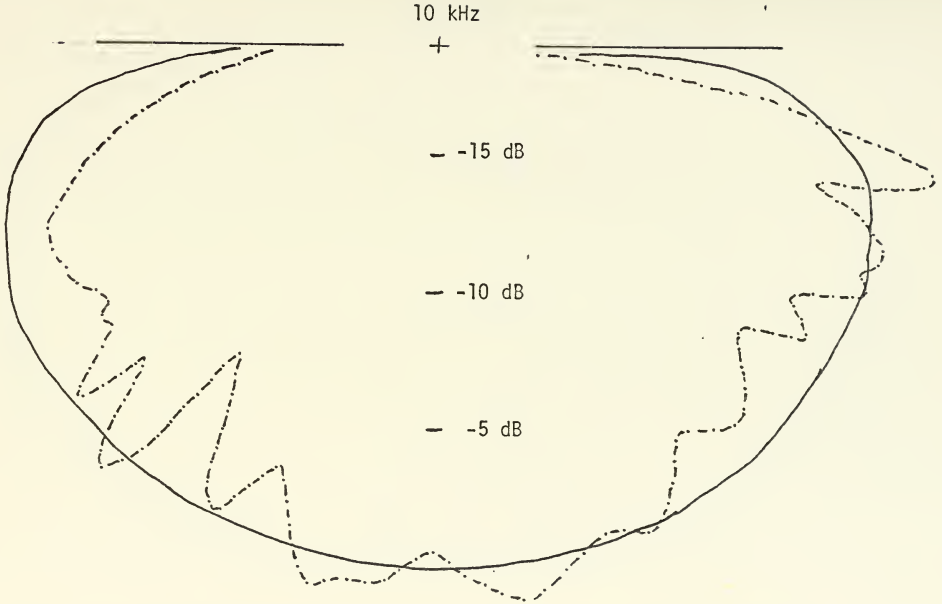

FIGURE 51. POLAR PLOT OF UNDERWATER FIELD AT 1 METER BELOW CENTER OF ENSONIFIED AREA (POINT SOURCE)

——— Theory —·—·— Experimental

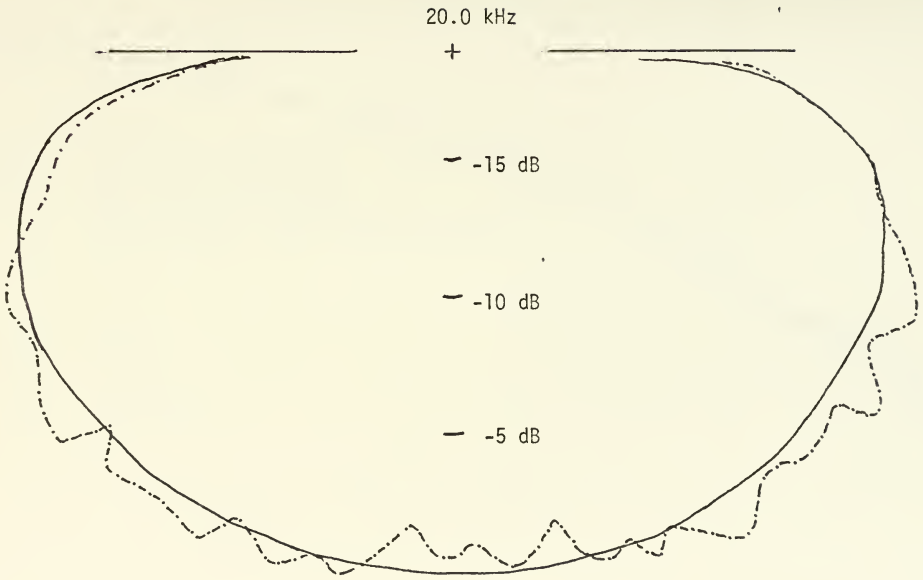

FIGURE 32. POLAR PLOT OF UNDERWATER FIELD AT 1 METER BELOW CENTER OF ENSONIFIED AREA (POINT SOURCE)

——— Theory —·—·— Experimental

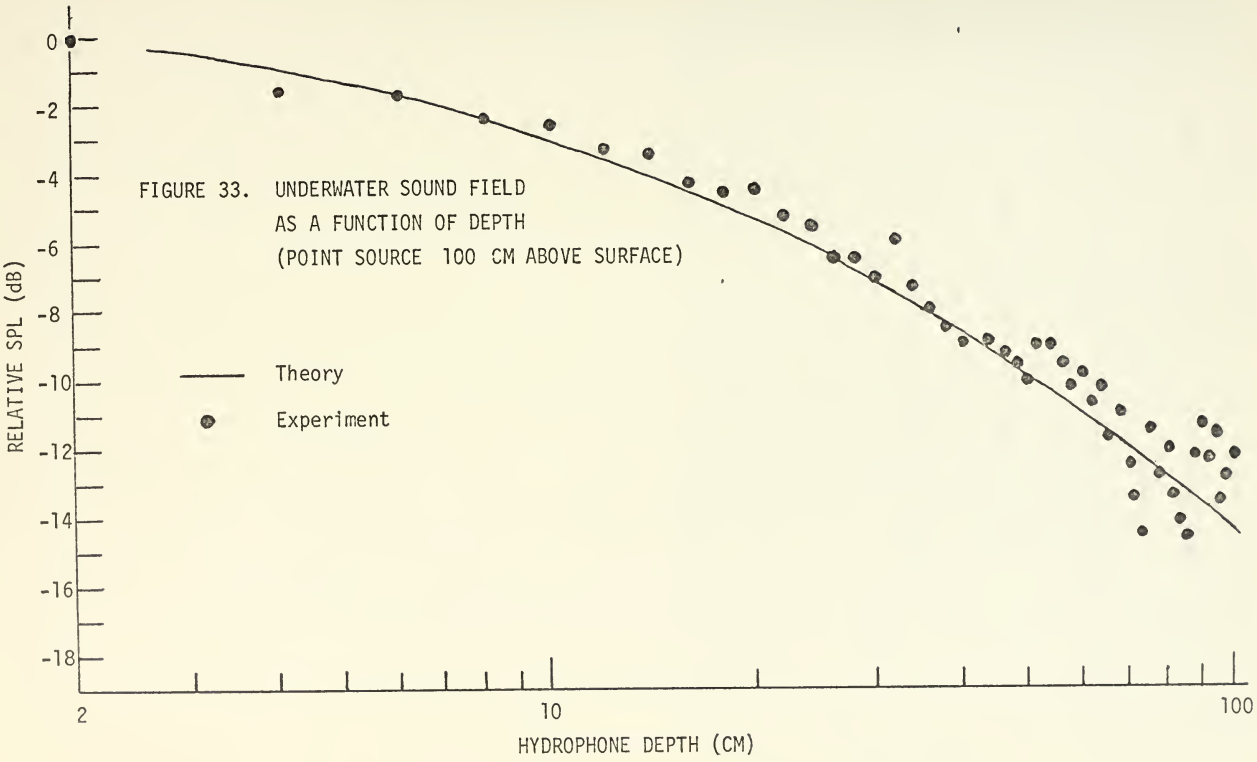

FIGURE 33. UNDERWATER SOUND FIELD AS A FUNCTION OF DEPTH (POINT SOURCE 100 CM ABOVE SURFACE)

Some data were taken for the rough surface (sea D) sound transmission from a point source. For this experiment the hydrophone was positioned at $\theta_{20} = 0°$ and a depth of one meter. The relative mean total intensity was measured in the manner described previously and the results are shown in Figure 34. Interpretation of these results is not easily done; a quantitative prediction to compare with these data is not available at this time. Figure 34 shows the relative mean square pressure beginning to fall with increasing roughness but then leveling off with a transmission loss of less than 1 dB. Qualitatively this effect can be attributed to incoherent contributions to the field at the receiver from areas that do not contribute significantly to the smooth surface field. A quantitative analysis of this phenomenon awaits further theoretical work as well as more extensive model studies.

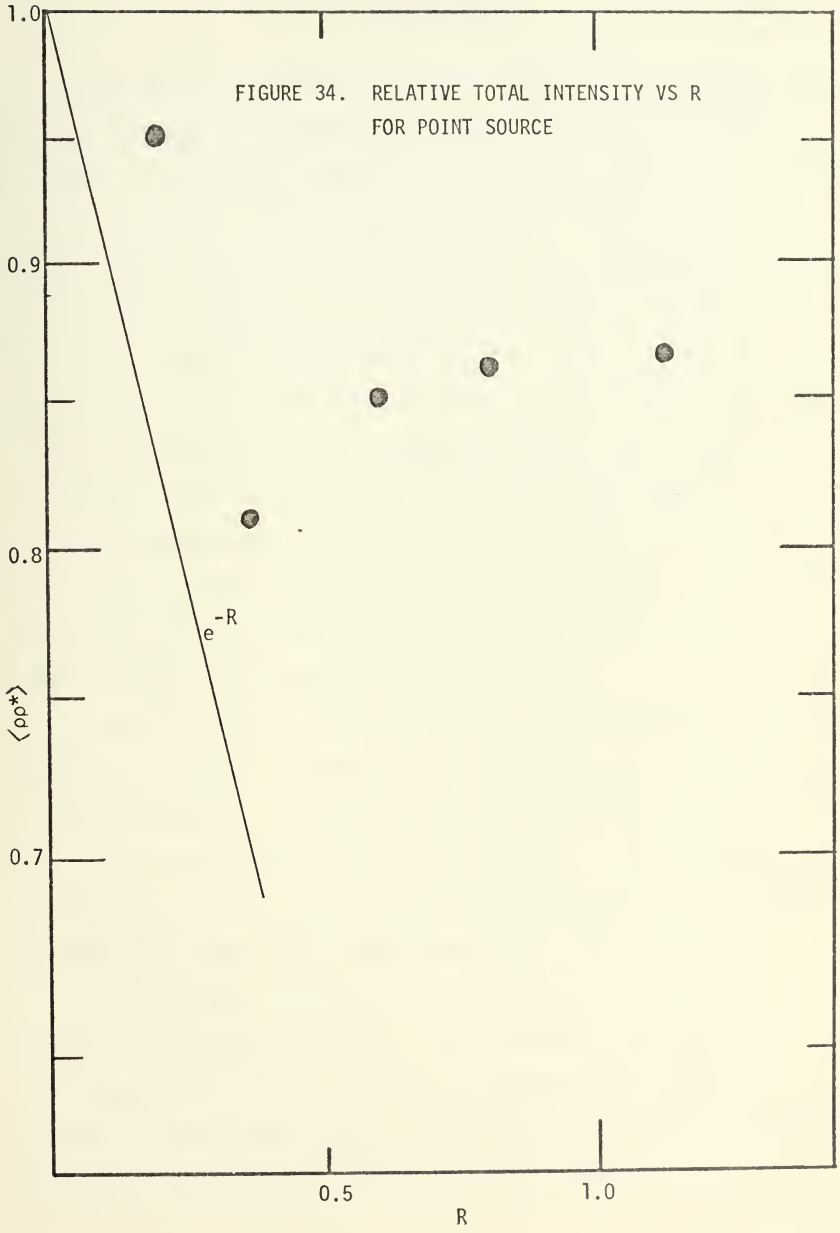

FIGURE 34. RELATIVE TOTAL INTENSITY VS R FOR POINT SOURCE

V. CONCLUSIONS

The model sea experiment has revealed that the theory based on the Kirchhoff method of evaluating the Helmholtz integral is not correct for many of the surfaces and acoustic frequencies that are most important in the problem of air-ocean sound transmission. However, the theory, which predicts that the coherent component of the transmitted intensity will decrease exponentially (e^{-R}) with the roughness parameter, R, can be used if an empirically-derived correction factor is introduced. The correction factor is a function of the surface correlation length only and multiplies the theoretical roughness parameter, R, to give a corrected acoustical roughness, αR. Defining the "correlation length", L_u, as the minimum distance over which the sea surface spatial correlation falls to e^{-1}, the correction factor, α, reduces to unity for $L_u/\lambda_2 \gg 1$ and corrects for the case where the sea surface correlation length is less than or equal to the acoustic wavelength in water.

When the correction factor is applied, the experimental results agree with the prediction of coherent sound transmission over a range from low to moderate acoustic roughness but depart significantly from the corrected theory for the roughness greater than $\alpha R \simeq 4.0$. This departure may be related to a similar phenomenon that has been observed for the coherent component of rough surface scattering by Mayo [8] and others.

The predictions of the corrected theory seem to describe the behavior of the total acoustic intensity. The incoherent component of the received signal appears to follow the predicted behavior within the limits of experimental accuracy. Experimental limitations prevented the testing of theory for the very high roughness case.

The wavefront curvature does not appear to be a critical factor for the range of curvature studied. Comparison of the results of the same experiment made with a near-plane wave generated by a parabolic reflector and a diverging wavefront with as much as $.17\lambda_1$ curvature across the ensonified area showed no detectable difference.

The limited experiments conducted with a nearly omnidirectional point source above an unlimited water surface seem to verify a theoretical prediction for the smooth surface underwater sound field derived by Medwin. The rough surface transmission results could be qualitatively explained based on theory.

A quantitative prediction for the point source problem may be achieved by partitioning the ensonified area into subareas that meet the specifications of the limited ensonified area used in the theory and by summing the contributions of each subarea. This procedure may not prove too difficult for determining the coherent component but it is not a trivial extension of the theory in the apparently important case of the incoherent contributions to the received intensity; for the incoherent contributions from subareas, the surface height correlation between subareas must be accounted for.

The discovery that correlation length must be used to empirically correct the roughness parameter seems to be consistent with the fact that the experiment strongly violated the Kirchhoff assumption, $L/\lambda_2 >> 1$. It suggests that additional theoretical work needs to be done for the case of surfaces and acoustic frequencies that do not meet the Kirchhoff restriction. The question arises as to whether the size of the ensonified area with respect to the correlation length might become a factor for the coherent component as it is in the present theory for the

incoherent component of intensity. The answer to this and other questions brought up by this study must be found before this very interesting problem can be considered to be solved.

APPENDIX A — STUDY OF SEA SURFACE CHARACTERISTICS

1. Probability Density Functions of Surface Wave Heights

The probability density of wave heights was determined for the wind-driven seas A and B as part of a study which used the CI5000/XDS9300 hybrid computer to process twenty-minute wave records of each sea. The procedures used in this study were as follows:

a. The wave probe was located at the center of the ensonified area and oscillated to provide a 10-minute calibration signal to the FM tape recorder. After the calibration signal, twenty-minute wave records of each sea were recorded.

b. The calibration signal and the wave records were replayed at ten times speed into the analog-to-digital converter of the hybrid computer facility. The converter sampled the wave record at an effective real-time rate of 50 times per second until an ensemble of 25,600 values was obtained.

c. The ensemble mean was computed and then adjusted to zero by subtracting the computed mean from each sample value. The mean square voltage for the two wave records and the calibration signal was computed and the calibration was used to determine root mean square wave heights, σ .

d. The digital computer then sorted the ensemble values into intervals of width 0.2σ . The results were normalized to give unit area and are plotted in Figures A1 and A2 . . A Gaussian distribution curve is included for comparison.

2. Spatial Correlation of the Sea Surface

The two-dimensional correlation function of the sea surfaces were determined by cross-correlation of the wave record from the two wave

probes, A and B, and recording the value computed with zero time delay. The wave probes were mounted on traverse that permitted one probe to be positioned at the center of the ensonified area and the other moved in any radial direction to any separation within about 30 cm. The wave probes were not calibrated as the correlation function could be computed as follows

$$C(\ell) = \frac{C_{AB}(\tau=0)}{[C_{AA}(\tau=0)\ C_{BB}(\tau=0)]^{1/2}}$$

where ℓ is the probe separation.

In order to determine the correlation for a given separation it was necessary to record the cross-correlation on the x-y recorder for at least 200 seconds and visually average the resulting plot. The mean square voltage of each probe was computed with a probe separation of 6 cm. and used to normalize the cross-correlations obtained for separations greater than 4 cm. For separations of 4 cm. or less it was necessary to determine the mean square voltage for each probe at each separation. This was required because the probe sensitivity decreased with separation until a spacing of at least 3 to 4 cm. was reached. Because of the long averaging times required to compute each point of the Spatial Correlation Function this was an extremely time consuming process.

Spatial correlation was determined for the upwind and crosswind directions as well as four intermediate angles. Figures A3 - A7 show the correlation functions obtained.

3. Wave-Number Sea Surface Spectrum

The two-dimensional surface spatial correlation data was used to compute a wave-number spectrum for sea A. The two-dimensional fourier transform of the correlation function, $C(\xi,\eta)$ yields the normalized directional spectrum of the sea surface:

$$G(\vec{k}) = \left(\frac{1}{2\pi}\right)^2 \iint_{\xi\eta} C(\xi,\eta)\, e^{-i(\vec{k}\cdot\vec{r})}\, d\vec{r}$$

where $\vec{r} = \hat{i}_1\xi + \hat{i}_2\eta$, $\vec{K} = \hat{i}_1 K_x + \hat{i}_2 K_y$ and $|\vec{k}| = 2\pi/\Lambda$,

Λ = surface wavelength.

To accomplish this transformation the HARM subroutine of the IBM/360 Scientific Subroutine Package was used. This subroutine uses the Cooley-Tukey (1965) fast fourier transform algorithm. The spatial correlation data was formed into a 16 by 16 array of sample values, (ξ,η), with one centimeter spacing. The upwind direction was taken to be the x-dimension of the array. The transformation of this array by HARM yielded an 8 by 8 array of fourier coefficients for wave numbers (K_x,K_y).

The resolution of the spectrum was limited by the maximum separation obtained in the surface spatial correlation. Although it would have been desirable to extend the correlation function out to greater distances, the uncertainty in such data due to the limited averaging time of correlator would have made the accuracy of the resultant spectrum somewhat questionable. If the correlation function had been sampled every 0.5 cm the spectrum could be extended to higher wave-numbers. This appears justified; however, it was not done.

The advantage of a wave-number spectrum as a description of a sea surface is that it clearly demonstrates the directional nature of the sea.

Figures A8, A9, and A10 show the wave-number spectrum in the upwind-downwind direction (K_y=0), the cross-wind spectrum (K_x=0) and 45° off the wind (K_x=K_y).

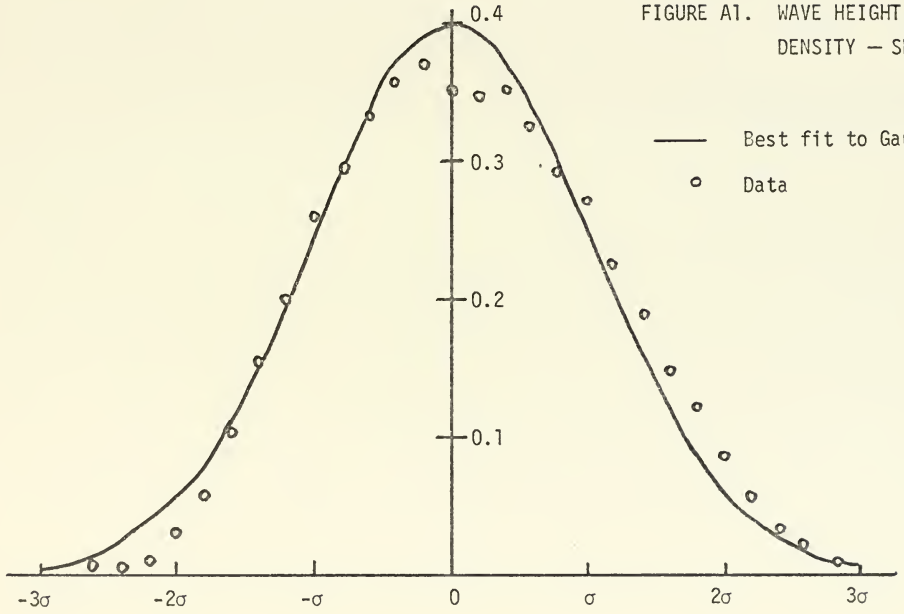

FIGURE A1. WAVE HEIGHT PROBABILITY DENSITY — SEA A

—— Best fit to Gaussian Distribution

o Data

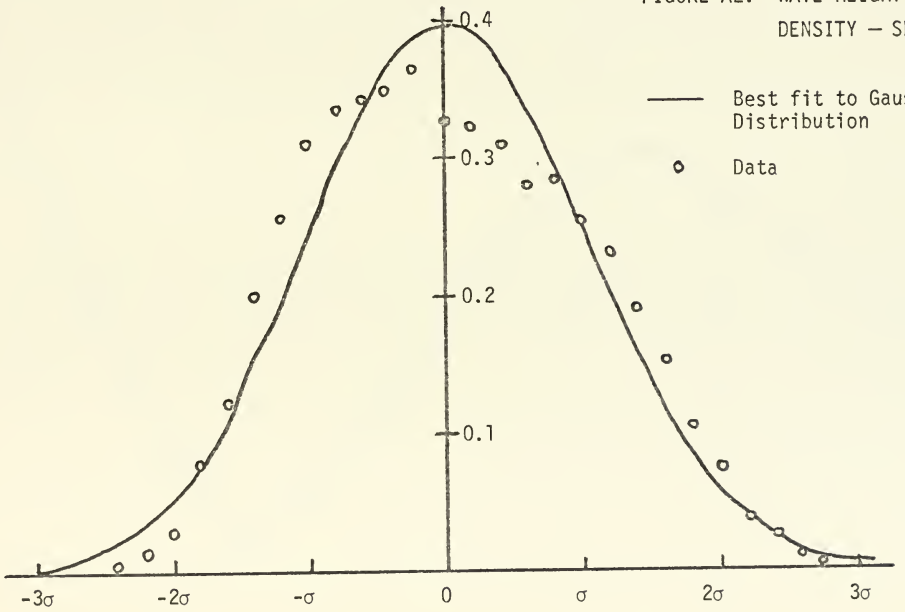

FIGURE A2. WAVE HEIGHT PROBABILITY DENSITY — SEA B

FIGURE A3. UPWIND SPATIAL CORRELATION
SEA A

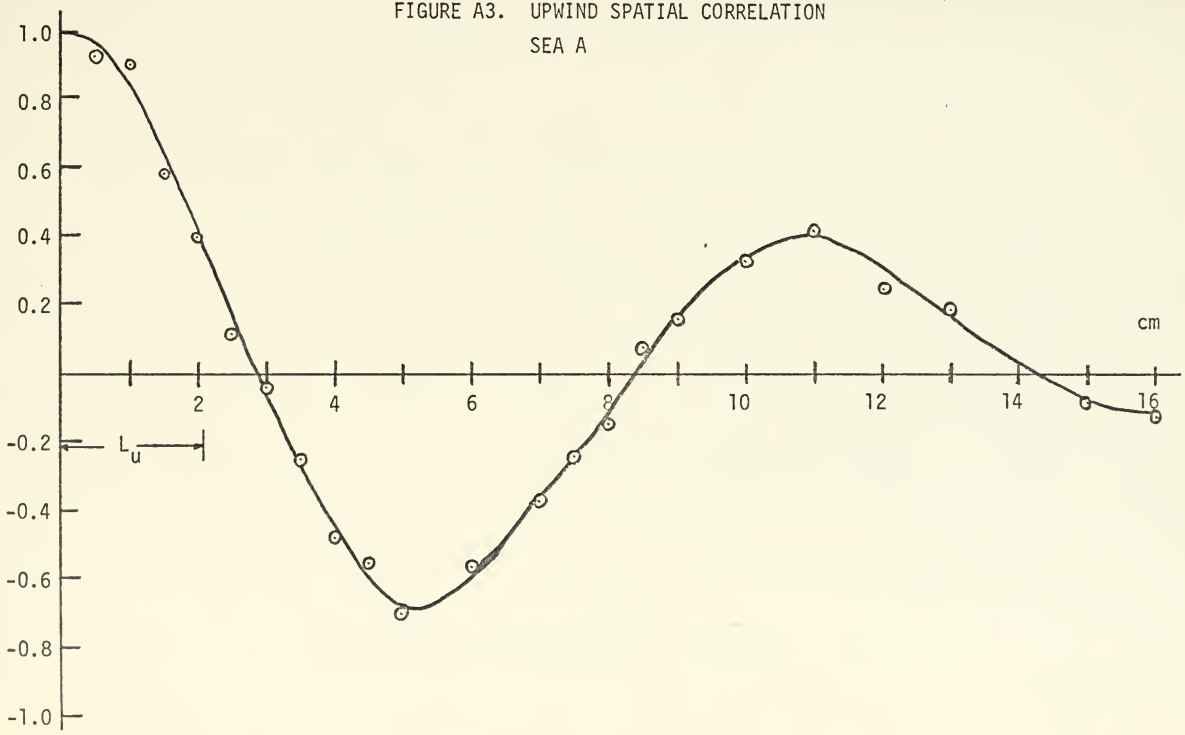

FIGURE A4. CROSSWIND SPATIAL CORRELATION
SEA A

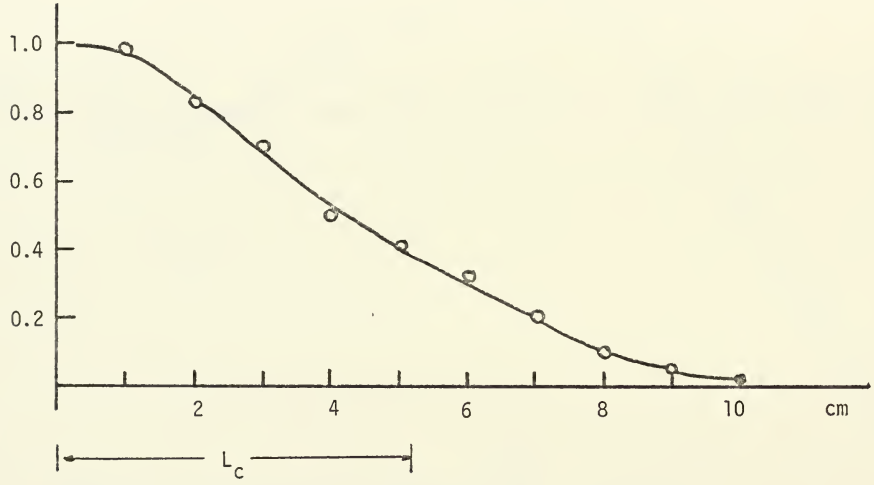

FIGURE A5. SPATIAL CORRELATION 040° RELATIVE TO UPWIND SEA A

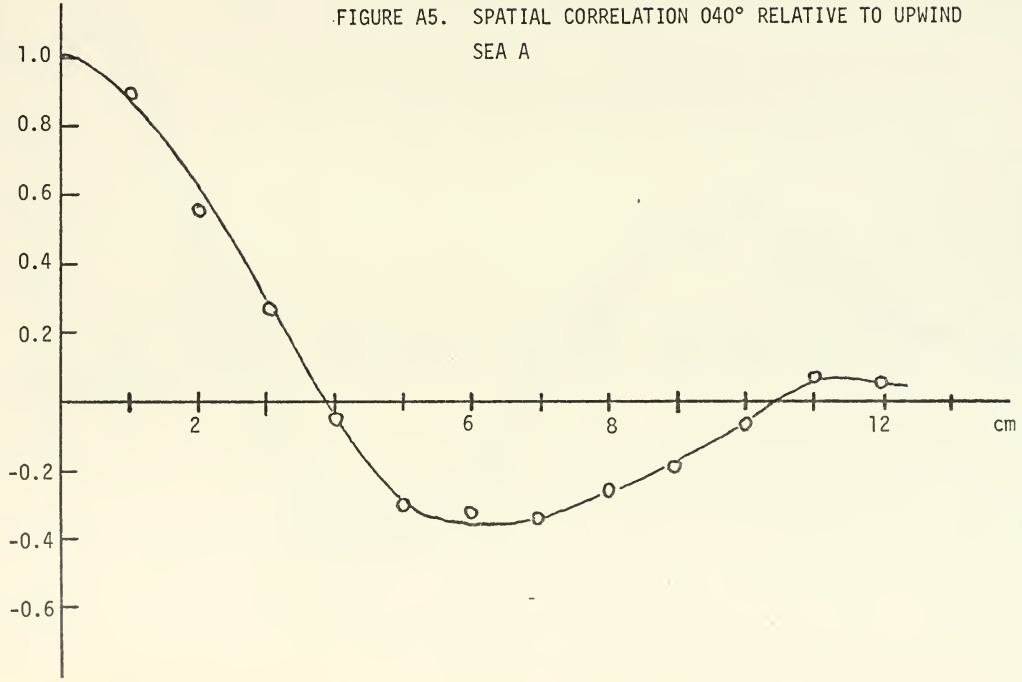

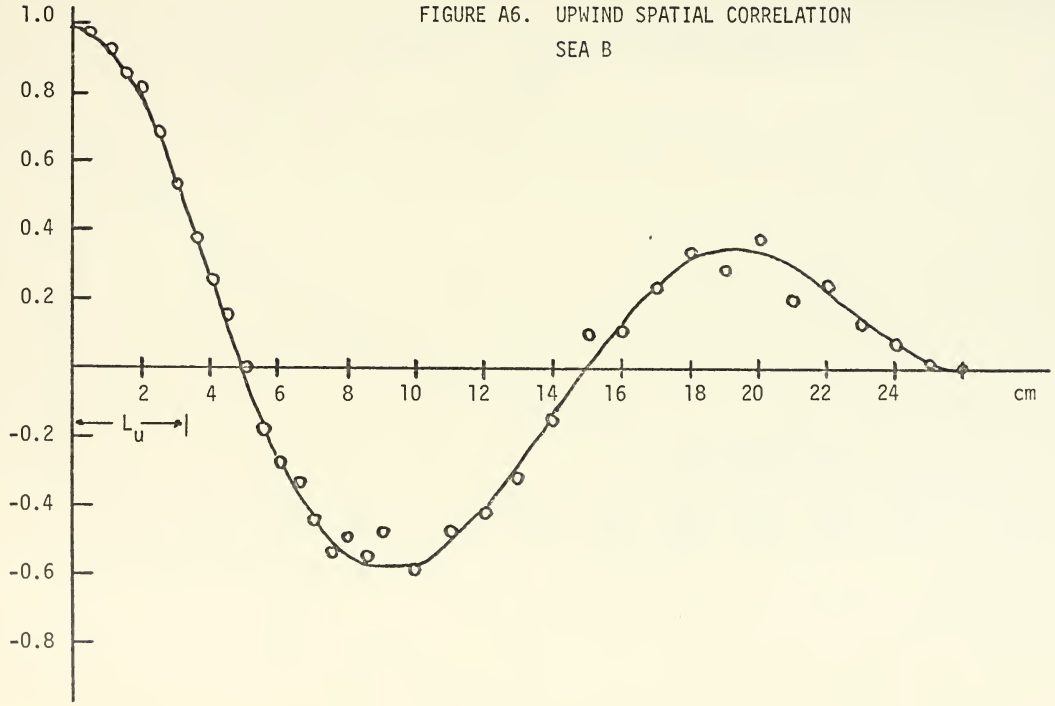

FIGURE A6. UPWIND SPATIAL CORRELATION
SEA B

FIGURE A7. CROSSWIND SPATIAL CORRELATION
SEA B

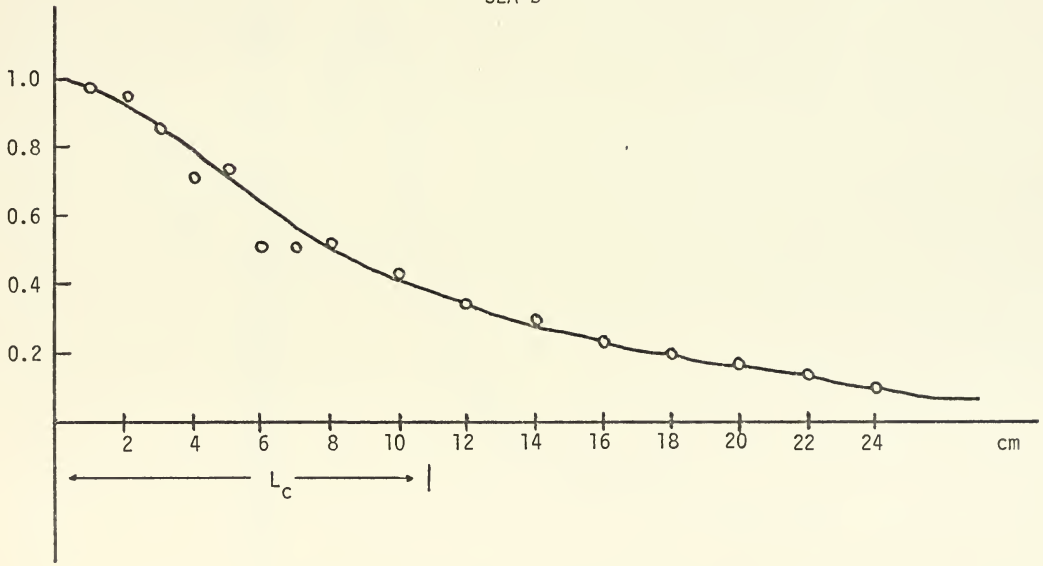

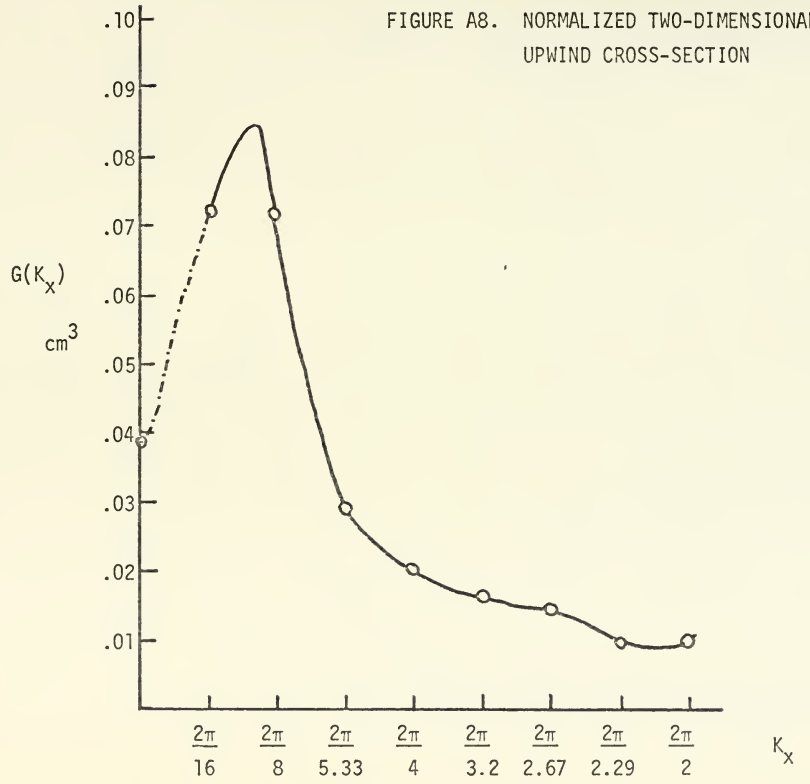

FIGURE A8. NORMALIZED TWO-DIMENSIONAL SPECTRUM UPWIND CROSS-SECTION

FIGURE A9. NORMALIZED TWO-DIMENSIONAL SPECTRUM CROSS-SECTION 045° RELATIVE TO WIND

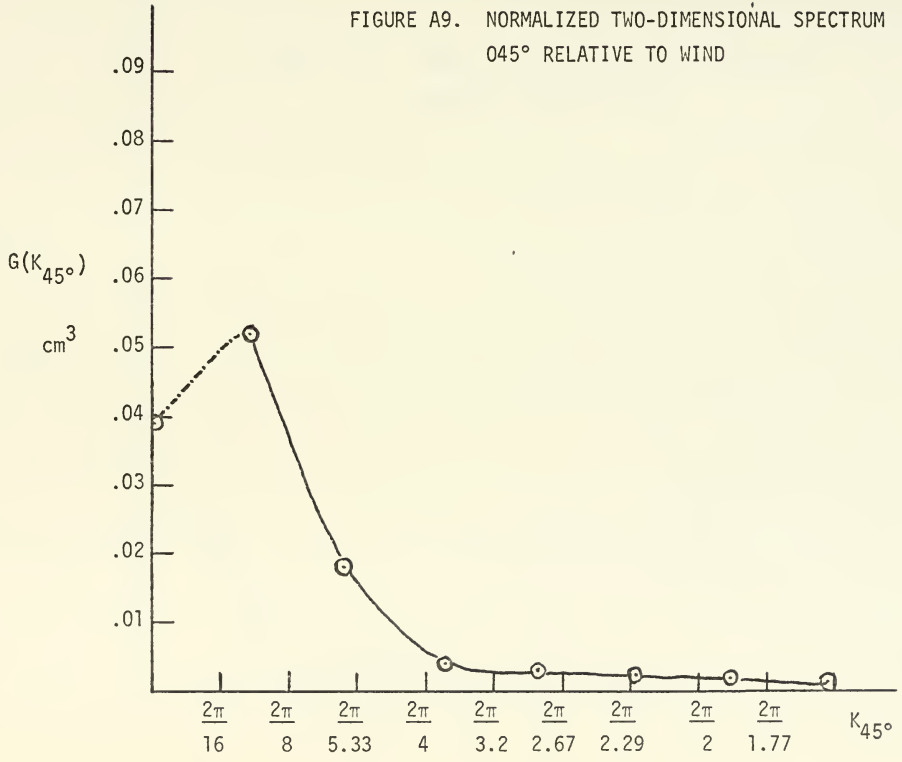

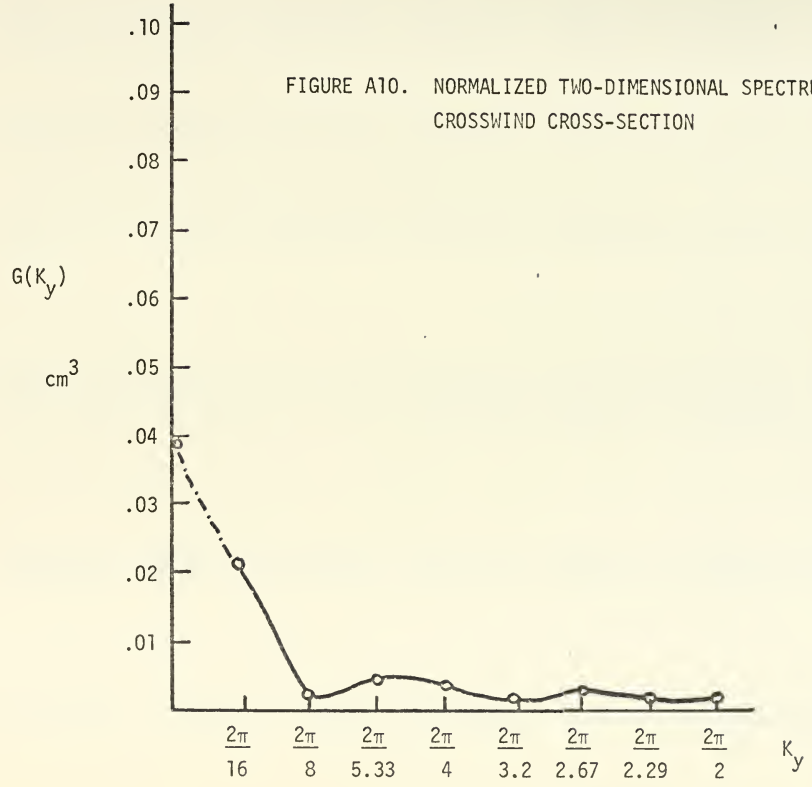

FIGURE A10. NORMALIZED TWO-DIMENSIONAL SPECTRUM CROSSWIND CROSS-SECTION

APPENDIX B — SUMMARY TABLES OF DATA

1. Basic Experiment Data

COHERENT AND TOTAL INTENSITY:

SEA A (σ = .173 cm, L_u = 2.1 cm)

freq	θ_1	θ_2	R	$\lvert\langle\rho\rangle\rvert^2$	$\langle\rho\rho^*\rangle$
10.0	0	0	.059	.89	.90
13.5	0	0	.107	.77	.78
17.5	0	0	.180	.69	.68
20.3	0	0	.240	.57	.60
24.3	0	0	.342	.52	.54
10.0	6	30	.063	.81	.82
13.5	6	30	.115	.72	.78
17.5	6	30	.193	.62	.64
20.3	6	30	.259	.53	.55
24.3	6	30	.366	.48	.50
10.0	12	60	.074	.85	.82
13.5	12	60	.135	.71	.72
17.5	12	60	.23	.57	.58
20.3	12	60	.306	.56	.60
24.3	12	60	.43	.40	.40
10.0	12	80	.087	.90	.90
13.5	12	80	.16	.67	.75
17.5	12	80	.27	.64	.69
20.3	12	80	.35	.55	--
24.3	12	80	.51	.36	.49
10.0	16	80	.085	.84	.81
13.5	16	80	.154	.72	.68
17.5	16	80	.26	.67	.64
20.3	16	80	.345	.45	--
24.3	16	80	.49	.29	--
10.0	16	85	.088	.88	.94
13.5	16	85	.16	.74	.79
17.5	16	85	.27	.56	.62
20.3	16	85	.36	.67	--
24.3	16	85	.51	.41	.42

COHERENT AND TOTAL INTENSITY (Continued)

SEA B (σ = .41 cm, L_u = 3.5 cm)

freq	θ_1	θ_2	R	$\lvert\langle\rho\rangle\rvert^2$	$\langle\rho\rho^*\rangle$
10.0	0	0	.33	.60	.63
13.5	0	0	.60	.39	.44
17.5	0	0	1.01	.20	.25
20.3	0	0	1.35	.15	.18
24.3	0	0	1.91	.078	.091
10.0	6	30	.353	.50	.53
13.5	6	30	.635	.34	.38
17.5	6	30	1.12	.18	.26
20.3	6	30	1.45	.12	.19
24.3	6	30	2.04	.060	.15
10.0	12	60	.42	.52	.57
13.5	12	60	.75	.32	.37
17.5	12	60	1.32	.15	.20
20.3	12	60	1.71	.12	.20
24.3	12	60	2.4	.056	.18
10.0	12	80	.49	.64	.64
13.5	12	80	.88	.28	.40
17.5	12	80	1.50	.17	.25
20.3	12	80	2.0	.11	--
24.3	12	80	2.82	.038	.12
10.0	16	80	.475	.57	.59
13.5	16	80	.86	.31	.38
17.5	16	80	1.45	.192	.24
20.3	16	80	1.95	.144	--
24.3	16	80	2.75	.022	--
10.0	16	85	.50	.60	.68
13.5	16	85	.89	.31	.42
17.5	16	85	1.51	.16	.24
20.3	16	85	2.02	.19	--
24.3	16	85	2.86	.09	.19

INCOHERENT INTENSITY:

freq	θ_1	θ_2	R	αR	$\langle \rho\rho^* \rangle_{incoh.}$	$\frac{\langle \rho\rho^* \rangle_{incoh.}}{\pi L^2/A}$
SEA A (α = 2.1 , $\pi L^2/A$ = .06)						
10.0	0	0	.059	.123	.01	.17
13.5	0	0	.107	.224	.01	.17
17.5	0	0	.180	.378	.00	.00
20.3	0	0	.240	.50	.03	.50
24.3	0	0	.342	.72	.02	.34
10.0	6	30	.063	.132	.01	.17
13.5	6	30	.115	.232	.06	1.0
17.5	6	30	.193	.405	.02	.336
20.3	6	30	.259	.543	.02	.336
24.3	6	30	.366	.77	.02	.336
10.0	12	60	.074	.150	.00	.00
13.5	12	60	.135	.284	.01	.17
17.5	12	60	.23	.483	.01	.17
20.3	12	60	.306	.642	.04	.67
24.3	12	60	.43	.90	.00	.00
SEA B (α = 1.43, $\pi L^2/A$ = .21)						
10.0	0	0	.33	.47	.03	.14
13.5	0	0	.60	.86	.05	.24
17.5	0	0	1.01	1.44	.05	.24
20.3	0	0	1.35	1.93	.03	.14
24.3	0	0	1.91	2.72	.013	.054
10.0	6	30	.353	.505	.03	.14
13.5	6	30	.635	.405	.04	.19
17.5	6	30	1.12	1.59	.08	.38
20.3	6	30	1.45	2.08	.07	.33
24.3	6	30	2.04	2.92	.09	.43
10.0	12	60	.42	.60	.05	.24
13.5	12	60	.75	1.07	.05	.24
17.5	12	60	1.32	1.88	.05	.24
20.3	12	60	1.71	2.45	.08	.38
24.3	12	60	2.4	3.43	.124	.59

2. Supplementary Experiment Data

freq	R	αR	$e^{-\alpha R}$	$\lvert\langle\rho\rangle\rvert^2$	$\frac{\lvert\langle\rho\rangle\rvert^2}{e^{-\alpha R}}$
SUPPLEMENTARY SEAS:					
SEA C (σ = .17 cm, L_u = 3.2 cm, α = 1.52) (θ_1=0°, θ_2=0°)					
10.0	.059	.09	.914	.88	.962
13.5	.107	.163	.850	.82	.965
17.5	.18	.274	.760	.78	1.03
20.3	.24	.365	.696	.71	1.02
24.3	.342	.52	.595	.58	.975
SEA E (σ = .051 cm, L_u = .8 cm, α = 3.7) (θ_1=0°, θ_2=0°)					
10.0	.0049	.018	.982	.987	1.01
13.5	.0089	.033	.968	.973	1.01
17.5	.0151	.056	.946	.935	.99
20.3	.0203	.075	.928	.955	1.03
24.3	.029	.107	.899	.94	1.04
PLANE WAVE (PARABOLIC REFLECTOR SOURCE):					
SEA A (σ = .173 cm, L_u = 2.1 cm, α = 2.1) (θ_1=0°, θ_2=0°)					
10.0	.059	.124	.884	.93	1.05
13.5	.107	.225	.798	.80	1.00
17.5	.18	.378	.686	.71	1.03
20.3	.24	.505	.604	.68	1.13
22.3	.293	.615	.541	.48	.89
24.3	.342	.72	.488	.51	1.04
27.0	.43	.90	.406	.42	1.03
30.0	.53	1.11	.33	.29	.88
34.5	.70	1.47	.230	.225	.98
37.0	.81	1.70	.183	.176	.96
43.0	1.09	2.29	.109	.109	1.00
SEA B (σ = .41 cm, L_u = 3.5 cm, α = 1.42) (θ_1=0°, θ_2=0°)					
10.0	.33	.468	.626	.63	1.01
13.5	.60	.852	.427	.39	.915
17.5	1.01	1.43	.240	.24	1.00
20.3	1.35	1.92	.147	.16	1.09
22.3	1.63	2.32	.098	.096	.98
24.3	1.91	2.72	.066	.069	1.05
27.0	2.40	3.41	.033	.038	1.15
30.0	2.96	4.20	.015	.0256	1.70
34.5	3.91	5.55	.0039	.0132	3.4
37.0	4.5	6.4	.0017	.008	4.7

PLANE WAVE (PARABOLIC REFLECTOR SOURCE) (Continued)

freq	R	αR	$e^{-\alpha R}$	$\lvert\langle\rho\rangle\rvert^2$	$\frac{\lvert\langle\rho\rangle\rvert^2}{e^{-\alpha R}}$
SEA D (σ = .32 cm, L_u = 4.2 cm, α = 1.26) (θ_1=0°, θ_2=0°)					
10.0	.20	.252	.778	.81	1.04
13.5	.365	.46	.632	.562	.89
17.5	.617	.777	.465	.482	1.03
20.0	.80	1.01	.366	.372	1.02
24.0	1.15	1.45	.235	.230	.98
27.0	1.46	1.84	.160	.162	1.01
30.0	1.80	2.27	.104	.090	.87
34.5	2.38	3.0	.050	.050	1.00
37.0	2.74	3.45	.032	.029	.91
43.0	3.69	4.65	.0096	.015	1.56

LARGER APERTURE (50 x 50 CM):

freq	R	$\lvert\langle\rho\rangle\rvert^2$	$\langle\rho\rho^*\rangle$
SEA A (σ = 0.173 cm, L_u = 2.1 cm) (θ_1=0°,θ_2=0°)			
10.0	.059	.79	.78
13.5	.107	.61	.58
17.5	.18	.62	.67
20.3	.24	.59	Not done
24.3	.342	.41	.47
SEA B (σ = 0.41 cm, L_u = 3.5 cm) (θ_1=0°,θ_2=0°)			
10.0	.331	.405	.44
13.5	.595	.23	.34
17.5	1.01	.23	.63
20.3	1.35	.15	Not done
24.3	1.91	.04	.425

(Note: The larger aperture data shows significant interference from reverberation — it was not used in the analysis.)

3. Point Source Experiment Data

SEA D (σ = .32 cm, L_u = 4.2 cm)

freq	R	$\langle \rho\rho^* \rangle$	$(S/N)_1$	$(S/N)_2$
10.0	.20	.95	20 dB	30 dB
13.5	.365	.81	20 dB	30 dB
17.5	.617	.85	15 dB	25 dB
20.0	.80	.86	15 dB	25 dB
24.0	1.15	.87	14 dB	25 dB

Note: $(S/N)_1$ is signal to total noise ratio

$(S/N)_2$ is correlated signal to noise ratio and is a measure of the coherent electrical feedthrough.

BIBLIOGRAPHY

1. Baker, W. L. and J. L. Macaluso, Underwater Sound Signatures of Flight Vehicles – Status Report No. 3, Ordnance Research Laboratory Report No. NOw 65-0123-d-30, The Pennsylvania State University, University Park, Pennsylvania.

2. Medwin, H., "Specular scatter of underwater sound from a wind-driven surface", Journal of the Acoustical Society of America, v. 41, pp. 1485-1495, June 1967.

3. Beckmann, P., and A. Spizzichino, The Scattering of Electromagnetic Waves from Rough Surfaces, Macmillan Co., New York, 1963.

4. Pierson, W. J., and L. Moskowitz, "A proposed spectral form for fully developed wind seas based on the similarity theory of S. A. Kitaigorodskii," Journal of Geophys. Res., v. 69, pp. 5181-5190, 1964.

5. Lastinger, J. L., "Acoustic characteristics of woods at high hydrostatic pressure", Journal of the Acoustical Society of America, v. 47, pp. 285-289, January 1970.

6. Clay, C. S., and H. Medwin, "Dependence of spatial and temporal correlation of forward-scattered underwater sound on the surface statistics – part I. Theory", Journal of the Acoustical Society of America", v. 47, pp. 1412-1418, May 1970.

7. Rudnick, I. and M. N. Stein, "Reciprocity free field calibration of microphones to 100 kc in air," Journal of the Acoustical Society of America, v. 20, pp. 818-825, November 1948.

8. Mayo, N. H., Near-grazing Specular Scattering of Underwater Sound from Sea and Swell, Master's Thesis, Naval Postgraduate School, July 1970.

9. Wright, W.M., "Study of model sea surface statistics", Part of an unpublished report of research conducted at the Naval Postgraduate School, July 1970.

10. Bendat, J. S. and A. G. Piersol, Measurement and Analysis of Random Data, John Wiley & Sons, New York, 1966.

11. Personal communication to author from Dr. H. Medwin.

INITIAL DISTRIBUTION LIST

		No. Copies
1.	Defense Documentation Center Cameron Station Alexandria, Virginia 22314	2
2.	Library, Code 0212 Naval Postgraduate School Monterey, California 93940	2
3.	Professor Herman Medwin Code 61Md Department of Physics Naval Postgraduate School Monterey, California 93940	16
4.	Professor G. A. Sackman Department of Electrical Engineering Naval Postgraduate School Monterey, California 93940	1
5.	Dr. Wayne Wright Kalamazoo College Kalamazoo, Michigan 49001	1
6.	LCDR Ned H. Mayo USS HENDERSON (DD785) FPO, San Francisco 96601	1
7.	LT. James D. Hagy FAIRKEF U.S. Naval Station, Keflavik FPO, New York 09571	1
8.	Mr. William Smith Department of Physics Naval Postgraduate School Monterey, California 93940	1

Blank

p 132

Security Classification

DOCUMENT CONTROL DATA - R & D

(Security classification of title, body of abstract and indexing annotation must be entered when the overall report is classified)

1 ORIGINATING ACTIVITY (Corporate author)

Naval Postgraduate School
Monterey, California

2a. REPORT SECURITY CLASSIFICATION

Unclassified

2b. GROUP

3 REPORT TITLE

Transmission of Sound Through a Randomly Rough Air-Sea Interface

4 DESCRIPTIVE NOTES (Type of report and inclusive dates)

Engineer's Thesis; September 1970

5 AUTHOR(S) (First name, middle initial, last name)

James Dixon Hagy, Jr.

6 REPORT DATE	7a. TOTAL NO. OF PAGES	7b. NO. OF REFS
September 1970	132	11

8a. CONTRACT OR GRANT NO.	9a. ORIGINATOR'S REPORT NUMBER(S)
b. PROJECT NO.	
c.	9b. OTHER REPORT NO(S) (Any other numbers that may be assigned this report)
d.	

10 DISTRIBUTION STATEMENT

This document has been approved for public release and sale; its distribution is unlimited.

11 SUPPLEMENTARY NOTES	12 SPONSORING MILITARY ACTIVITY
	Naval Postgraduate School Monterey, California 93940

13. ABSTRACT

The Helmholtz integral and the Kirchhoff approximation have been used to develop predictions for the transmission of sound through a rough air-sea interface. A model study was conducted with wind-driven surfaces generated in a large anechoic tank. Root mean square wave heights, σ, ranged from .05 to .41 cm, windward correlation lengths, L_u, from 0.8 to 4.2 cm. The frequencies used (10-43 kHz) were scaled to be equivalent to low audio frequencies with moderate seas. Although the coherent component of the transmitted acoustic intensity showed an exponential decrease with increasing values of the roughness parameter, $R\ [= k_2^2\sigma^2\ (c_2/c_1 \cos\theta_1 - \cos\theta_2)^2\ ]$, the decrease was greater than predicted. (Subscript 2 refers to propagation constant, speed and angle of transmission in water; subscript 1, in air.) This lack of agreement appeared to be caused by violation of the Kirchhoff requirement, $L/\lambda_2 >> 1$. An empirical correction factor $\alpha = 1 + 4.8\ e^{-Lu/1.75}$ was determined to give a corrected roughness, αR. The corrected theory appears to be valid for both coherent and incoherent components of intensity for all values of L/λ_2 provided that $R < 4.0$. For higher values of roughness there is a "leveling off" of the transmission loss of the coherent component similar to that recently observed but unexplained in rough surface scattering.

DD FORM 1 NOV 65 1473 (PAGE 1)

S/N 0101-807-6811

Security Classification

A-31408

14 KEY WORDS	LINK A		LINK B		LINK C	
	ROLE	WT	ROLE	WT	ROLE	WT
Sound Transmission						
Underwater Sound						
Air-Sea Interface						
Rough Water Surface						
Wave Height Distribution						
Wave Spectrum						
Correlation						
Coherent						

Gaylord
SHELF BINDER
Syracuse, N.Y.
Stockton, Calif.

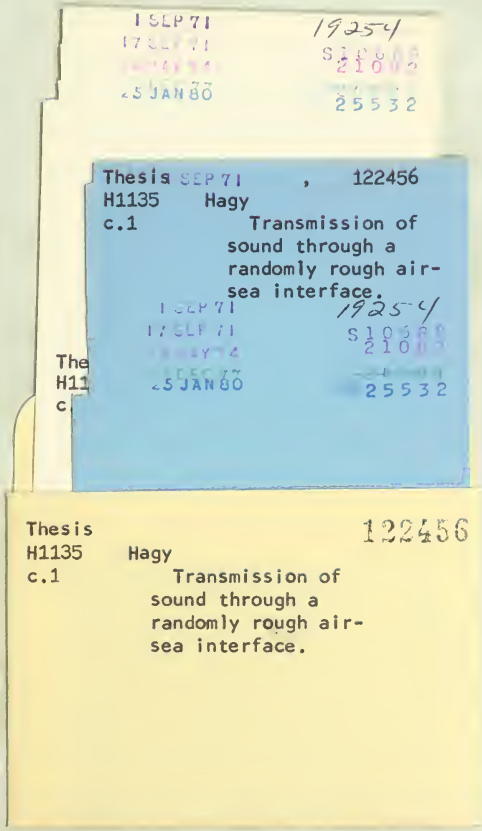
1 SEP 71
17 SEP 71
25 JAN 80
1925
S10660
21003
25532

Thesis SEP 71 , 122456
H1135 Hagy
c.1 Transmission of sound through a randomly rough air-sea interface.
1 SEP 71
17 SEP 71
25 JAN 80
1925
S10660
21003
25532

The
H11
c

Thesis 122456
H1135 Hagy
c.1 Transmission of sound through a randomly rough air-sea interface.

thesH1135
Transmission of sound through a randomly
3 2768 001 03720 3
DUDLEY KNOX LIBRARY